Dissertation

submitted to the

Combined Faculties of the Natural Sciences and Mathematics

of the Ruperto-Carola-University of Heidelberg. Germany

for the degree of

Doctor of Natural Sciences

Put forward by

Dipl. Phys. Frank Hantschel

born in: Halle an der Saale

Oral examination: 21.01.2014

Energy transport in the medium of interacting two-level systems

Referees: Prof. Dr. Boris Fine
PD. Dr. Andreas Komnik

Energy transport in the medium of interacting two-level systems

This thesis investigates a medium of disordered two-level systems with dipolar interaction. This investigation is relevant to the dynamics of nuclear spins 1/2 in solids and to the dynamics of low temperature glasses. Our main tool is a hybrid quantum classical simulation, which enables us to study the time evolution of three-dimensional systems consisting of up to 1000 two-level systems.
The results indicate, that the dynamics of the full system is delocalized up to very large disorders. We derive an estimate for the time scale of energy transport. When the disorder is larger than a certain value, this time scale becomes proportional to the disorder.

Energietransport in wechselwirkenden Zwei-Level Systemen

Die vorliegende Arbeit untersucht das Verhalten ungeordneter Zwei-Niveau Systeme mit dipolarer Wechselwirkung. Das zugrundeliegende Modell beschreibt sowohl die Dynamik für Kernspins in Festkörpern, als auch die Dynamik von Gläsern bei tiefen Temperaturen. Wir studieren dieses Modell mithilfe einer Computersimulation, die quantenmechanischen Berechnungen auf Systeme mit wenigen Teilchen eingrenzt. Durch diese Vereinfachung ist es möglich, die Zeitevolution von dreidimensionalen Systemen mit insgesamt 1000 Zwei-Niveau Systemen zu simulieren.
Die Ergebnisse zeigen eine Delokalisierung des Systems bis zu einem großen Unordnungsgrad. Mithilfe der Verteilung von Wechselwirkungen schätzen wir die Zeitskala des Energietransports ab. Wir zeigen, dass ab einem gewissen Unordnungsgrad diese Zeitskala proportional zur Unordnung des Systems wird.

Contents

Chapter 1

Introduction

In this thesis, we investigate energy transport at atomic scale in a medium of disordered quantum two-level systems (TLS). These investigations are, in particular, relevant to the dynamics of nuclear spins measured by the technique of nuclear magnetic resonance (NMR). They are also relevant to the dynamics of low temperature glasses.

We consider the simplest case of a many-particle system: a system of spin 1/2 particles. We assume dipolar interaction between TLS, which is common in the fields of NMR and low temperature glasses.

Interaction between particles leads to fluctuation of the energy of individual particles. This process is depicted in Figure 1.1. It leads to the transport of energy. Energy conservation requires that the energy differences of two particles match each other.

Energy transport in the medium of disordered TLS can be suppressed because of the phenomenon of many-body localization. Our goal is to investigate, whether this suppression happens, and, if not, to determine the characteristic timescale for the onset of energy transport. The main tool to examine these properties is a computer simulation.

An exact numerical treatment of a quantum system is limited to about 30 particles, since the dimension of the Hilbert space grows exponentially with the number of particles. In contrast, a classical simulation allows to investigate larger systems. But by ignoring quantum effects, it automatically neglects the quantum localization phenomenon, which may play the crucial role in the energy transport. Therefore, we introduce a hybrid quantum classical approach for the simulation of the system. The dynamics of these systems can be explained using the notion of resonant pairs [9], which emerge from quantum treatment of spin pairs. We identify resonant spin pairs

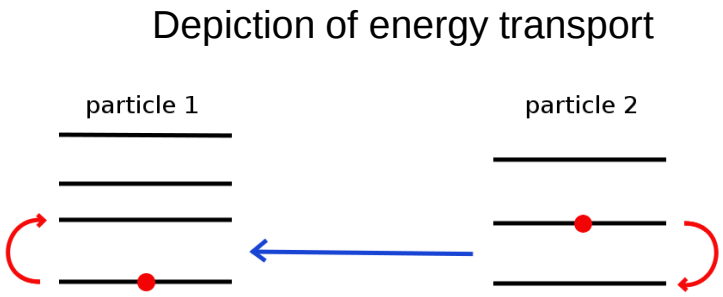

Figure 1.1: This figure depicts transport of energy between two particles, whose energy levels are indicated as black lines. The energy of particle 1 is raised, whereas the energy of particle 2 is lowered. Thus, energy is transported from 2 to 1.

and simulate the dynamics quantum mechanically, while the rest of the simulation is implemented classically.

1.1 Localization

The properties of a quantum particle are determined by its wave function $\psi(x,t)$. The probability to find the particle with coordinates x at time t is

$$p(x,t) = |\psi(x,t)|^2 \,, \tag{1.1}$$

A delocalized wave function spreads over the entire space. Therefore, the probability to find the particle around any position x tends to zero for an infinite system: $\lim_{t\to\infty} p(x_i,t) = 0$. In contrast, if a wave function ψ is localized, the probability $p(x,t)$ remains significant for a compact range of coordinates x. Localized wave functions typically decay exponentially far from their localization region.

Let us consider a wave function ψ, which is localized at initial time $t = 0$. Its time evolution is determined by the Schrödinger Equation

$$i\hbar \, \frac{\partial \psi}{\partial t} = \mathcal{H} \, \psi \tag{1.2}$$

which includes the Hamiltonian $\mathcal{H}$ of the system. By Equation (1.2), $\mathcal{H}$ determines the dynamic properties of the quantum system of interest.

We phrase the general agenda of localization vs. delocalization investigations as three separate questions:

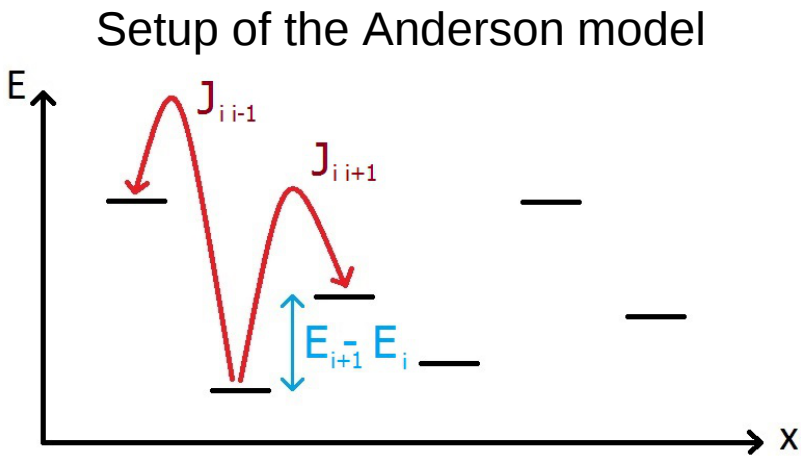

Figure 1.2: Depiction of the setup of Anderson model. Energy levels of different positions are distributed randomly, therefore the energy difference ΔE between adjacent levels varies as well. Hopping between adjacent sites is indicated by red arrows.

- If ψ is localized at time $t = 0$, will it stay localized in the limit $t \to \infty$?
- If not, how much time does it take for a particle to drift by distance d away from its initial position?
- How does this time depend on the properties of the system?

In this work, we address these questions not for the drift of a particle, but energy transport. We focus on the dependence of the delocalization time scale on the disorder of the system.

1.1.1 Anderson localization

In 1958, P.W. Anderson investigated the behaviour of one particle, whose wave function ψ is initially localized in a disordered potential on a lattice [4]. The situation is parametrized by energy levels E_i of different lattice sites and hopping terms J_{ij}, which describe the transition of the particle from one site to another. Figure 1.2 depicts this situation for a one dimensional lattice. Its main feature is the disorder of on-site energy levels. The disorder in the Anderson model is controlled by a parameter W, defining the uniform probability distribution of energy levels in the interval $[-W/2, W/2]$. This affects the diffusion of the wave function: If the energy difference of two levels is small, the probability for a transition from one level to another is large. This probability depends on the hopping J_{ij} between different sites as well.

The hopping is assumed to be sufficiently short range: J_{ij} decreases for $r_{ij} \to \infty$ faster than r_{ij}^{-d}, where d is the dimension of the system and r_{ij} denotes the distance of the two sites i and j. The transport properties of the system are determined using a perturbation in different hopping orders, where the first order is defined as the direct transition between two sites.

As the main result, no diffusion occurs for systems with disorder values W larger than a certain critical value W_c. This critical value is equal to zero for one and two dimensional systems [2, 13, 16]. Hence, an arbitrarily small disorder causes the breakdown of diffusion transport for short range interaction and small dimensions $d \leq 2$. This effect is denoted as *Anderson localization* of a single particle wave function.

Anderson evaluated the critical value W_c to be of the order of the nearest neighbour interaction for three dimensions. Recent results indicate $W_c = 16.530$ for a system with nearest neighbour interaction of strength 1 [22].

Experimentally, localization has been reported for light waves [24], microwaves [12], sound waves [27], electron gases [3] and 1D matter waves [6].

Anderson localization can be viewed as the result of interference between multiple scattering of particles by disorder [15]. The interference increases the probability of time reversible paths and thus, the net resistivity of the system.

$J_{ij} \sim r_{ij}^{-3}$ as the marginal case for the localization-delocalization transition in three-dimensional systems

Beside of the study of systems with short range hopping, Anderson investigated the properties of his model with dipolar-type hopping $J_{ij} \sim r_{ij}^{-3}$ [4]. Two results for these systems were determined:

- There is no critical value W_c as for systems with short range hopping. Single particle states are always delocalized.
- Nonetheless, diffusion is logarithmically slow.

He supported this claim using the notion of pairs with resonant levels. A pair of sites is labeled as resonant, if their energy difference is smaller than the hopping J_{ij} coupling the sites:

$$|E_i - E_j| < J_{ij}. \tag{1.3}$$

Pairs that satisfy condition (1.3) have a large transition amplitude, which leads to particle transport. For $J_{ij} \sim r_{ij}^{-3}$, the mean number of resonant

partners of every lattice site depends on the logarithm of the distance R of the site as

$$N_{RP} \sim \log(R)\,. \tag{1.4}$$

For an infinite size of the system, each particle finds at least one resonant partner. This leads to delocalization, independent of the disorder W. But then, the resulting diffusion is logarithmically slow. As a result, for large enough disorder, this diffusion may never happen on experimental time scales.

If we assume a faster decaying hopping $r^{-3-\alpha}$, the dependence in Equation (1.4) is altered to $N_{RP} \sim r_{ij}^{-\alpha}$. Hence, the value of N_{RP} is bounded for $r_{ij} \to \infty$. The value of the upper bound depends on the disorder of the system as $1/W$. For large disorder W, these systems have only few resonant pairs and are localized.

In contrast, for slower decaying hopping $r^{-3+\alpha}$, N_{RP} increases proportionally to r^{α}, which is much faster than logarithmically. As a result, delocalization and the resulting diffusion become efficient.

In summary, the hopping law $J_{ij} \sim r_{ij}^{-3}$ leads to a borderline behaviour with respect to the localization-delocalization transition in one particle systems [4, 9].

1.1.2 Lifshitz Model

So far, we examined systems that possess a disorder in on-site energies, but we assumed no disorder of the hopping elements between system sites.

In 1964, I.M. Lifshitz considered a system of potential wells, which were located randomly in three-dimensional space. The potential wells have identical binding energies, but the hopping elements depend on the random distances r_{ij} between wells as

$$J_{ij} \sim e^{-\gamma r_{ij}}\,. \tag{1.5}$$

The inverse of the parameter γ is a measure for the range of the hopping. Another important parameter is the concentration n of potential wells. Lifshitz derived, that delocalized states exist for $\gamma n^{-1/3} \sim 1$, whereas the system is localized for $\gamma n^{-1/3} \gg 1$. Numerical simulations indicate that delocalized states appear at $\gamma n^{-1/3} \approx 3$ [11].

1.1.3 Many-body localization

Many-body localization (MBL) is a phenomenon, that may possibly exist in systems of interacting particles with disorder. These systems would exhibit single-particle localization in the absence of interactions between particles. However, interactions between particles tend to destroy localization [7]. Numerical simulations of one dimensional spin chains with disorder produce results consistent with possible MBL [14, 17]. These studies use a full diagonalization procedure to calculate many-body eigenstates and study their properties. Therefore, they are limited to systems consisting of about 30 particles.

Another approach is the application of the renormalization group technique to such systems [26]. It was also reported to support the existence of MBL.

Closest to the scope of the present thesis was the investigation of MBL in a medium of dipolar coupled two-level systems (TLSs) by Burin and Kagan [9]. Their investigation was focused on the properties of low temperature glasses.

Burin and Kagan (BK) studied the dynamics of the system by examining the properties of resonant TLSs. Their results indicate, that there exists a critical distance between TLSs with corresponding critical coupling J_*, when resonantly coupled TLSs form a "resonant cluster". The formation of the resonant cluster then leads to the onset of energy transport (i.e. breakdown of MBL).

The idea, that interaction between resonant pairs is leading to dynamics in the system, is the basic principle for our approach to simulate the time evolution in a spin system. In this work, we extract a value for J_* from our numerical simulations. Thereby, the order of magnitude estimates of Burin and Kagan are substituted by explicit numbers. In addition, we identify a mechanism for resonant cluster, which is different from that of BK.

Generally, the phenomenon of many-body localization is not completely understood at present.

1.2 Experimental context

In this section, we introduce two experimental settings, namely:

1. Nuclear magnetic resonance (NMR) in solids and
2. Low temperature glasses.

Both settings involve disordered TLSs with dipolar interactions.

1.2.1 Nuclear spins in solids

In order to obtain a specific Hamiltonian for our model, the next section introduces the basic principles of nuclear magnetic resonance (NMR). Here, spin 1/2 particles assume the role of TLSs and are described by spin operators S^α.

One spin in magnetic field

We assume a strong magnetic field $\vec{H} = H_0\vec{e_z}$ along the z-axis. This field couples to the spin operator S^z via the magnetic moment

$$\mu = \gamma h S^z \tag{1.6}$$

as

$$\mathcal{H} = -\gamma h H_0 \; S^z, \tag{1.7}$$

where γ is the gyromagnetic ratio. In most molecules, this field is influenced by screening of electrons and therefore differs for different positions in the molecule. Moreover, the gyromagnetic ratio varies slightly for different atoms. Both effects are combined to a variation ΔH_i of the static field. Using this notion, we obtain the full magnetic field acting on the particle as $\vec{H} = (H_0 + \Delta H_i)\vec{e_z}$. The fluctuations ΔH_i are called chemical shifts.

The static field H_0 generates a precession of the magnetic moment $\vec{\mu}$ around the z-axis. In order to obtain a constant magnetic moment, we define a new reference frame, which rotates around the z-axis with frequency $\vec{\Omega} = -\gamma H_0\vec{e_z}$. This frame is called Larmor rotating reference frame and leads to a correction of the magnetic field:

$$\vec{H} \to \vec{H} + \frac{\vec{\Omega}}{\gamma}. \tag{1.8}$$

As a result, Equation (1.7) transforms to

$$\mathcal{H} = -\gamma\hbar(H_0 + \Delta H_i - \frac{\Omega}{\gamma}) \; S_i^z = -\gamma\hbar \, \Delta H_i \; S_i^z. \tag{1.9}$$

Truncated magnetic-dipolar interaction

Dipolar interaction contributes the term

$$\mathcal{H}_{\text{dipole}} = \sum_{i=1}^{N}\sum_{j=1}^{N} \frac{\boldsymbol{\mu_i} \cdot \boldsymbol{\mu_j}}{r_{ij}^3} - \frac{3\,(\boldsymbol{\mu_i} \cdot \boldsymbol{r_{ij}})\,(\boldsymbol{\mu_j} \cdot \boldsymbol{r_{ij}})}{r_{ij}^5} \tag{1.10}$$

to the Hamiltonian $\mathcal{H}$ [25]. Here, N denotes the number of particles in the system and r_{ij} the distance between two particles. In the Larmor rotating

frame, we express the magnetic moments $\boldsymbol{\mu}$ by spin operators (equation (1.6)), and expand all products in Equation (1.10). This yields

$$\mathcal{H}_{\text{dipole}} = \frac{\gamma_i \gamma_j \hbar^2}{r_{ij}^3} \left(A + B + C + D + E + F\right), \tag{1.11}$$

where

$$\begin{aligned}
A &= \left(1 - 3\cos^2\theta\right) S_i^z S_j^z \\
B &= -\frac{1}{4}\left(1 - 3\cos^2\theta\right)\left(S_i^+ S_j^- + S_i^- S_j^+\right) \\
C &= -\frac{3}{2}\sin\theta\cos\theta\ e^{-i\theta}\left(S_i^+ S_j^z + S_i^z S_j^+\right) \\
D &= -\frac{3}{2}\sin\theta\cos\theta\ e^{i\theta}\left(S_i^- S_j^z + S_i^z S_j^-\right) \\
E &= -\frac{3}{4}\sin^2\theta\ e^{-2i\theta} S_i^+ S_j^+ \\
F &= -\frac{3}{4}\sin^2\theta\ e^{2i\theta} S_i^- S_j^- \ .
\end{aligned}$$

Whereas term A is completely diagonal, the off diagonal term B simultaneously flips one spin up and one spin down. The admixture related to all remaining terms is very small [25]. Hence, these terms can be neglected and we obtain a simplified Hamiltonian of the form

$$\mathcal{H} = -\sum_i \gamma\hbar\,\Delta H_i\ S_i^z + \sum_{i,j} J_{ij}\ \left(S_i^z S_j^z - \frac{1}{4}\left(S_i^+ S_j^- + S_j^+ S_i^-\right)\right), \tag{1.12}$$

where we used Equation (1.9) to obtain local fields. The simplified interaction is referred to as *truncated dipole interaction*. The prefactors were combined to a new variable J_{ij} as

$$J_{ij} = \frac{\gamma^2\hbar^2\left(1 - 3\cos^2(\theta_{ij})\right)}{r_{ij}^3}. \tag{1.13}$$

Equations (1.12) and (1.13) define the Hamiltonian of our model.

1.2.2 Low temperature glasses

Now, we introduce a second experimental setup, which is related to the model of this thesis: The setup of low temperature glasses. One interesting property of glasses at low temperatures is their specific heat, which is nearly proportional to the temperature [29]. This contradicts Debye theory, which predicts a T^3 dependence of the specific heat. In order to explain this discrepancy, microscopic structures of glasses were examined.

In the medium of glasses, tunneling of atoms between two nearby positions can be described by double-well potentials. Typically, the energy splitting of the lowest two eigenstates is much smaller than the splitting to the next available eigenstate. Therefore, such a double well can be approximated well by a TLS. The TLSs influence the mean path of phonons, which results in a linear specific heat [5,20] and thereby explains the deviation from the T^3 prediction of Debye Theory. Small deviations from the linear dependence [29] can be explained by taking into account the interaction of TLS [28].

The same is true for dephasing in dielectric glasses at ultra low temperatures: Whereas the tunneling model predicts $\tau_1^{-1} \sim T^3$ [5], experiments in the range of μK indicate a $\tau_1^{-1} \sim T$ behaviour in dielectric glasses [23]. This characteristics is explained by taking into account a dipolar interaction of TLS, which is mediated via strain fields [10]. These interactions induce delocalized collective excitations in the system. An important concept of this calculation is the idea of resonant pairs.

Recent research investigates higher orders of interaction. For example, Bodea and Würger examined the influence of resonant triples of TLS [8], whereas Polishchuk and Burin regarded the effect of nuclear quadrupole interaction on the thermal conductivity [21].

In general, low temperatures lead to a higher population of lower energy states. However, TLS with large energy splittings (compared to the temperature) are isolated from the dynamics [10]. By neglecting these particles, the setup of low temperature glasses can be mapped onto the infinite temperature setup of NMR.

The glassy properties of examined systems generate a random distribution of these two level systems in three-dimensional space. The distribution of energy splittings is uniform in the range of interest. We adopted these characteristics of low temperature glasses for the model of our simulation.

1.3 Organization of the thesis

In Chapter 2, the Hamiltonian of the problem is introduced and the framework of the simulation is described. One central aspect is the notion of resonant spin pairs, which is widely-used in this field [8, 9]. We discuss the realization of this notion and examine its implementation. Additionally, we compare analytical and numerical distributions of variables characterizing resonant spin pairs. Thereby, in particular, we can assess the influence of the finite-size effects on our simulation and control the accuracy of the algorithms used.

In Chapter 3, we present a simulation that restricts full quantum calculations on the behaviour of spin pairs. We use the concept of resonant pairs to determine a time evolution of the full system. The time evolution is investigated by examining correlations in the system. We obtain the functional form of these correlations and focus on their dependence on the disorder. We find, that part of the system is isolated from the dynamics. We examine the properties of this isolated region in detail.

In the algorithm of Chapter 3, interaction of resonant pairs leads to violation of energy conservation. We address the question, whether these processes should be suppressed by a detailed study of four spin systems. As a result of this examination, a modified condition for resonant pairs is derived, which is described in Chapter 4.

Since this modification complicates the algorithm, a direct time evolution is not possible anymore. Instead, we investigate the formation of resonant cluster, which are formed by the interaction of spin pairs. Results of the time evolution indicate, that such a cluster can transport energy and lead to spin diffusion. The properties of such a cluster are important for the dynamics of the spin system. We found, that pairs with large interaction are excluded from this dynamics. From this fact we predict a lower bound for the time scale of energy transport, which is the main result of Chapter 4.

The last chapter collects and discusses the results of this thesis. Furthermore, we present an outlook.

In order to justify these results, it is necessary to discuss the implementation of the model. Along with technical derivations, we moved this discussion to the appendix, which is a vital part of this thesis. In addition, the appendix contains a detailed study of small spin systems, namely, systems consisting of two, four and six spins.

Chapter 2

Disordered two-level systems with dipolar interaction

The theoretical setting of this thesis is identical to the one described in Section 1.2.1 for solid-state NMR. It also shares features with the TLS model for low-temperature glasses, namely: two level structure of the primary microscopic objects, disordered energy splitting between the two levels and r^{-3} type interaction between the primary objects.

Throughout the thesis, we always use a system with an interaction prefactor $u_0 = 1$ and a density of spins $\rho_{\text{Spins}} = 1$. All units are normalized with respect to these two constants. Therefore, units are omitted in the further course of the thesis.

2.1 Theoretical model

We consider a spin system of N spins 1/2, that interact via a version of dipolar interaction occurring in solid-state NMR (see Section 1.2.1). We obtain its Hamiltonian as

$$\mathcal{H} = -\sum_{i=1}^{N} h_i S_i^z + \sum_{i,j} J_{ij} \left(S_i^z S_j^z - \frac{1}{4} \left(S_i^+ S_j^- + S_j^+ S_i^- \right) \right), \tag{2.1}$$

where $S_i^{\pm} = S_i^x \pm i S_i^y$ and

$$J_{ij} = \frac{u_0 \left(1 - 3\cos^2\left(\theta_{ij}\right)\right)}{r_{ij}^3}, \tag{2.2}$$

where r_{ij} is the distance between spin i and spin j, and

$$\cos(\theta_{ij}) = \frac{z_i - z_j}{r_{ij}} \tag{2.3}$$

with z-coordinates z_i and z_j. The parameter θ_{ij} is defined as the angle between $\mathbf{r_{ij}}$ and the z-axis.

We choose the on-site fields h_i from a uniform distribution $[0, \varepsilon]$. The ratio $\frac{\varepsilon}{u_0}$ defines the on-site variation of energy compared to the typical interaction between spins, which are separated by a distance $r_{ij} = 1$. The variable ε refers to the disorder value of the system.

Our simulation investigates the dynamics of a spin system consisting of 1000 spins confined to a cubic box of size $10 \times 10 \times 10$ with periodic boundaries. The positions of the spins are chosen randomly within the box, where we define a minimum distance of $r_{\min} = 0.05$ between spins. This cutoff value corresponds to an interaction of 8000, which is much larger than the typical interaction between spins. The probability p, to find a spin with distance $r < r_{\min}$ to a given spin, can be estimated as $p = \frac{4\pi}{3} \cdot (0.05)^3 \approx 5 \cdot 10^{-4}$.

The introduction of $r_{\min}$ is based on the structure of glasses and the NMR setup: In glasses, the minimum radius corresponds to the distance between two adjacent atoms. For the NMR setup, it arises from the smallest distance of two nuclei.

The results of this thesis indicate, that spin pairs with a large interaction do not influence the dynamics of the system. Hence, the actual value of the minimum radius is not important, if it is considerably smaller than the average nearest neighbour interaction.

2.2 Resonant pairs

According to Eq. (2.1), the Hamiltonian of a spin pair reads as

$$\mathcal{H}_{12} = -h_1 S_1^z - h_2 S_2^z + J_{12} \left(S_1^z S_2^z - \frac{1}{4} \left(S_1^+ S_2^- + S_2^+ S_1^- \right) \right). \tag{2.4}$$

A detailed analysis of this system is presented in Appendix A.3. Since the only non-vanishing coupling of $\mathcal{H}_{12}$ connects states $|\uparrow\downarrow\rangle$ and $|\downarrow\uparrow\rangle$, we truncate the full basis to the *product basis*

$$\mathbb{B} = \{|\uparrow\downarrow\rangle, |\downarrow\uparrow\rangle\} \, . \tag{2.5}$$

The two basis states of $\mathbb{B}$ are denoted as ψ_1 and ψ_2. We obtain the matrix representation of the Hamiltonian as

$$\mathcal{H}_{12} = \frac{1}{2} \begin{pmatrix} -h_{12} - \frac{1}{2} J_{12} & -\frac{1}{4} J_{12} \\ -\frac{1}{4} J_{12} & -h_{12} - \frac{1}{2} J_{12} \end{pmatrix}, \tag{2.6}$$

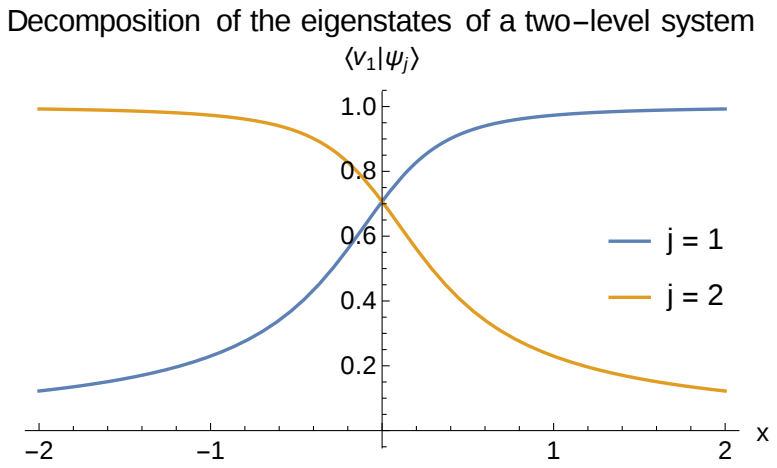

Figure 2.1: Plot of the projection $\langle v_1|\psi_j\rangle$ of eigenvector v_1 on the product states ψ from Equation (2.5) in dependence of $x = \frac{h_{12}}{J_{12}}$.

where $h_{12} = h_1 - h_2$ is called on-site field of the pair. Further, we introduce the dimensionless variable

$$x = \frac{h_{12}}{J_{12}}, \tag{2.7}$$

which describes the ratio of on-site field and interaction. First, we consider very small and very large absolute values of x:

1. $|x| \gg 1$. In this case, the matrix of Equation (2.6) is dominated by its diagonal elements. Spin pairs of the this type behave as two independent spins. Their eigenstates v_1 and v_2, are nearly equal to the product states $\psi_j \in \{|\uparrow\downarrow\rangle, |\downarrow\uparrow\rangle\}$, and we obtain the projection $\langle v_i|\psi_j\rangle$ of v_i on ψ_j as $\langle v_i|\psi_j\rangle \approx \delta_{ij}$. This implies, that the probability for a transition $|\uparrow\downarrow\rangle \leftrightarrow |\downarrow\uparrow\rangle$ is small.

2. $|x| \ll 1$. Here, the off-diagonal elements dominate $\mathcal{H}_{12}$.

Two-spin systems, which satisfy $|x| \ll 1$, possess eigenstates close to

$$\begin{aligned} v_1 &= \frac{1}{\sqrt{2}}\left(|\uparrow\downarrow\rangle + |\downarrow\uparrow\rangle\right) \\ v_2 &= \frac{1}{\sqrt{2}}\left(|\uparrow\downarrow\rangle - |\downarrow\uparrow\rangle\right) . \end{aligned}$$

Their projection $\langle v_i|\psi_j\rangle$ is about $1/\sqrt{2}$ for any i and j. Therefore, the probability for a transition $|\uparrow\downarrow\rangle \leftrightarrow |\downarrow\uparrow\rangle$ is large. Spin pairs of this type are called *resonant pairs*.

The two cases $|x| \gg 1$ and $|x| \ll 1$ are connected by the regime $x \approx 1$. Figure 2.1 shows a continuous dependence of the projection $\langle v_i|\psi_j\rangle$ on the

value of x.

In order to obtain a simple model, we approximate this continuous change by a sharp condition: Spin pairs satisfying $|x| < 1$ are identified as resonant pairs, whereas pairs with $|x| > 1$ are treated as two independent spins. This condition is called *resonance condition* and is also used elsewhere [4,9]. Further in this thesis, we compute the resonance condition as

$$|h_{12}| < |J_{12}|\,. \tag{2.8}$$

Introduction of the resonance range S_{ij}

We can transform the resonance condition (2.8) to

$$S_{12} \equiv |J_{12}| - |h_{12}| > 0, \tag{2.9}$$

where we introduced a new variable S_{12}, which we call the "resonance range". If $S_{12} > 0$ holds, the spin pair $(1, 2)$ is resonant. Otherwise, it is non-resonant.

The absolute value of S_{ij} is a measure for the stability of a pair state with respect to a change of its parameter. If $|S_{ij}|$ is small, a small modification of the local field h_{ij} can lead to a change of its identity from resonant to non-resonant or vice versa.

2.2.1 First estimates of the number of resonant pairs

We estimate the number of resonant pairs by calculating the probability $p(R)$, that an arbitrary spin has a resonant partner within distance $r < R$:

$$p(R) = 2\pi \int_{r_{\min}}^{R} \frac{2J(r,\theta)}{\varepsilon}\, \mathrm{d}\varepsilon\; r^2 \mathrm{d}r \sin(\theta)\mathrm{d}\theta\,. \tag{2.10}$$

We insert the dipole interaction $J(r, \theta)$ given by Equation (2.2) and obtain

$$p(R) = \frac{4\pi u_0}{\varepsilon} \cdot \frac{2}{3\sqrt{3}}\; \log\left(\frac{R}{r_{\min}}\right), \tag{2.11}$$

where the factor of $\frac{2}{3\sqrt{3}}$ arises from the θ dependence of J. For isotropic dipole interaction, this factor is 2 and $p(R)$ is calculated as [8]

$$p(R) = \frac{8\pi u_0}{\varepsilon} \cdot \log\left(\frac{R}{r_{\min}}\right). \tag{2.12}$$

In both cases, the probability to find a resonant partner is proportional to $\log(R)$ and to ε^{-1}.

This implies, that in a system with infinite size every spin finds a resonant partner. However, for practical purposes, the probability $p(R)$ can be small due to large disorder ε and the weak dependence on the finite size R.

In this case, a large value of ε results in a small number of resonant pairs, which leads to little dynamics of the system. In contrast, for small values of ε, many resonant pairs exist and we expect large dynamics.

2.2.2 Resonant pair as a composite two-level system

Spins, which belong to a resonant pair, are not in one of the basis states $|\uparrow\rangle$ or $|\downarrow\rangle$, but in a superposition of both states. While this is true for every spin pair, the prefactors of the superposition for non-resonant pairs are typically close to δ_{ij}. This is not the case for resonant pairs. Therefore, we study resonant pairs in their eigenbasis

$$\begin{aligned} |\Uparrow\rangle &= c^+|\uparrow\downarrow\rangle - c^-|\downarrow\uparrow\rangle \\ |\Downarrow\rangle &= c^-|\uparrow\downarrow\rangle + c^+|\downarrow\uparrow\rangle, \end{aligned}$$

where the coefficients

$$c^{\pm} = \frac{1}{\sqrt{2}} \left(1 \pm \frac{h_{12}}{H}\right)^{\frac{1}{2}} . \tag{2.13}$$

are determined in Appendix A.3. Here, denoting the eigenstates as $|\Uparrow\rangle$ and $|\Downarrow\rangle$ substitutes the previous notation of eigenvectors v_1 and v_2. The energy splitting H is defined as the difference of the eigenvalues $\lambda_{1,2}$:

$$H = \langle \Uparrow |\mathcal{H}| \Uparrow \rangle - \langle \Downarrow |\mathcal{H}| \Downarrow \rangle = \lambda_1 - \lambda_2 = \frac{1}{2}\sqrt{4\,h_{12}^2 + J_{12}^2}\,. \tag{2.14}$$

We interpret a resonant pair as a composite two level system with energy H and describe its interaction with other spins using pair operators I^α. In the following, these operators are shortly introduced.

In Appendix A.1, we formally define the basis of the spin pair. This basis is used in Appendix A.2 to derive the matrix representation of the pair operators I. We obtain I as 2×2 matrices in terms of the Pauli matrices σ_α as

$$I^\alpha = \frac{1}{2}\sigma_\alpha. \tag{2.15}$$

This reproduces the expected behaviour of the operators I:

$$I^z|\Uparrow\rangle = \frac{1}{2}\,|\Uparrow\rangle \quad \text{and} \quad I^z|\Downarrow\rangle = -\frac{1}{2}\,|\Downarrow\rangle. \tag{2.16}$$

This configuration is equivalent to the notion of a spin with spin operators S. Hence, we identify a resonant pair as a two level system with basis states

$\{|\Uparrow\rangle, |\Downarrow\rangle\}$ and operators I^α. The Hamiltonian written in pair operators I^α is obtained as

$$\mathcal{H} = -HI^z, \tag{2.17}$$

where the energy H was defined in Equation (2.14).

In contrast, non-resonant pairs are treated as two independent spins and are therefore studied in the product basis $\{|\uparrow\downarrow\rangle, |\downarrow\uparrow\rangle\}$.

Change of the resonance state

As a result of a change of the full local fields h'_{ij}, the resonance state of a pair can change from non-resonant to resonant or vice versa.

First, we consider the case, that a non-resonant spin pair is modified such, that it becomes a resonant pair. In this case, we change the basis from the product basis to the eigenbasis of the pair. We obtain two possible states for the resonant pair: $|\Uparrow\rangle$ and $|\Downarrow\rangle$. In order to select the new state from these two possibilities, we calculate the projections of the initial product state onto both eigenstates. These yield the probabilities for the transitions to $|\Uparrow\rangle$ and $|\Downarrow\rangle$. Based on these probabilities, we choose the new state randomly from $\{|\Uparrow\rangle, |\Downarrow\rangle\}$.

Similar to this procedure, we choose the state of a non-resonant pair, which previously was resonant, from the product states $|\uparrow\downarrow\rangle$ and $|\downarrow\uparrow\rangle$. The probabilities for the transition into each state are given by the projections of the former eigenstate onto both product states.

All projections and the resulting probabilities are determined in Appendix A.3.7.

In order to introduce a time scale, we delay both transformations by the time

$$t_d = \frac{T}{4} = \frac{\pi}{2H}\,, \tag{2.18}$$

which originates from the time evolution of the resonant pair (Appendix A.3.3) and is called *delay time*. Since t_d depends on the splitting H of the spin pair, different pairs typically have different delay times.

2.2.3 A spin in resonance with several other spins

Since we have a system consisting of many spins, a certain spin can be in resonance with several spins at once. We call this situation a conflict. The situation is resolved by comparing time scales of the evolution of all possible resonant pairs involving this spin. As a result of this argumentation, we

confirm the resonant pair with the largest interaction and discard all other resonant pairs involving the same spin. In the following, we justify this procedure.

As derived in Appendix A.3.3, the time evolved wave function $\psi(t)$ of a product state $\psi(0)$ oscillates between ψ_0 and ψ_1 with period $T \sim H^{-1} \sim \frac{1}{J_{12}}$. If the interaction J_{12} of a resonant pair is large, the period of its oscillation is short.

Let us now consider the situation of a spin i, which is in resonance with different spins j and k. The oscillation of their time evolutions acts on different time scales. For the spins of the "slow" pair, spin i is not in its original state anymore, instead it is in an eigenstate of the "fast" pair. On the contrary, the fast pair does not feel a similar effect, since it interacts on a much shorter time scale. Therefore, the interaction with the shorter period suppresses the resonance of the pair with the longer period.

This argumentation is not valid if both interactions are equal. However, the probability for a conflict with equivalent interactions is small in the case of a spin system with random positions and large disorder. In the case of small disorder, the results of our simulation are certainly influenced by this approximation.

2.2.4 Influence of interactions on the resonance condition

In the previous subsections, we discussed the case of resonant spins. If that is not the case, we neglect the off diagonal terms of the Hamiltonian in Equation (2.6). Beside of the on-site field h_{12}, the interaction due to the term $J_{12}\ S_1^z S_2^z$ remains. This interaction is called J^z interaction and affects the on-site field h_i. By factoring out the operator S_1^z in Equation (2.6), we obtain its prefactor as $-h_1' = -h_1 + J_{12} S_2^z$. Hence, the on-site field h_1 of the first spin is shifted by the interaction $J_{12} S_2^z$ to a new level $h_1' = h_1 - J_{12} S_2^z$. In order to discriminate between h and h', we call h' the *full local field*. The shift $J_{12} S_2^z$ is named J^z contribution of spin 2 on spin 1.

For a system consisting of N spins, we combine all J^z contributions on a particular spin i to the J^z field

$$f_i = -\sum_{j \neq i} J_{ij}\, S_j^z \tag{2.19}$$

of spin i, which emerges from the prefactors of all product operators $S_i^z\, S_j^z$.

Equation (2.19) takes into account all J^z fields, which originate from spin-spin interaction. This modifies the resonance condition (2.8) to

$$|h_{ij} + f_{ij}| < |J_{ij}|. \tag{2.20}$$

The term $f_{ij} = f_i - f_j$ is named J^z field of the pair. The two contributions h_{ij} and f_{ij} to the full local field are different: The distribution of h_{ij} is uniform with width ε, whereas the distribution of f_{ij} is Lorenzian (Section 2.5.2). The J^z field is generated by interaction between spins and does not depend on ε. We analyze its distribution and its effect on the number of resonant pairs in Section 2.5.2.

The resonance condition (2.20) of the spin pair consisting of spins i and j includes the J^z contribution of spin i on j, too. However, in the two-spin Hamiltonian from Equation (2.6), the term S^zS^z is constant and therefore does influence neither the behaviour of the pair nor its resonance condition. Hence, we exclude the contribution of term $J_{ij}S_i^zS_j^z$ from the J^z field. This is achieved by introducing a correction κ, which cancels the contribution of $J_{ij}S_i^zS_j^z$ in condition (2.20). The explicit value of κ is determined in Appendix A.3.8.

As a result of this correction, we obtain the final version of the resonance condition as

$$|h_{ij} + f_{ij} + \kappa| < |J_{ij}|. \tag{2.21}$$

2.3 Interaction of a spin with a resonant spin pair

After studying the spin-spin interaction, we now examine the interaction of a resonant pair and a spin.

Let us consider a system consisting of three spins. Two spins, labeled as 1 and 2, form a resonant pair, whereas the third spin does not belong to a resonant pair. We use the pair operators I_1^α to describe the resonant pair, where $\alpha = x, y, z$. The third spin is represented by operators S_3^α, whereas the interaction between spin and pair is represented by products of these operators.

The transformation of $\mathcal{H}$, given by Eq. (2.1), to the new form is described in Section A.2. We obtain

$$\mathcal{H} = -h_3\, S_3^z - H\, I_1^z + B_{zz}\, I_1^z\, S_3^z + B_{xz}\, I_1^x\, S_3^z, \tag{2.22}$$

where the energy splitting H of the pair is defined in Equation (2.14). Since the truncated dipole Hamiltonian $\mathcal{H}$ does not allow an uneven number of

spins to flip at once, only two coupling terms remain. We use Equation (A.16) to calculate their prefactors as

$$B_{zz} = \frac{h_{12}\, J_{sp}}{H_1} \tag{2.23}$$

$$B_{xz} = \frac{J_{12}\, J_{sp}}{2\, H_1}\,. \tag{2.24}$$

Here,

$$J_{sp} = J_{13} - J_{23} \tag{2.25}$$

represents the spin-pair interaction. Using the general notions from the previous subsection, the contribution of the resonant pair of spin i and j to the J^z field of spin k is obtained as

$$f_k^{\text{pair-spin}} = -B^{zz}_{k,(i,j)} I^z_{(i,j)}, \tag{2.26}$$

where $I^z_{(i,j)}$ has one of the values $\pm 1/2$.

Now, we combine (2.26) with the spin-spin field of Eq. (2.19) to obtain the full expression for the J^z field of spin i as

$$f_i = f_i^{\text{spin-spin}} + f_i^{\text{pair-spin}} = -\sum_{j\neq i} J_{ij}\, S^z_j - \sum_{(k,l)} B^{zz}_{i,(k,l)} I^z_{(k,l)}\,, \tag{2.27}$$

which substitutes f_i in the resonance condition (2.21).

In contrast to the term $B^{zz}\ I^z_1\, S^z_3$, the term $B^{xz}\ I^x_1\, S^z_3$ induces a coupling of both eigenstates of the resonant pair. In the algorithm of Chapter 3, we neglect this term for the simplicity of the model and keep only the diagonal coupling B^{zz} as a contribution to the J^z field of the single spin.

The routine of Chapter 4 already includes the spin-pair interaction as part of the coupling terms of interacting pairs and neglects explicit interaction of pairs and spins completely.

2.3.1 Influence of the resonance state on J^z fields

Equations (2.19) and (2.26) determine different J^z contributions for resonant and non-resonant pairs on a third spin. Therefore, a modification of the resonance state of spin pair (i,j) induces a change of the field it imposes on other spins. We derive this change in the following subsection.

Let us consider the J^z field of the pair (i,j) on spin $r \neq i,j$ for both resonance states. They are defined in Eq. (2.19) and (2.26) as

$$f_{\text{non-res}} = J_{(i,j),r} \tag{2.28}$$

$$f_{\text{res}} = \frac{J_{(i,j),r}\ h_{ij}}{\sqrt{h_{ij}^2 + \frac{1}{4}J_{ij}^2}}\,, \tag{2.29}$$

where $J_{(i,j),r} = J_{ir} - J_{jr}$ is the spin-pair interaction of Equation (2.25), expressed in general notions. The field $f_{\text{non-res}}$ denotes the field, if pair (i,j) is non-resonant, and f_{res} describes the field, if (i,j) is resonant. The difference $f_{\text{non-res}} - f_{\text{res}}$ depends on the ratio of the pair parameter h_{ij} and J_{ij} and is large for $h_{ij} \ll J_{ij}$.

There are two ways to change the field of a spin:

1. Identification of a resonant pair. The field f changes by $f_{\text{res}} - f_{\text{off-res}}$.
2. Destruction of a resonant pair. The field f changes by $-f_{\text{res}} + f_{\text{off-res}}$.

In both cases, the change of field is proportional to $J_{(i,j),r}$. Since $J_{(i,j),r}$ strongly depends on the distances of the spins belonging to the pair to the remote spin ($J \sim r^{-3}$), the change of field is strong only in the direct vicinity of the modified pair. Nonetheless, the interplay between the identification of resonant pairs and J^z fields leads to a dynamics in the full spin system, if the value of the disorder ε is small enough (Chapter 3).

2.4 Investigation of the interaction of pairs

Finally, we consider the interaction of two resonant pairs.

First, we rewrite the Hamiltonian $\mathcal{H}$ of two interacting spin pairs, where we use operators I_1^α to describe the first pair consisting of spins $(1,2)$, and operators I_2^α to describe the second pair consisting of spins $(3,4)$. Similar to the approach of the previous subsection, the Hamiltonian $\mathcal{H}$ is obtained as

$$\mathcal{H} = -H_1\, I_1^z - H_2\, I_2^z + A_{zz}\; I_1^z\, I_2^z + A_{zx}\; I_1^z\, I_2^x + A_{xz}\; I_1^x\, I_2^z + A_{xx}\; I_1^x\, I_2^x, \quad (2.30)$$

where H_i are the energy splittings of the pair defined in Equation (2.14). Using Eq. (A.16), the prefactors of the couplings in Equation (2.30) are calculated as

$$A_{zz} = \frac{h_{12}\, h_{34}\, J_{pp}}{H_1\, H_2} \quad (2.31)$$

$$A_{xz} = \frac{J_{12}\, h_{34}\, J_{pp}}{2\, H_1\, H_2} \quad (2.32)$$

$$A_{zx} = \frac{h_{12}\, J_{34}\, J_{pp}}{2\, H_1\, H_2} \quad (2.33)$$

$$A_{xx} = \frac{J_{12}\, J_{34}\, J_{pp}}{4\, H_1\, H_2}, \quad (2.34)$$

where

$$J_{pp} = (J_{13} - J_{23}) - (J_{14} - J_{24})\,. \quad (2.35)$$

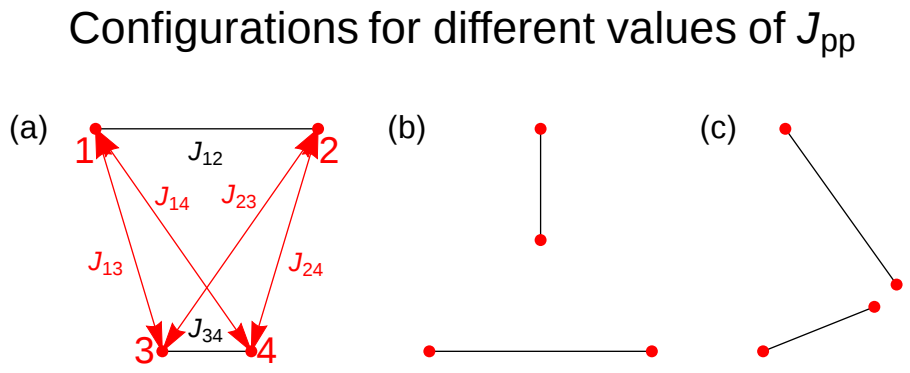

Figure 2.2: Three constellations of two spin pairs. The pair-pair interaction J_{pp} vanishes for configurations (a) and (b). For configuration (c), J_{pp} is large compared to internal interactions.

If the pairs are separated by a large distance, J_{pp} is small compared to the internal couplings J_{12} and J_{34}. In this case, the interaction between the two pairs is negligible. The same is true for a symmetric constellation of the two pairs, as indicated in pictures (a) and (b) of Figure 2.2. On the other hand, if two spins of different pairs are close together (compared to all other distances), the value of J_{pp} is large. This situation is depicted in plot (c) of Figure 2.2.

Similar to the last subsection, the algorithm of Chapter 3 neglects all terms but the J^z interaction $A_{zz}\, I_1^z\, I_2^z$ for simplicity.

In contrast, the algorithm of Chapter 4 takes into account all couplings of the pair-pair Hamiltonian of Equation (2.30). Adding the off diagonal terms significantly affects the resonance condition (2.21).

2.5 Preliminary investigations of the model

In this section, we determine an expression for the number of resonant pairs by determining probability distributions of pair interactions J_{ij}, local fields h_{ij} and J^z fields, which appear in the resonance condition (2.21). To achieve this, we use transformation rules for density functions, which are stated in Appendix A.6.

In the following, we compare the distribution of the isotropic interaction

$$J = \frac{u_0}{r^3} \tag{2.36}$$

to the distribution of the anisotropic interaction from Equation (2.2).

2.5.1 Distribution of the pair interaction J

In order to obtain the distribution of interactions, first, we determine the distribution of the distance r of two spins. For small distances $r < 5$, this distribution is independent of the finite size. The uniform distribution of the spin coordinates yields

$$p_r(r) \sim r^2. \tag{2.37}$$

For $r > 5$, the probability density function $p_r(r)$ deviates from Equation (2.37). In Appendix A.7, a full analytic expression is derived for $p_r(r)$ considering the finite size effect.

The density function is normalized using the condition $\int p_r(r)\mathrm{d}r = 1$. We introduce a cutoff $r_{\max}$ to approximate the finite size effect and obtain

$$p_r(r) = \frac{3}{r_{\max}^3} r^2 \text{ for } r \in [0, r_{\max}]. \tag{2.38}$$

$r_{\max}$ corresponds to a minimum interaction

$$J_{\min} = \frac{u_0}{r_{\max}^3}\,, \tag{2.39}$$

which is used to normalize the probability distribution of the interaction J. By Equation (2.39), the parameter $J_{\min}$ is connected to the size of the system.

Using Equation (A.90), $p_J(J)$ is derived from Equations (2.36), (2.38) as

$$p_J(J) = p_r(r) \left|\frac{\mathrm{d}r}{\mathrm{d}J}\right| = \frac{J_{\min}}{J^2}\,. \tag{2.40}$$

Note, that the integral of $p_J(J)$ is already normalized to 1.

In the further course of this work, we often examine J^{-1} instead of J. In contrast to $p_J(J)$, the probability distribution $p_{J^{-1}}(J^{-1})$ for J^{-1} is constant, which simplifies the analysis of coupling distributions in Chapter 4.

The distribution of J^{-1} is derived as

$$p_{J^{-1}}(J^{-1}) = p_J(J) \left|\frac{\mathrm{d}J}{\mathrm{d}(J^{-1})}\right| = J_{\min}\,, \tag{2.41}$$

where $J^{-1} \in [0, J_{\max}^{-1}]$ and $J_{\max}^{-1} = (J_{\min})^{-1}$.

Figure 2.3 shows the distribution of J^{-1} obtained from the numerical simulation. Pairs satisfying $J^{-1} < 125$ are not influenced by the finite size effect and their coupling distribution obeys Equation (2.41). We fit the numerical

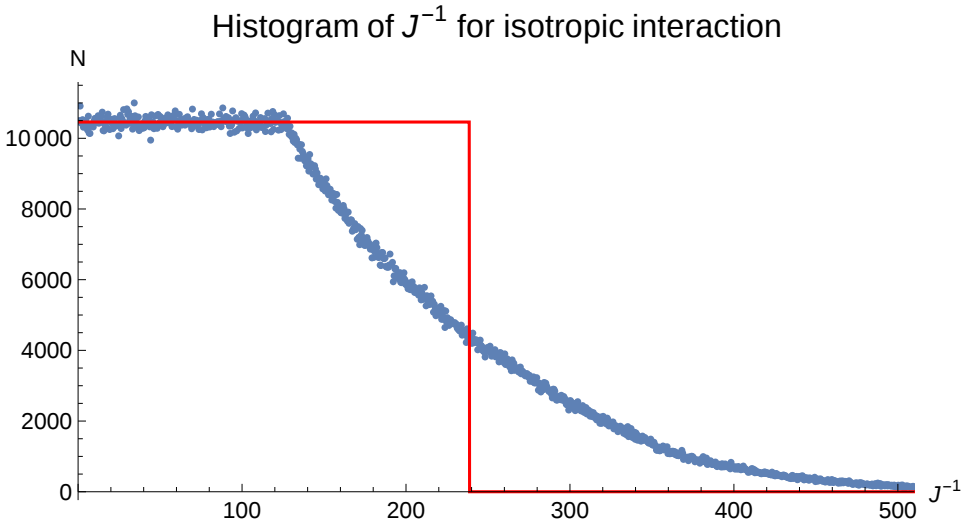

Figure 2.3: Histogram of the values J^{-1} obtained from all spin pairs of 10 different spin systems with isotropic $J = r^{-3}$ interaction between spins. Numerical results are presented by blue dots and the fit from eq. (2.41) by a red line. In summary, $5 \cdot 10^6$ pairs were examined.

data in Fig. 2.3 by a constant distribution and obtain $J_{\min} = 0.0042$, which corresponds to a cutoff value of $r_{\max} = 6.2$. The minimum distance $r_{\min}$ corresponds to a small values $J^{-1} = 1.25 \cdot 10^{-4}$ and does not influence the distribution significantly.

Now, we compare the distribution of the inverse isotropic interaction of Eq. (2.36) to the inverse anisotropic dipole interaction of Eq. (2.2). Figure 2.4 shows a plot of both distributions. Since the isotropic interaction is always positive, whereas the anisotropic interaction can be negative, we use the absolute value to compare both interactions. From fitting numerical data, we obtain $J_{\min} = 0.0032$ for the anisotropic interaction (inset of Figure 2.4).

In summary, the statistics of $p_J(J)$ using anisotropic interaction J has two differences compared to the distribution emerging from isotropic r^{-3} interaction. First, the $\cos(\theta)$ dependence decreases the average magnitude of interaction by a factor of 0.77. Second, since the anisotropic interaction can be arbitrarily small due to the dependence on θ, the values of J^{-1} have no upper limit. As a result of these two effects, the number of pairs, for which the distribution of J^{-1} is constant, is smaller for anisotropic interaction. This fraction is 52% for isotropic interaction and 20% for anisotropic interaction.

On the other hand, both interactions can be approximated well by $p_J(J) \sim$

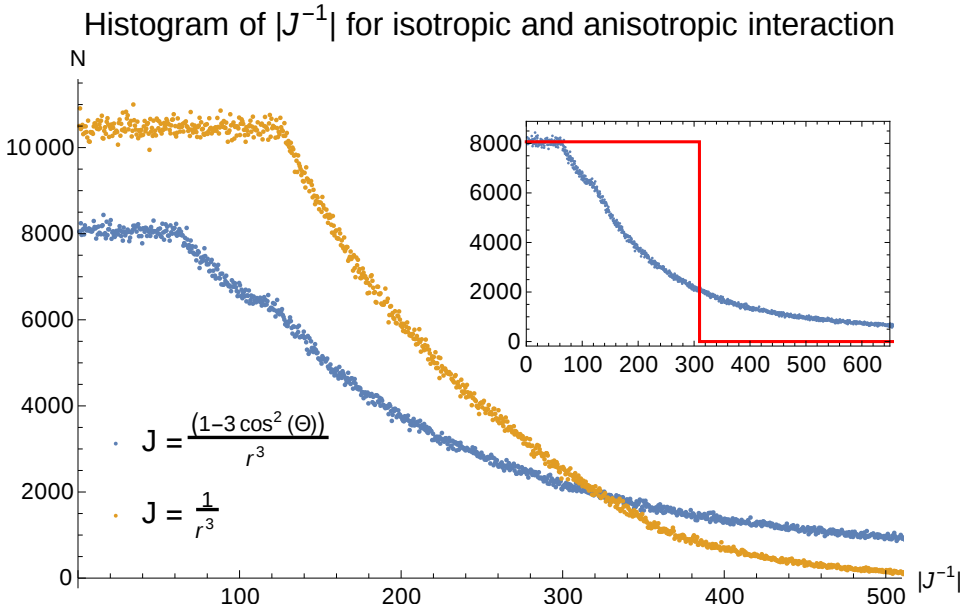

Figure 2.4: Histogram of the absolute values $|J^{-1}|$ for isotropic r^{-3} interaction from Equation (2.36) (yellow dots) and anisotropic dipole interaction from Equation (2.2) (blue dots) between spins. In summary, $5 \cdot 10^6$ pairs were examined. The inset shows the cutoff approximation for anisotropic interaction (blue dots) with $p_J(J) = const.$ (red line).

J^{-2} with a cutoff at $J_{\min}$. The value of this parameter differs for both interactions. The ratio of the two values is used as a correction to compare analytical estimates taking into account isotropic interaction to numerical results using the anisotropic interaction.

2.5.2 Distribution of the local fields h_{ij} and the J^z fields f_i

The distribution of local pair fields h_{ij} is derived from the uniform distribution of local spin fields $h_i \in [0, \varepsilon]$. Since we never use the distribution of local spin fields explicitly, we denote the distribution of local pair fields as $p_h(h_{ij})$. This distribution is determined as

$$p_{\mathrm{h}}(h_{ij}) = \frac{1}{\varepsilon^2}(\varepsilon - |h_{ij}|), \tag{2.42}$$

which is valid for $h_{ij} \in [-\varepsilon, \varepsilon]$.

As a next step, we consider the distribution of J^z fields between spins. Here, we need both the distribution of J^z fields f_i on spins and the distribution of J^z fields $f_{ij} = f_i - f_j$ on pairs. We denote the first by $p_f(f_i)$, whereas the

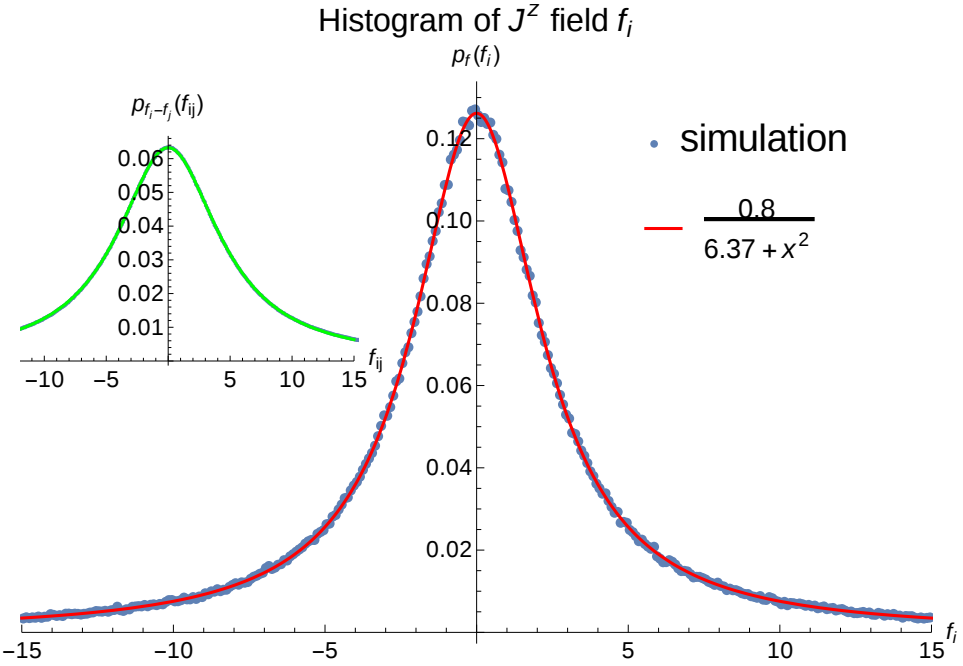

Figure 2.5: Plot of the distribution of J^z fields f_i (main plot). Numerical data is presented as blue dots (both inset and main plot). The inset shows the distribution of the variable $f_{ij} = f_i - f_j$.

pair fields are represented by the distribution function $p_{f_i - f_j}(f_{ij})$.

Anderson derived [1], that the distribution $p_f(f_i)$ has the shape of a Lorenzian function

$$p_f(f_i) = \frac{a}{b + f_i^2}. \tag{2.43}$$

As presented in Figure 2.5, this fits well with numerical data of our simulation. We obtain $a = 0.8$ and $b = 6.37$. The minimum radius $r_{\min}$ corresponds to $f_i = 4000$ and does not influence the probability distribution p_f significantly.

As a next step, we use this distribution to determine the distribution of f_{ij}. The convolution of the Lorenzian from Equation (2.43) with itself gives another Lorenzian

$$p_{f_i - f_j}(f_{ij}) = \frac{2\pi a^2}{\sqrt{b}} \cdot \frac{1}{4b + f_{ij}^2}. \tag{2.44}$$

This result is confirmed by numerical data for f_{ij} (see inset of Figure 2.5).

Finally, we determine the distribution $p_{h'}$ of full local fields h'_{ij} as another

convolution of $p_{f_i - f_j}$ (Eq. (2.44)) and p_h (Eq. (2.42)). We obtain

$$\begin{aligned} p_{h'}(x) &= \frac{0.8}{\varepsilon^2}\Big[2\log\left(25+x^2\right) - \log\left(25+(\varepsilon+|x|)^2\right) \\ &- \log\left(25+(\varepsilon-|x|)^2\right) - 0.8x\arctan(0.2\cdot|x|) \\ &+ 0.4\,(\varepsilon-|x|)\arctan(0.2\cdot(\varepsilon-|x|)) + 0.4\,(\varepsilon+|x|)\arctan(0.2\cdot(\varepsilon+|x|))\Big]\,, \end{aligned}$$

where ε denotes the value of the energy disorder and x the value of h'_{ij}. In Figure 2.6, the distribution $p_{|h'|}(x)$ of the absolute value $|h'_{ij}|$ is compared with numerical data of the simulation for a disorder $\varepsilon = 50$. Additionally, the figure takes into account two approximations based on Equation (2.42), namely: The direct implementation of Equation (2.42) using $\varepsilon = 50$ (red line), and an implementation of Equation (2.42) using a fitted value of the disorder $\varepsilon \approx 58$ (green line). The first approximation is equivalent to neglecting the presence of J^z fields and using the probability distribution p_h of the on-site fields h_{ij}.

The deviation ε_f of the fitted disorder from the disorder of the system is presented in the inset of Figure 2.6.

From Figure 2.6, we deduce the following statements:

First, the function $p_{|h'|}(x)$ is in a perfect agreement with numerical data.

Second, both approximations work well for $0 \ll h'_{ij} \ll \varepsilon$, but not for small or large values of the full local field h'_{ij}.

At large values $h'_{ij} \approx \varepsilon$, the distribution $p_{h'_{ij}}$ has a tail, which p_h has not. This tail is not influenced by the disorder value, but originates from the presence of J^z fields. Hence, even for a system with zero disorder in energy, there is a certain probability, that a spin has a large value of the full local field h'_{ij}. This effect is important for the analysis in Chapter 4.

The deviation of the distributions $p_{h'}$ and p_h for small values h'_{ij} influences the number of resonant pairs (see Figure 2.7). Hence, we expect, that the number of resonant pairs decreases significantly, when we substitute p_h by $p_{h'}$.

2.5.3 Obtaining the number of resonant pairs

In the following, we derive the number of resonant pairs without the consideration of J^z fields. First, we use the probability distributions p_h and p_J to derive the probability distribution of the resonance range S_{ij} in Appendix

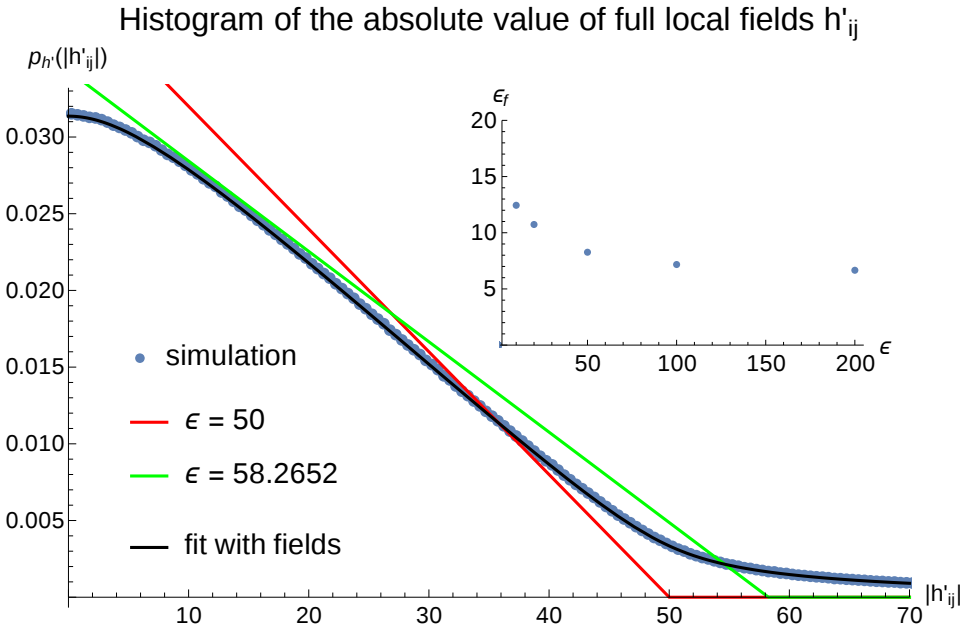

Figure 2.6: Histogram of the full local fields h'_{ij} for all spin pairs of a spin system where $\varepsilon = 50$ (blue dots) including spin-spin fields. We used 100 different starting configurations, which result in $5 \cdot 10^7$ examined spin pairs. The histogram was normalized to compare it to the analytical expression (red for $\varepsilon = 50$ and green for $\varepsilon = 58.2652$, which corresponds to $\varepsilon_f = 8.2652$) for $p_h(h_{ij})$ from Equation (2.42). The inset shows the deviation ε_f of the fitted disorder value from the disorder of the system.

A.3.5. In Appendix A.3.6, this probability distribution yields the probability

$$P_{\mathrm{RP}} = \frac{J_{\mathrm{min}}^2}{\varepsilon^2} + \frac{2J_{\mathrm{min}}}{\varepsilon} \ln\left(\frac{\varepsilon}{J_{\mathrm{min}}}\right), \tag{2.45}$$

that a pair is resonant. Equation (2.45) agrees with the widely-used formula (2.12) (see Appendix A.3.6).

We convert this result to the average number of resonant pairs N_{RP} via

$$N_{\mathrm{RP}} = \frac{1}{2} N_{\mathrm{Pairs}} \cdot P_{\mathrm{RP}}, \tag{2.46}$$

where we obtain the factor $\frac{1}{2}$ from excluding pairs of state $|\uparrow\uparrow\rangle$ or $|\downarrow\downarrow\rangle$.

As described in Section 2.2, the simulation does not allow a spin to participate in more than one resonant pair at the same time. This effect is not included in Equation (2.46). In order to compare the results of the simulation with Equation (2.46), we introduce the variable N_{RC}. N_{RC} denotes

the number of resonance conditions, that are evaluated as true. By using different initial configurations, we obtain a distribution of N_{RC} values with mean μ_{RC}. Such a distribution is presented in the inset of Figure C.1 of Appendix C. Additionally, this figure shows a perfect agreement of analytical prediction and numerical results for the dependence of the average number of resonant pairs μ_{RC} on ε. This confirms the cutoff approximation done of the finite size effect.

Whereas the last paragraph determined the number of resonant pairs without J^z fields, we now use a routine including spin-spin fields and the anisotropic dipole interaction. We present the results in Figure 2.7. It shows a good agreement of data from the simulation and the number of resonant pair with J^z fields, which was determined using the convolution of $p_{h'}$ and p_J. The figure indicates, that the effect of J^z fields is important for small disorder values, whereas for large disorder the fits with and without J^z fields coincide.

We conclude, that Equation (2.12), which is widely used in literature, does not give accurate results for a system with J^z fields between spins.

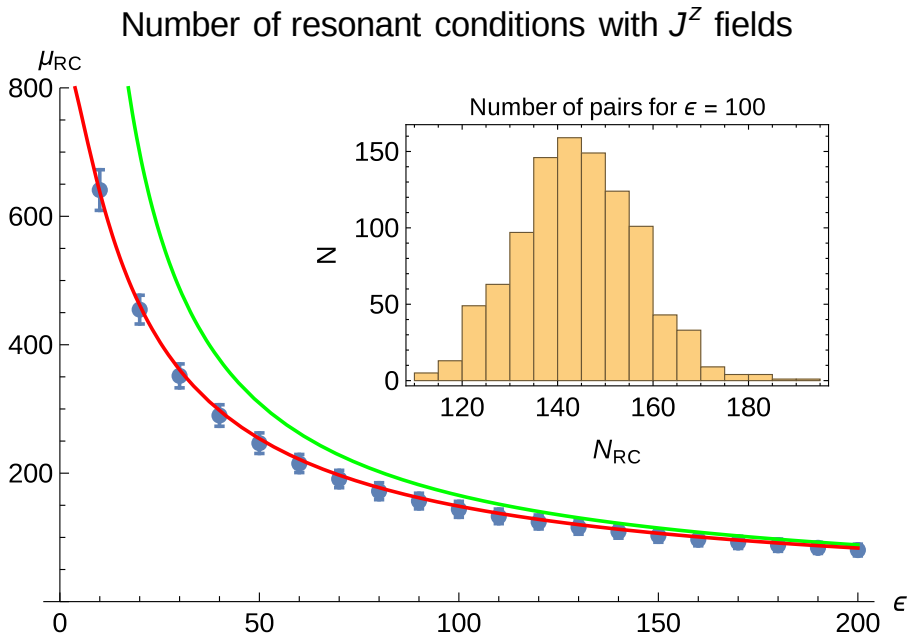

Figure 2.7: The main plot shows the dependence of the average number μ_{RC} of resonant conditions on the disorder ε using dipole interaction and spin-spin fields. For each disorder value, 1000 different initial configurations of the spin system were examined. The mean values μ_{RC} of the resulting distributions of N_{RC} are indicated by blue dots, the standard derivation by an error bar. The distribution of N_{RC} for $\varepsilon = 100$ is presented as inset. The green curve represents the analytical prediction (Eq. (2.46)) neglecting J^z fields, and the red curve uses the density function $p_{h'}(h'_{ij})$ of the full local fields.

Chapter 3

Time evolution

In this chapter, we describe and implement an algorithm imitating the time evolution of disordered TLSs with dipolar interactions. The algorithm simulates the time evolution rather crudely: namely it focuses only on creation and destruction of resonant spin pairs. A more accurate dynamical simulation is impractical even classically, because the problem involves multiple time scales. We still expect that this simulation captures the essential aspects of the energy transport in the system.

3.1 Conceptual description of the time evolution algorithm

As discussed in Section 2.3.1, the resonance state of a pair influences the field, which it imposes on other spins. On the other hand, the resonance condition (2.21) of this pair, and thus its resonance state, depends on the J^z field itself. These two relations make it possible to obtain a crude time evolution of the system, which is generated by the interplay of fields and the resonance state of pairs of the spin system.

This mechanism is implemented as follows: First, the time axis is discretized using time steps, where the i^{th} time step describes the time evolution from t_i to $t_{i+1} = t_i + \Delta t$.

In each time step, we consecutively apply the following two intermediate steps on each spin pair:

1. The algorithm checks, whether the resonance condition (2.21) is satisfied and identifies, if the resonance state of the pair changed.

2. If it changed, the routine recalculates the J^z contribution of the pair on other spins. This recalculation is delayed by the delay time t_d, which is determined individually for this pair from Eq. (2.18).

All pairs are organized in a list, which is sequenced in descending order with respect to the absolute value of the pair interaction. We present a detailed description of the algorithm in Appendix B.2.

The recalculation of J^z contributions changes the resonance condition of all spin pairs. Therefore, the next time step can produce a different distribution of resonant pairs in the system, which again causes a modification of the J^z fields. By performing many time steps, the system evolves and the simulation monitors properties of spins and pairs. Since a spin pair can flip from state $|\uparrow\downarrow\rangle$ to $|\downarrow\uparrow\rangle$ by undergoing two consecutive changes of its resonance state, the polarization S^z of individual spins changes in the course of the time evolution.

3.2 Results

The evolution of the full system depends strongly on the value of the disorder ε. If ε is large, the number of resonant pairs is small and likewise are thes change of J^z fields after identifying all pairs.

On the other hand, a system with small disorder value ε does incorporate a large number of resonant pairs. Then, each time step results in a large change of fields and this greatly changes the distribution of resonant pairs for the next time step.

If we increase the disorder from very small to large values, we expect a transition from a system with fast dynamics to a system with slow dynamics.

3.2.1 Correlation function of interest

In order to investigate and to quantize the dynamics of the system, we examine the decay of the correlation of the system at time t to its initial configuration. This correlation is described by the *correlation function*

$$C_{\text{spins}}(t) = \langle 4 \sum_{i=1}^{N_{\text{Spins}}} S_i^z(t)\ S_i^z(0) \rangle\,, \tag{3.1}$$

where $S_i^z(t)$ is the z projection of spin i at time t and the bracket $\langle\rangle$ denotes the average over many initial conditions. The prefactor 4 normalizes the correlation function to a maximum value of

$$C_{\text{spins}}(0) = 4 \sum_{i=1}^{N_{\text{Spins}}} \frac{1}{4} = N_{\text{Spins}}\,.$$

In contrast, for a completely uncorrelated system, half of the spins have the same polarization as in the initial configuration, which results in $C(t) = 0$.

Equation (3.1) includes all spins, which are not part of a resonant pair. Since the wave function of a resonant pair is defined in the diagonal basis $\psi \in \{|\Uparrow\rangle, |\Downarrow\rangle\}$, the calculation of the correlation function for spins belonging to a resonant pair differs from Equation (3.1).

We use the Heisenberg representation to pass the time dependence from the wave function to the operators as

$$\langle\psi(t)|S_z(0)S_z(t)|\psi(t)\rangle = \langle\psi(0)|e^{i\mathcal{H}t}S_z e^{-i\mathcal{H}t}S_z|\psi(0)\rangle = e^{i(\lambda_1-\lambda_2)t}\,, \qquad (3.2)$$

where λ_i are the eigenvalues of the resonant pair. We define the initial time $t = t_0$ at the time of the identification of the resonant pair and reduce the result of Eq. (3.2) to its real part. Since a pair substitutes two spins in Equation (3.1), we include a factor of 2 and obtain

$$C_{\text{pair}}(t) = 2\cos\left(H_{(i,j)}(t - t_0)\right) \qquad (3.3)$$

as the contribution of the resonant pairs (i, j) to the total correlation function $C(t) = C_{\text{spins}} + C_{\text{pairs}}$.

We are interested in the following properties of the function $C(t)$:

- Does $C(t)$ decay to 0 for long times or does it saturate at some level $c > 0$?
- How fast does $C(t)$ change and what is its functional dependence on t?
- How does the function $C(t)$ depend on disorder?

In the following, we address these questions.

3.2.2 Summary of main results

For a large range of disorder and long times, the value of $C(t)$ decreases to a finite saturation value of 5% of its maximum. This indicates, that about 95% of the system is delocalized, even though much less spins belong to a resonant pair at the same time. Therefore, the delocalization is caused by the interaction between pairs and the resulting fluctuation of the distribution of resonant pairs.

We found, that long time behaviour of the correlation function $C(t)$ can be described by a stretched exponential function

$$f(t) = (1000 - c) \cdot e^{-(b\cdot t)^d} + c\,, \qquad (3.4)$$

which fits many relaxation processes in disordered media [19]. The parameter b, c and d depend smoothly on the value of disorder ε. Of particular interest is the behaviour of the finite saturation value, represented by the offset parameter c.

This offset is a measure for the number of spins, that do not take part in the dynamics of the system. We denote these spins as isolated spins. In the range $0 < \varepsilon < 150$, the value of c, and thus the number of isolated spins, is independent of the disorder. Hence, there is always a part of the system, that is localized with respect to spin diffusion and energy transport. The isolation of the spins is not caused by a large value of the local field h_i, but by a large value of the J^z field imposed on the spins. This claim is discussed in Section 3.2.4 and explains the independence of the number of isolated spins on the value of disorder ε.

Additionally, pairs with large interactions are isolated from the dynamics as well. We denote these pairs as isolated pairs.

If we add the number of isolated spins and the number of spins, that are part of an isolated resonant pair, we obtain a large fraction of the spin system. The remaining spins are involved in resonant pairs, which change their resonance due to the fluctuation of fields. We denote these pairs as fluctuating pairs. These spins are responsible for the long time decay of the correlation function. We analyze the properties of fluctuating pairs in detail.

3.2.3 General shape of the correlation function

In this subsection, we examine the time dependence of $C(t)$, which was defined in 3.2.1. A plot of $C(t)$ is presented in Figure 3.1. The fast decrease of $C(t)$ at small times is caused by resonant pairs with large interactions. Their contribution to $C(t)$ is described by a cosine function (Equation (3.3)), which has a different period for each pair. After a short time of the order of these periods, the sum of all these contributions averages to 0.

We resolve this effect in Figure 3.4, which shows $C(t)$ for three different time scales: $t \in [0, 2]$, $t \in [0, 50]$ and $t \in [0, 500]$. From this resolution, we estimate the delay times of strong resonant pairs as $0.01 \ldots 1$.

After the initial jump, we use the stretched exponential from Equation (3.4) as a fit for the long time behaviour of $C(t)$. Figure 3.1 shows a linear plot of $C(t)$ and $f(t)$ for $\varepsilon = 0$, where the fit is indicated as a green line. A logarithmic and a double-logarithmic plot of $C(t)$ for $\varepsilon = 0, 30, 90, 150$ is presented in Figure 3.5. More linear plots for medium ($t < 2000$) and large times ($t \in [0, 50000]$) are shown in Figure C.3 in Appendix C.

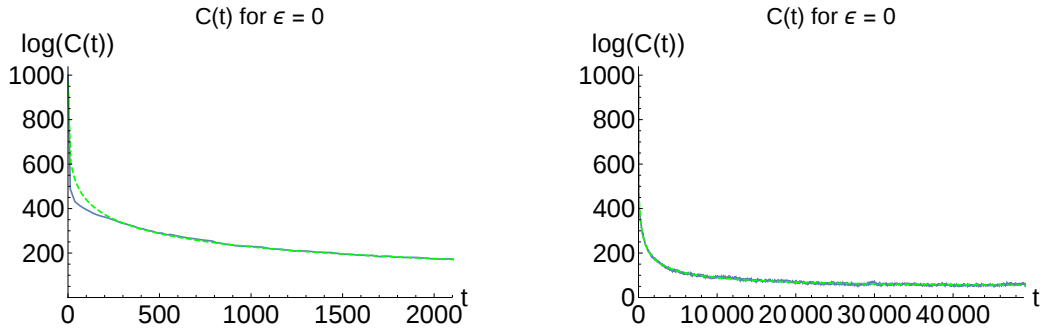

Figure 3.1: Linear plots of the correlation function $C(t)$ for disorder $\varepsilon = 0$. We present one plot for times $t \in [0, 2000]$ and one plot for $t \in [0, 50000]$, thereby we averaged over about 35 different initial configurations of spins. The blue dots indicate the data obtained from the simulation whereas the green line is a stretched exponential function as defined in (3.4). Similar plots for disorder $\varepsilon = 10, 80, 150$ are presented in Figure C.3 in the appendix. We resolve the initial behaviour in Figure 3.4.

The fit (3.4) does not agree with $C(t)$ for short times $t < 200$ (Figure 3.1). On this time scale, the dynamics of the system is still dominated by the initial identification of resonant pairs. For longer times $t \gg 200$, the fit works very well.

Dependence of the shape of $C(t)$ on the disorder

Figure 3.2 shows the correlation function for several different disorder values $\varepsilon < 200$. In this range, $C(t)$ decreases to about 5% of its initial value.

If we increase the disorder beyond $\varepsilon = 200$, the saturation value increases significantly (Figure 3.3). This effect is investigated using the parameter c from Equation (3.4), which describes the finite saturation level. Figure 3.6 shows a plot of c over the disorder value ε. We see a clear separation of three different phases:

- $c \approx 50$ for $\varepsilon < 150$.
- a crossover region for $\varepsilon \in [150, 700]$.
- $c \approx 950$ for $\varepsilon > 700$.

The third region ($\varepsilon > 700$) features a small number of resonant pairs. Hence, there is a small probability for a significant change in the J^z field of spins and we obtain only a small fluctuation of the distribution of resonant pairs in the system. As a result, nearly all spins of the system are frozen in their

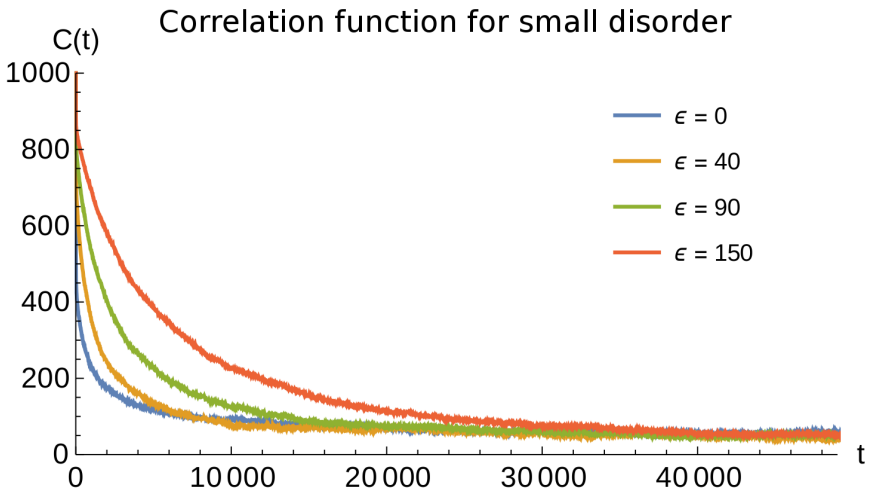

Figure 3.2: Plot of the correlation function $C(t)$ for long times and small disorder $\varepsilon < 200$. We averaged over about 35 different initial configurations of spins.

initial state and the system is localized.

In this regime, the finite size of the system is very important. For larger sizes, there are more resonant partners available for every spin. As shown in the introduction, the probability of finding a resonant partner increases as $\log(R)$, where R is a measure for the size of the system. We expect that the marginal ε values of the transitions depend on the probability of finding a resonant partner and therefore scale with $log(R)$. For large systems, we expect this localized phase to appear at very large disorder, which might be out of an experimentally achievable range.

The crossover regime features some dynamics in the system, but depending on the value of ε, only a fraction of the system participates in this dynamics. This regime corresponds to the localization-delocalization transition of the system.

Last, we consider the regime of small disorder $\varepsilon < 150$. Here, the correlation function decreases to a small value. This indicates, that a large part of the system is delocalized. Note, that for the marginal case $\varepsilon = 150$, only 20% of all spins are part of a resonant pair at the same time step. However, the fluctuation of the distribution of these pairs involves about 95% of all spins and thereby causes a decrease of $C(t)$ to 5%. We discuss the properties of these pairs further in Subsection 3.2.4.

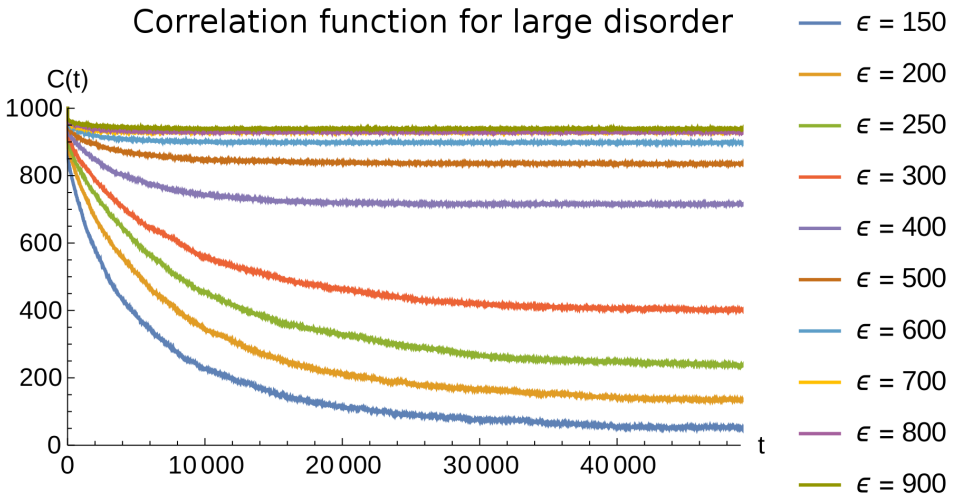

Figure 3.3: Plot of the correlation function $C(t)$ for long times and large disorder $\varepsilon > 200$. We averaged over about 35 different initial configurations of spins.

In contrast to our expectation, the correlation function $C(t)$ does not drop to zero, but remains at a level of $c = 50$ even for long times (figure 3.2). This finite level is independent of the disorder ε. Both claims are supported additionally by Figure 3.5.

We discuss the finite saturation in more detail in Subsection 3.2.4. In contrast to the behaviour of the saturation value, the general shape of $C(t)$, or more specific the parameter b and d, always depend on the value of disorder ε. The dependence of b and d on the disorder ε is shown in Figure 3.6. These dependencies change the decay of $C(t)$ in opposite ways: For increasing value of ε, d increases and leads to a faster decay, whereas the value of b decreases and therefore slows the decay.

We also chose another approach to investigate the speed of the decay: We fix the time t to a constant value t_c and plot the value of the correlation function $C(t_c)$ as a function of ε. A plot for several choices of t_c can be seen in Figure 3.7. For large values of t_c, the dependence of $C(t_c)$ on ε is similar to the dependence of the offset parameter c in Figure 3.6, namely, $C(t_c)$ is independent of ε for small disorder values. On the contrary, $C(t_c)$ depends strongly on ε for small values of t_c. The latter effect is explained by the fact, that the magnitude of the initial jump is proportional to the number of initially identified resonant pairs. As derived in Section 2.5.3, this number depends on ε as $1/\varepsilon$.

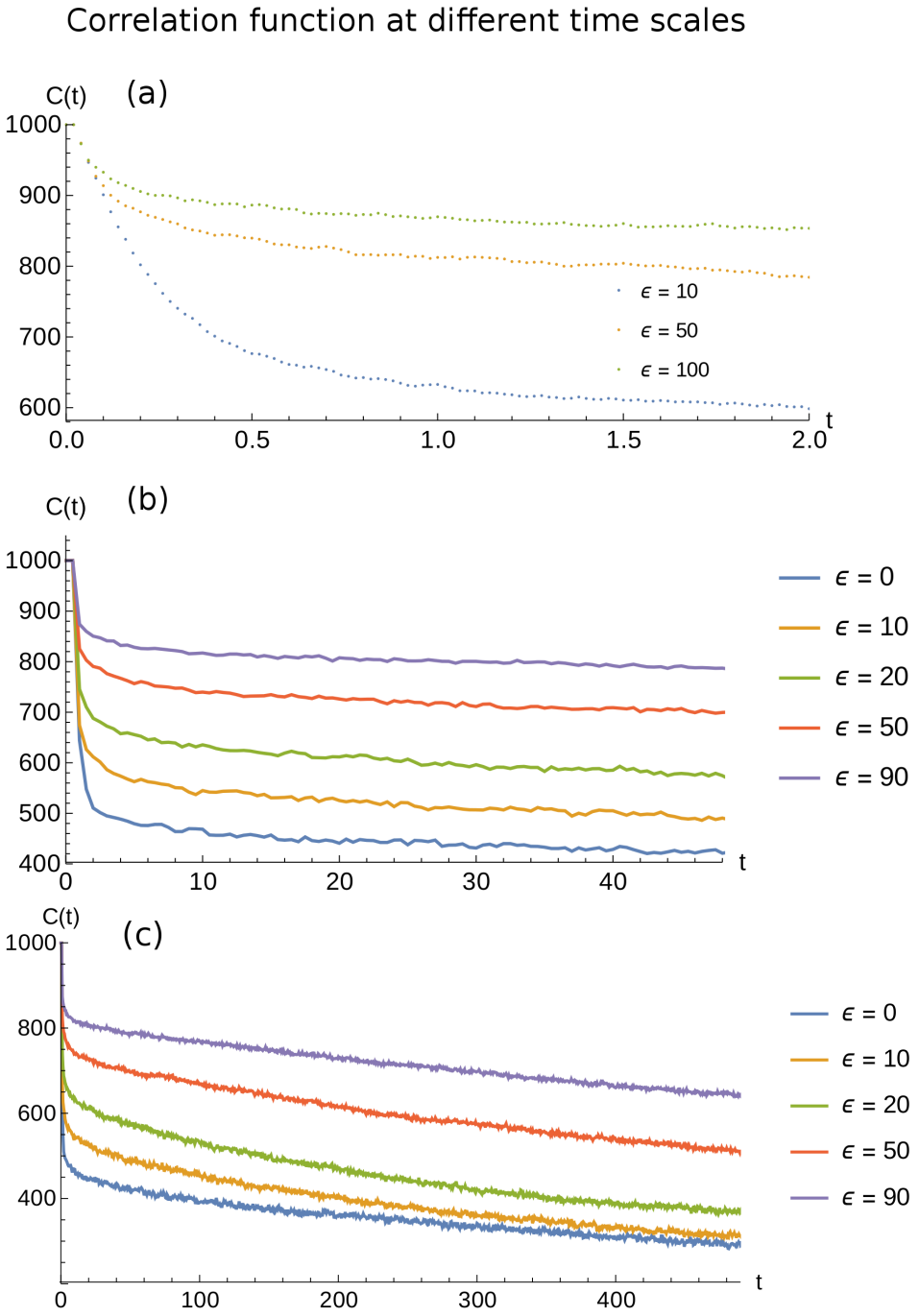

Figure 3.4: Plot of the correlation function $C(t)$ for several disorder values and three different time scales: $t \in [0, 2]$ (a), $t \in [0, 50]$ (b) and $t \in [0, 500]$ (c). In order to resolve small times, we decreased the time increment to $\Delta t = 0.02$ for plot (a). The remaining two plots were generated using the standard time increment $\Delta t = 0.5$.

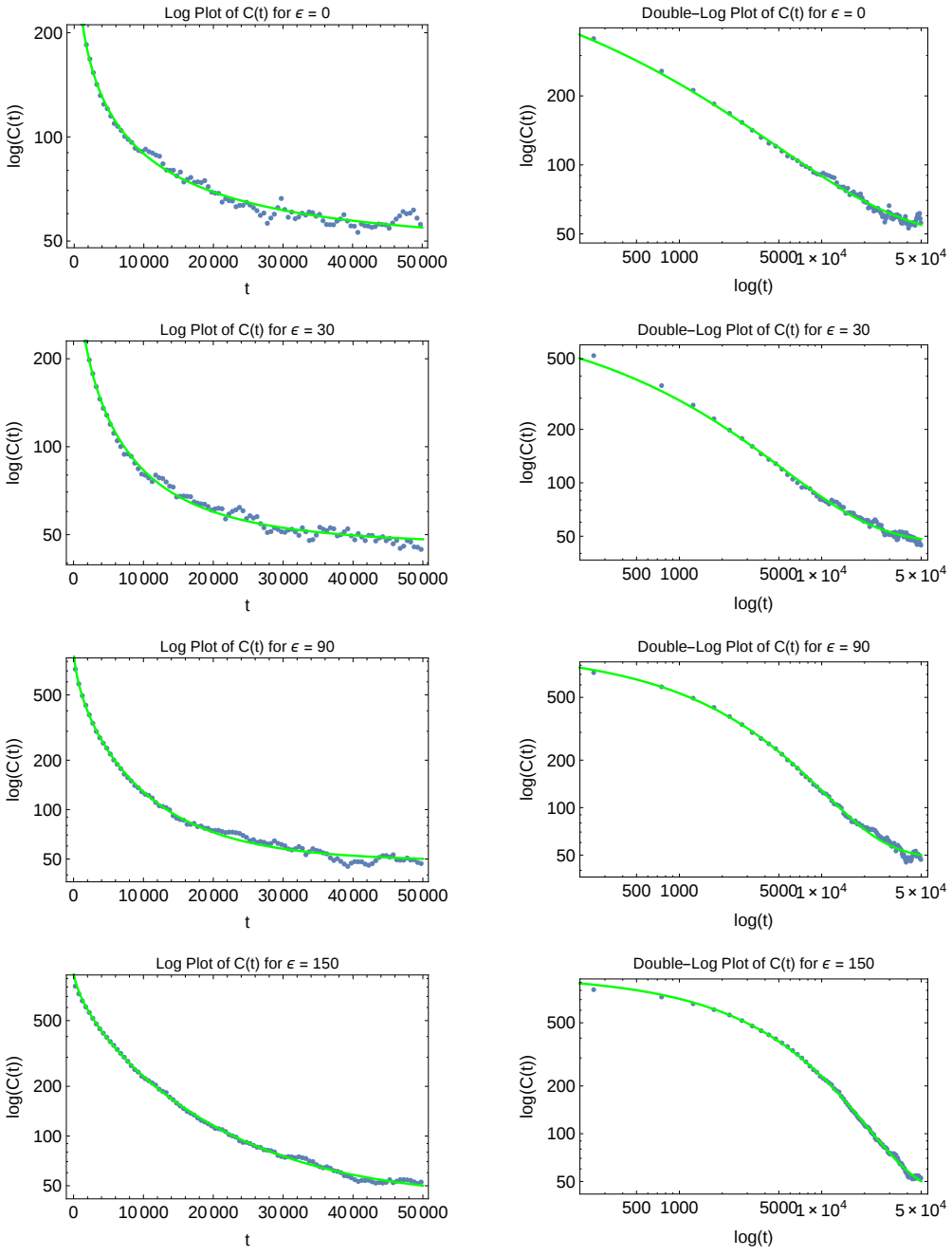

Figure 3.5: Collection of logarithmic plots of the correlation function $C(t)$ for disorder values $\varepsilon = 0, 30, 90, 150$ and a time increment $\Delta t = 0.5$ for long times. We averaged over about 35 different initial configurations of spins. The blue dots indicate the data obtained from the simulation whereas the green line is a stretched exponential function as defined in (3.4). A similar collection for large disorder value can be found in Figure C.4 in the appendix.

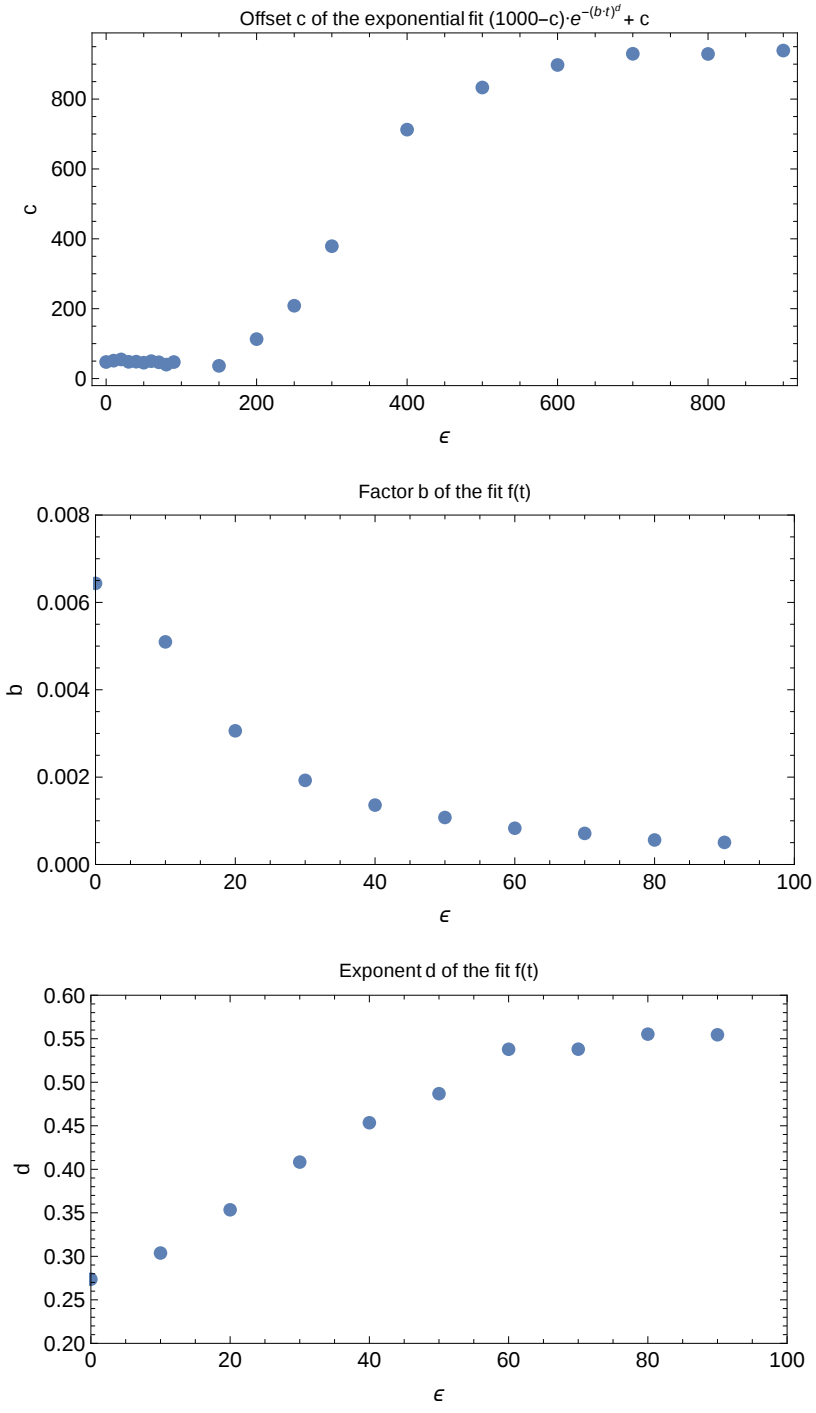

Figure 3.6: Plot of the parameter of the fit $f(t) = (1000 - c) \cdot e^{-(b \cdot t)^d} + c$ over the value of disorder ε. We used $\Delta t = 0.5$ and averaged over 35 initial configurations.

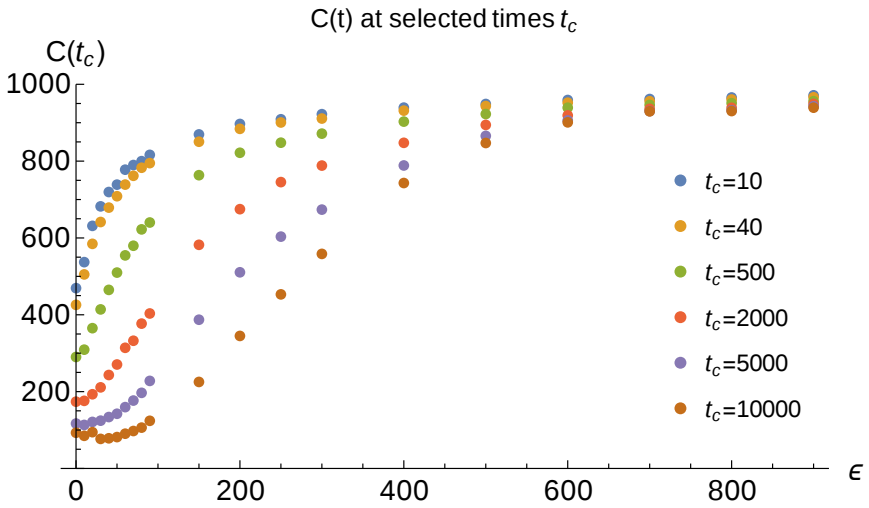

Figure 3.7: Mean number of fluctuating pairs at $t = 50000$ for varying disorder value ε.

For further analysis of the decay rate, we examined the half time $t_{1/2}$, which is defined as the time the correlation function $C(t)$ needs, to drop to half of its initial value $C(t_0)$. We define the initial time as $t_0 = 10$, to exclude the initial drop caused by the identification of strong pairs. Additionally, we subtract the value of the offset c for both values. Hence, the half time $t_{1/2}$ is defined by the equation

$$C(t_{1/2}) - c = \frac{1}{2}\left(C(10) - c\right) . \tag{3.5}$$

Figure 3.8 compares $t_{1/2}$ with the time scale $1/b$ from fit (3.4). In this figure, we observe a smooth increase of $t_{1/2}$ and $1/b$ for $\varepsilon \in [20, 150]$. For $\varepsilon \in [0, 20]$, the half time $t_{1/2}$ has a minimum at $\varepsilon \approx 10$ and increases for smaller disorder values. The time scale $1/b$ has no minimum, but changes its slope.

Investigation of small disorder values

As a final part of this subsection, we investigate the decay of $C(t)$ for small disorder values. Figure 3.8 indicates a maximum for the decay rate around $\varepsilon \approx 10$. We resolve this behaviour in Figure 3.9. The half time $t_{1/2}$ has a minimum in $\varepsilon \in [10, 15]$. Figures C.5 and C.6 in Appendix C show plots of the correlation function $C(t)$ for these disorder values. The initial behaviour ($t < 10000$) differs, but then it is not possible to discriminate between functions with different disorder values.

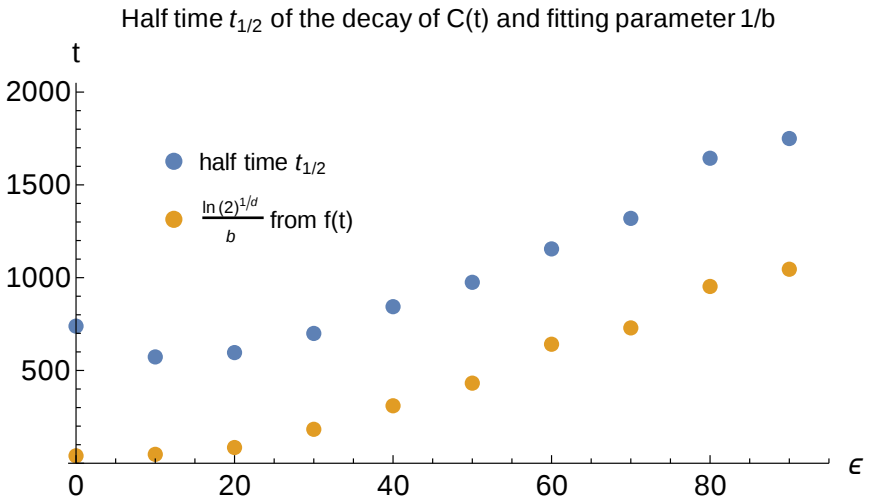

Figure 3.8: Half time for varying disorder value ε.

3.2.4 Further investigations

In the last section, we examined the decay of the correlation function. We found, that the decay has a finite saturation level in the range $\varepsilon \in [0, 150]$. Next, we discuss implications of this finite saturation level. Then, we examine the existence time of resonant pairs to explain the decay of $C(t)$ for long times.

Isolated spins

The finite saturation of $C(t)$ corresponds to the existence of a small part of the spin system, which is not affected by the dynamics. Figures C.11 and C.10 in Appendix C investigate the number of spins, that are never part of a resonant pair. We call these spins *isolated spins* and denote their number as N_{isolated}. Figure C.11 shows the time dependence of N_{isolated}, whereas Figure C.10 examines the value of N_{isolated} at the longest available time $t = 50000$ in dependence of disorder. The last plot shows the same characteristics as Figure 3.6. However, the saturation level c of $C(t)$ is considerably larger than the number of isolated spins N_{isolated}.

We believe, that next to fully isolated spins, there is a set of nearly isolated spins. While these spins can become part of a resonant pair, these pairs are separated by a long distance and therefore have a long delay time. Typically, pairs of this kind are destroyed long before their delay time is reached. As a result, the flipping probability for nearly isolated spins is very small and they keep their correlation to the initial configuration. Figure C.12 in Appendix C investigates this statement by examining all spins, that did not

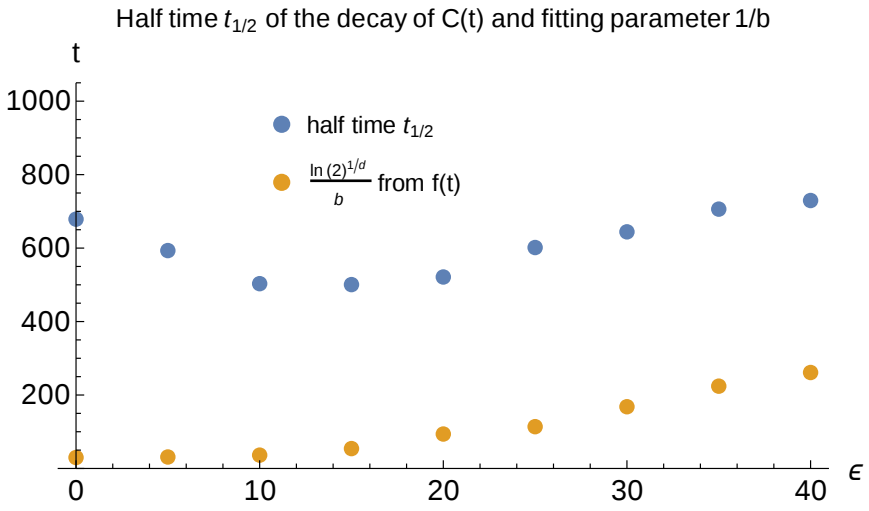

Figure 3.9: Half time for varying disorder value ε.

flip at $t = 50000$. It shows a histogram of the number of time steps, which these pairs have been part of a resonant pair. Next to fully isolated spins, there are many spins which flipped only a small number of times.

The most important property of the finite saturation value is its independence of disorder. Figures C.11 and C.6 indicate, that the long time dynamics of the system is independent of ε for a large range of disorder values. In the following, we investigate the distribution of J^z fields to explain this effect.

The J^z fields imposed on spins are distributed as a Lorenzian function with a maximum value at $f = 0$ and a width of 2.5 (see Figure 2.5). As a result, there exist some spins i with very large J^z field f_i. This leads to a large value of the full local field $h_i' = h_i + f_i$. For small disorder values, the contribution of the on-site field h_i to the full local field h_i' can be neglected. Therefore, the number of isolated spins is independent of disorder for a certain range of small disorder values.

In order to test this explanation, we examine the value of the field for spins which remain isolated from the dynamics for long times ($t = 50000$). The histogram of fields for these spins is presented in Figure 3.10. As one can see, this distribution differs much from the original Lorenzian (figure 2.5) and has maxima around $f \approx \pm 100$. This indicates, that isolated spins typically have very large J^z fields.

Since the J^z field is generated by interaction between spins and pairs, a large

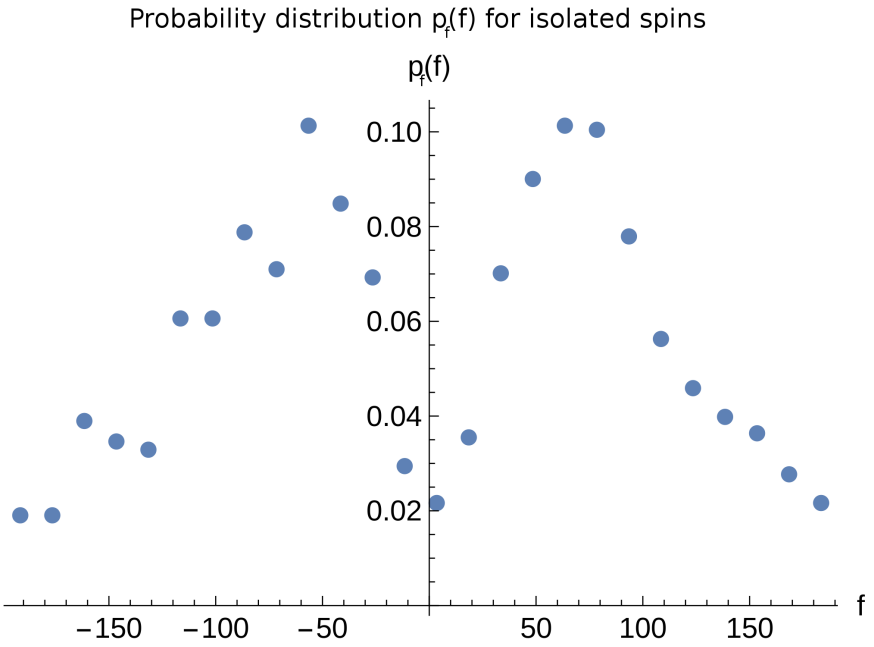

Figure 3.10: Histogram of field values for spins that are isolated from the dynamics of the system ($\varepsilon = 0$). The distribution is very different from the histogram of f for all spins (figure 2.5). We obtained the histogram by simulating 77 different initial configurations with $\varepsilon = 0$ for $t = 50000$. The averaged correlation function $C(t)$ for these parameter is shown in Figure C.5 in Appendix C.

J^z field on one spin is related with a nearby spin that has a large J^z contribution to this spin. If the two spins do not have the same S^z polarization, they form a resonant pair with large interaction. Otherwise, the strong field suppresses the probability for both spins to find a resonant partner. These spins remain isolated and form a non-resonant isolated pair.

We conclude, that even for zero disorder, a part of the spin system remains isolated. The size of this isolated region does not depend on the disorder for $\varepsilon < 150$. From $\varepsilon \approx 150$, the number of isolated spins grows for increasing value of ε. At about $\varepsilon \approx 700$, only few spins ($< 5\%$) take part in the dynamics.

We are aware that the absolute and relative size of the isolated region depends on the size of the system. However, since pairs with a small interaction and small local field have very long delay times and typically are destroyed before they lead to dynamics, we believe that the dependence of this effect on the finite size is weak.

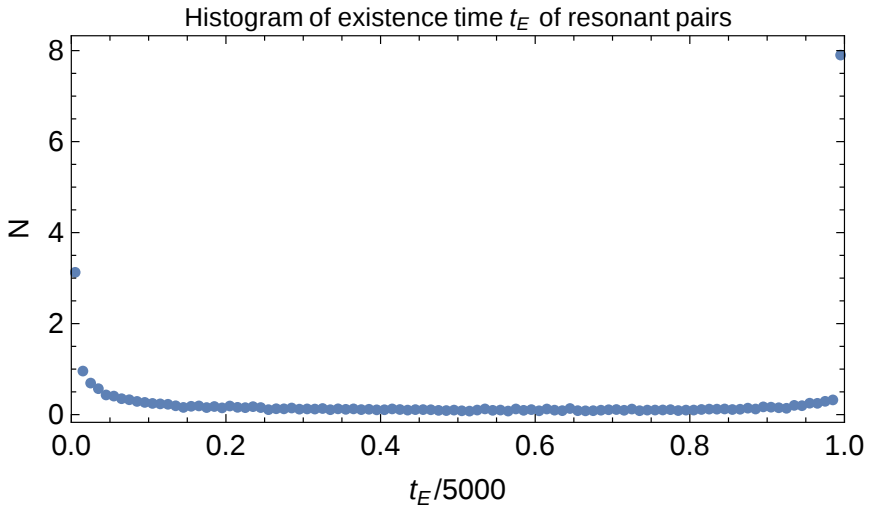

Figure 3.11: Histogram of the relative existence time t_E/t for long times $t = 5000$ and $\varepsilon = 10$, $\Delta t = 0.5$. The plot is logarithmic to show all regimes. We averaged over 100 different initial configurations.

Analysis of the existence time of resonant pairs

In order to explain the decay of $C(t)$ for long times, we investigate the distribution of existence times of resonant pairs.

We define the *existence time* t_E of a resonant pair as the time difference between the current time t, and the latest time t_I, where this pair was identified as a resonant pair: $t_E = t - t_I$. Figure 3.11 examines the existence times of all resonant pairs, that exist at a time $t = 5000$. There are two maxima, thus two main accumulations of resonant pairs:

First, pairs with very long existence times $t_E \approx t$. These pairs were identified during the first time steps of the simulation and typically have a large interaction. Since these pairs do not change their resonance identity, they do not contribute to the long time dynamics of the system.

Second, pairs with small existence times. We present these pairs in a histogram of absolute values of t_E in Figure 3.11 (appendix). These pairs are crucial for the dynamics of the system, since their changing resonance state leads to a fluctuation of fields. We call these pairs *fluctuating pairs*.

In Figure 3.12, we compare the magnitude of both groups. An interesting fact can be extracted from this figure for $\varepsilon > 400$: Even though that the total number of resonant pairs is still noticeable (≈ 50), almost all of these pairs belong have long existence times and do not contribute to the dynam-

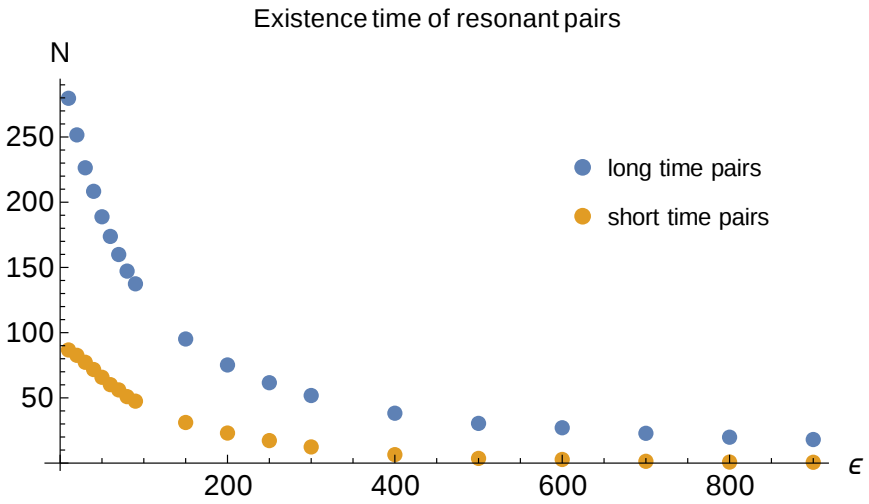

Figure 3.12: Number of resonant pairs with long existence times compared to the number of pairs with short existence times. The time increment was chosen as $\Delta t = 0.5$ and the value of disorder ε is varied (x-axis).

ics. This explains the increase of the number of isolated spins around this disorder value.

Fluctuating pairs

In the following, we further examine the properties of fluctuating pairs. They form a network of pairs, whose resonance states and therefore J^z fields fluctuate. This network is essential for dynamics in the system. In order to obtain the number N_{fluct} of fluctuating pairs, we determine the number of pairs, whose resonance state changed from resonant to non-resonant in a time interval $\Delta t = 1$. Figures 3.13 and 3.14 plot the dependence of N_{fluct} on the time t. We observe the following properties of N_{fluct}:

- After an initial fast decrease, N_{fluct} decreases very slow.
- N_{fluct} depends strongly on disorder for $\varepsilon > 20$.
- For smaller disorder values, the value of N_{fluct} does not depend on ε.

In order to examine this dependence, we plot the mean number of fluctuating pairs at large time $t = 5000$ in Figure 3.15. We expect, that the value of N_{fluct} influences two properties of the spin system:

First, it influences the number of isolated spins that do not participate in the dynamics. This corresponds to the saturation value of the correlation function $C(t)$.

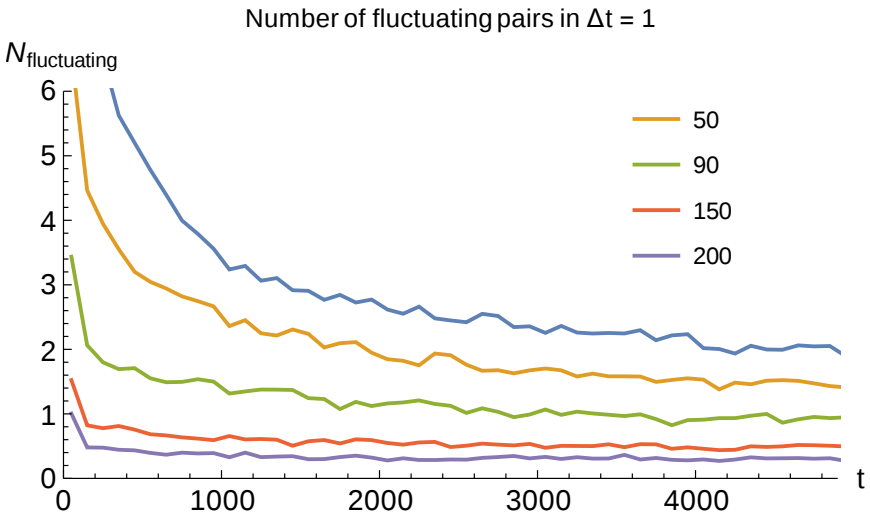

Figure 3.13: Plot of the number of fluctuating pairs over time t for a time increment of $\Delta t = 0.5$ and several different disorder values.

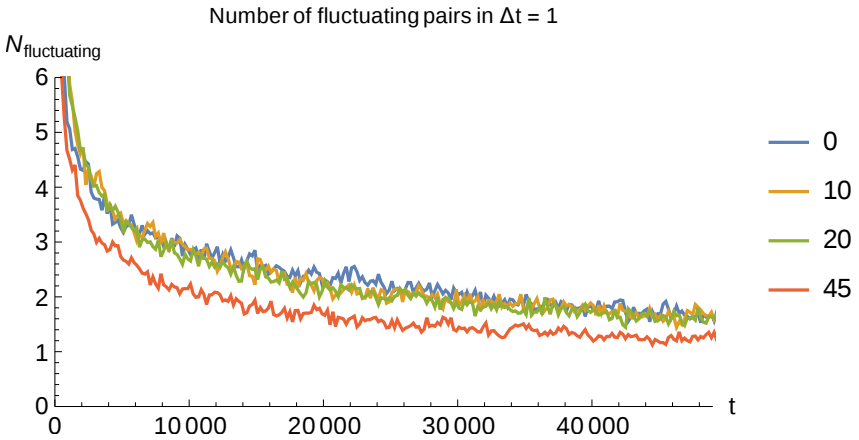

Figure 3.14: Plot of the number of fluctuating pairs over time t for small disorder values.

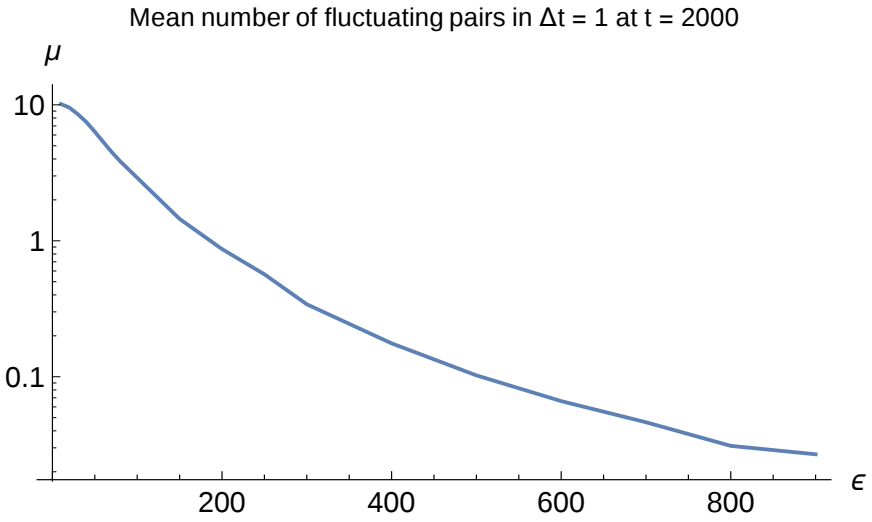

Figure 3.15: Mean number of fluctuating pairs at $t = 5000$ for varying disorder value ε.

And second, it influences the decay rate of $C(t)$, which is related to the speed of spin diffusion.

From previous analysis we know, that the saturation value of $C(t)$ is constant for small disorder value $\varepsilon < 150$. For larger disorder values, the number of fluctuating pairs becomes so small, that the dynamics of the system is not sufficient to decrease $C(t)$ to a finite saturation value of 5%. We conclude, that for large networks ($N_{\text{fluct}} > 1$), the size of the resonant network does not influence the number of isolated spins. If the number of fluctuating pairs decreases below a certain marginal value $N_{\text{crit}} \approx 1$, the number of isolated spins increases for decreasing value of N_{fluct}.

We investigated the speed of the decay in the end of subsection 3.2.3. Figure 3.9 indicates, that the decay rate has a maximum around $\varepsilon \approx 10$. As shown in Figure C.14 of Appendix C, the same behaviour is found for N_{fluct}. In the following, we explain this maximum by an analysis of the distribution of delay times of fluctuating pairs.

Figure 3.17 shows a histogram of delay times for resonant pairs. In this figure, we discriminate between the set of all resonant pairs and the set of fluctuating pairs. The latter shows a sharp decrease for $t_d < 0.2$. Since the delay time t_d of a pair is related to its interaction J by $t_d \sim J^{-1}$, this result indicates, that pairs with large coupling constants do not contribute to the resonant network.

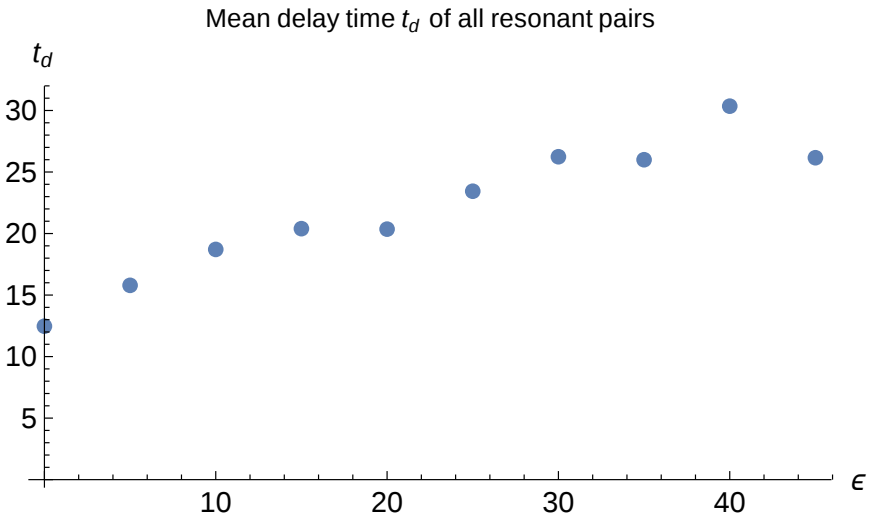

Figure 3.16: Mean value of the delay time in dependence of the disorder value ε.

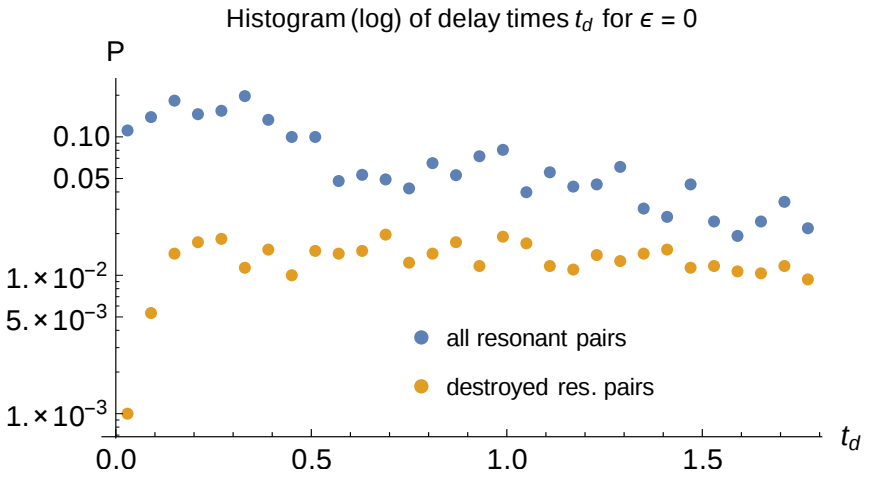

Figure 3.17: Histogram of delay times for short times $t_d < 2$ and disorder $\varepsilon = 0$.

This effects leads to a decrease of the number of fluctuating pairs for decreasing disorder. However, the increasing number of resonant pairs affects this number in the opposite way. We believe, that both effects balance each other for $\varepsilon \approx 10$. For larger disorder values, the influence of the number of resonant pairs dominates and the number of fluctuating pairs decreases for increasing disorder. For smaller disorder values, the opposite is the case and the number of fluctuating pairs increases for increasing disorder value ε.

3.3 Validity of model

After the presentation of the results, in this section we discuss the validity of the time evolution algorithm. We focus on the situation, that a pair with small interaction controls the resonance of a pair with large interaction. We expect, that the prospect of changing the identification of the pair with large interaction blocks the change of the resonance state of the pair with small interaction. Therefore, this setup is called blocking.

3.3.1 Blocking

Let us consider two interacting spin pairs, which we call "strong" and "weak" pair. These names arise from the assumption, that the absolute value of the interaction J_1 of the strong pair is considerably larger than the absolute value of the interaction J_2 of the weak pair: $|J_1| \gg |J_2|$. Initially, we assume that pair 1 is resonant and pair 2 is not.

By a change in the environment of the weak pair, it becomes a resonant pair. Because of a large coupling of the two pairs, the resonance condition of the strong pair is altered such, that it is not resonant any more. In this case, the weak pair 2 controls the resonance of the strong pair 1. As a effect of this progress, the energy of the full system is changed by a value of the order of J_1. Therefore, tiny energy changes are allowed to have big impacts on the energy of the system. This raises the question, if such processes should be suppressed.

We address this question in two steps: First, we determine a time evolution of the total energy of the system. This is done in the next subsection. Second, we investigate the interaction between pairs with respect to the question, if the prospect of changing the identity of other pairs influences the resonance condition. This analysis is done in Chapter 4.

3.3.2 Energy conservation

In the course of the time evolution, the distribution of resonant pairs changes. Since a resonant pair in its eigenstate differs in energy from the same pair

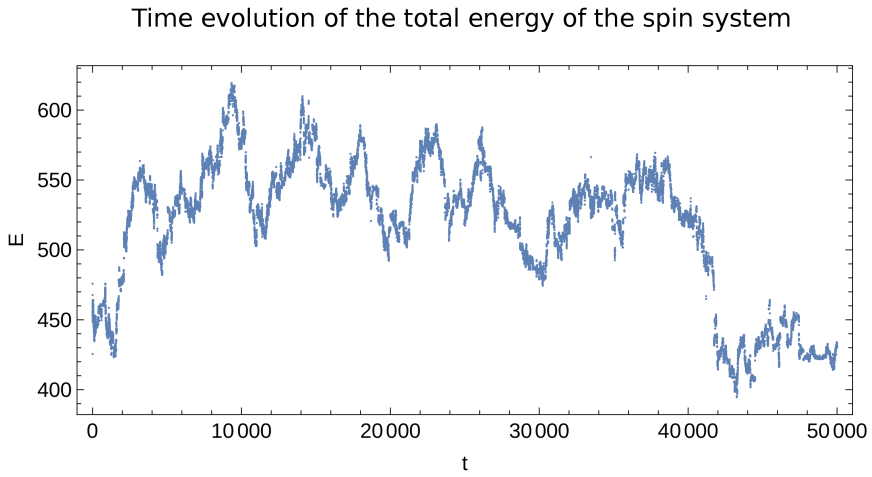

Figure 3.18: Total energy as defined in Equation (B.8) for one initial configuration with $\varepsilon = 0$ and $\Delta t = 0.5$.

in a product state, we expect a fluctuation of the total energy present in the system.

In Appendix B.2.5, we determine the contribution of isolated spins and resonant pairs to the energy of the system separately. As a result, we obtain Equation (B.8) to calculate the full energy E. Figure 3.18 shows an example of the time evolution of E for $\varepsilon = 0$. The energy fluctuates in the range of ± 200, but there is no long time drift to positive or negative values.

Nonetheless, there remains the question, if the implementation of a time evolution as described in this chapter resembles the real behaviour of a spin system. Our main concern is the following: The underlying mechanism of the evolution is the situation, in which a resonant pair destroys or creates other resonant pairs by the means of J^z fields. In this case, the total energy in our simulation is not conserved as shown above.

Chapter 4

Creation of a resonant cluster

In this Chapter, we introduce a proper way to identify the resonance condition in the case of Section 3.3, where a weak pair affects the resonance condition of a strong pair. This leads to a modified resonance condition, which conserves energy through the joint dynamics of strong and weak pairs. This, in turn, becomes a part of a new mechanism for the formation of resonantly coupled spin cluster capable of transporting energy across the system. The cluster is formed when a typical strong pair becomes coupled to more than one weak pair and vice versa. We believe that such a coupling becomes the leading mechanism of the energy transport.

The modification of the resonance condition increases the complexity, and thus the computational calculation time requirement, of the algorithm significantly. Hence, it is not possible to obtain a time evolution of the spin system. Instead, we focus on the formation of the resonant cluster through the mechanism indicated above.

4.1 Interaction between "weak" and "strong" pairs

First, we consider a system of two spin pairs and neglect the influence of other spins and pairs. We denote the first pair as $(1, 2)$ and the second pair as $(3, 4)$. We assume, that the first pair has a stronger coupling: $|J_{12}| > |J_{34}|$. As introduced in Section 3.3, the two pairs are addressed as strong and weak pair. The Hamiltonian $\mathcal{H}$ of the two pair system was derived in Equation (2.30).

Of special interest are resonant transitions of this system. To determine these transitions, we diagonalize $\mathcal{H}$ and identify avoided eigenvalue crossings. As an adjustable parameter, we choose the on-site field h_{34} of the

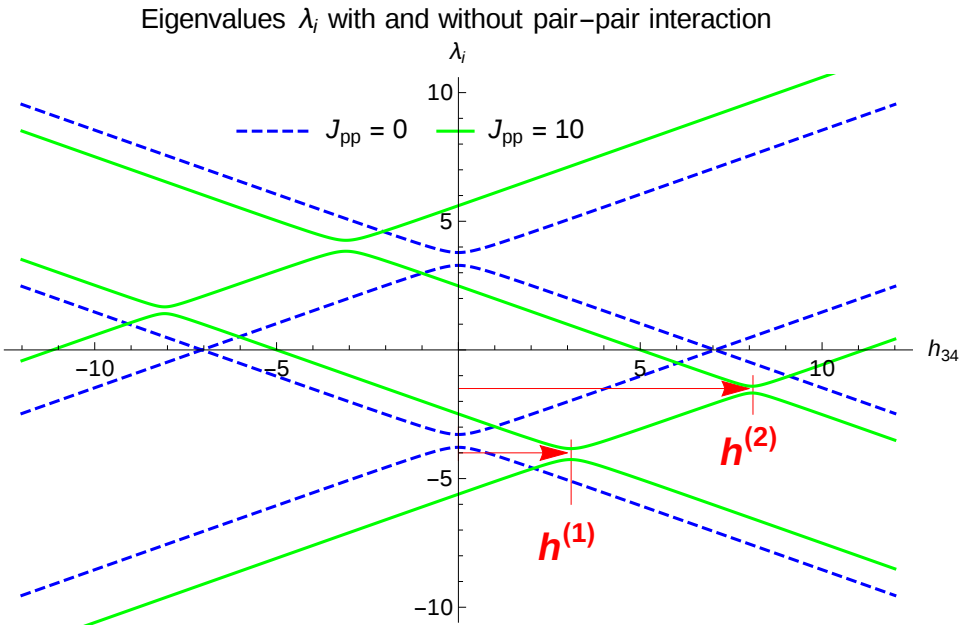

Figure 4.1: Avoided level crossing for $J_{34} = 1$, $J_{12} = 10$, $h_{12} = 5$ and two values of J_{pp}: $J_{pp} = 5$ (green, solid) and $J_{pp} = 0$ (blue, dashed). For $J_{pp} = 0$, we obtain an avoided level crossing at $h_{34} = 0$. For $J_{pp} = 5$, avoided crossings are seen for $h_{34} = \pm h^{(1)}$ and $h_{34} = \pm h^{(2)}$, where $h^{(1)} \approx 3$ and $h^{(2)} \approx 8$.

weak pair. A plot of the eigenvalues λ_i in dependence of h_{34} is shown in Figure 4.1.

First, we examine the case, that both pairs are decoupled ($J_{pp} = 0$). This is represented by the blue dashed curves in Figure 4.1. For this situation we obtain an avoided level crossing at $h_{34} = 0$, which represents the only possible resonant transition of the weak pair for this set of parameter. This transition is equivalent to the classical resonant condition from Section 2.2:

$$|h_{34}| < J_{34}, \tag{4.1}$$

which also predicts resonance at $h_{34} = 0$. The width of the transition, and thus the transition amplitude, is controlled by the value of J_{34}. This agrees with the analysis of the avoided crossing: The distance d of eigenvalues at the avoided crossing is $d = \frac{1}{2}J_{34}$, which corresponds to the off-diagonal matrix element $\frac{1}{4}J_{34}$ in of $\mathcal{H}$ in Equation (2.6).

Next, we examine the case of two coupled spin pairs. An example of such a system is shown by the green solid lines in Figure 4.1. Here, we obtain

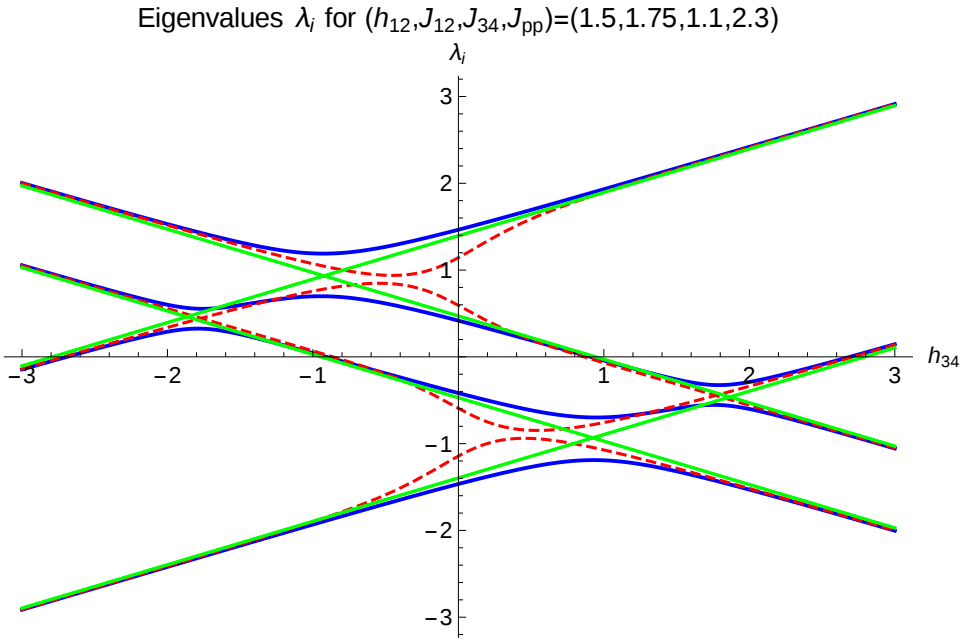

Figure 4.2: Comparison of the full eigenvalues (blue solid line) with the eigenvalues of the truncated Hamiltonian H_0 (red dashed line). They differ for small values of h_{34}, especially at $h_{34} \sim h^{(1)}$. For this reason we use the approximation $h_{34} = -H_2$ for the calculation of $w^{\pm}$ and obtain the green solid line.

four values of h_{34}, where the four-spin system has a transition between two eigenstates. The values of h_{34}, where a transition occurs, are labeled as $\pm h^{(1)}$ and $\pm h^{(2)}$. We call $h^{(1)}$ and $h^{(2)}$ *shifts*, since the resonance condition is shifted from 0 to one of these values. The transition amplitude of all transitions (given by the vertical width of the avoided level crossing) is smaller compared to the decoupled case $J_{pp} = 0$.

Hence, instead of the resonance condition (4.1), we obtain four modified resonance conditions of the form

$$|h_{34} \pm h^{(i)}| < |J^{(i)}|, \tag{4.2}$$

where $i = 1, 2$ and $J^{(i)} < J_{34}$.

4.1.1 Modified resonance condition for a weak pair interacting with a strong pair

In the following, we derive expressions for the parameter $h^{(i)}$ and $J^{(i)}$, which determine the modified resonance condition (4.2). We describe this scheme

in detail in Section A.4.1 in the appendix.

It is not possible to do a direct analytical diagonalization of the general pair-pair Hamiltonian from Equation (2.30). In order to solve this problem, we introduce a small parameter, namely, the weak pair interaction J_{34}. We assume

$$J_{34} \ll h_{34} \sim h_{12} \sim J_{12} \sim J_{pp}\,. \tag{4.3}$$

Using this assumption, the Hamiltonian $\mathcal{H}$ is separated into two parts $\mathcal{H} = \mathcal{H}_0 + \Delta\mathcal{H}$, which are of different order in J_{34}. This approximation works well for $h_{34} \gg J_{34}$. Therefore, we approximate the eigenvalues

$$\begin{aligned} \lambda_{1,2} &= \mp\frac{1}{4}w_- + \frac{1}{2}H_2 \\ \lambda_{3,4} &= \mp\frac{1}{4}w_+ - \frac{1}{2}H_2 \end{aligned}$$

of $\mathcal{H}_0$ by straight lines, which we obtain in the limit $h_{34} \gg J_{34}$. This condition yields $H_2 = h_{34}$, and we obtain

$$w_\pm = \sqrt{4H_1^2 + J_{pp}^2 \mp 4h_{12}J_{pp}}\,. \tag{4.4}$$

Figure 4.2 compares the Eigenvalues of the full Hamiltonian $\mathcal{H}$ with the eigenvalues of $\mathcal{H}_0$ and its linear approximation. The approximated eigenvalues have no avoided but a normal crossing and we obtain the shifts $h^{(1)}$ and $h^{(2)}$ as

$$h^{(1)} = \frac{1}{4}(w_+ - w_-) \tag{4.5}$$

$$h^{(2)} = \frac{1}{4}(w_+ + w_-)\,, \tag{4.6}$$

with $w_\pm$ from Equation (4.4). The transition amplitudes $J^{(i)}$ are determined as

$$J^{(i)} = \langle v_i|\mathcal{H}|v_j\rangle\,, \tag{4.7}$$

where v_i are the eigenvectors, which are involved in the respective avoided eigenvalue crossing. Appendix A.4.1 derives an analytical expression for $J^{(i)}$. This result is given in Equations (A.59) to (A.64). Since these expressions have a factor $\frac{1}{4}J_{34}$ each, introduce a new variable $j^{(i)}$ as

$$J^{(i)} = j^{(i)} \cdot \frac{1}{4}J_{34}\,, \tag{4.8}$$

where $j^{(i)} \in [0,1]$ does not depend on J_{34}. Numerical results show, that the equation

$$\left(j^{(1)}\right)^2 + \left(j^{(2)}\right)^2 = 1 \tag{4.9}$$

holds.

Hence, the value of $j^{(i)}$ leads to a decrease of the transition amplitude of the modified resonance condition (4.2). This compensates the fact, that we have four possible transitions instead of one.

Using the expressions from Equations (A.59) to (A.64), we determine $j^{(i)}$ as

$$j^{(1)} = \frac{\left(\frac{J_{pp}^3\, h_{12}\, h_{34}^2}{2\, H_1\, H_2^3} + \frac{2\, J_{pp}^2\, h_{34}}{H_2} - \frac{J_{pp}\, h_{12}}{2\, H_1\, H_2}\left(2H_1(w_+ + w_-) + 4H_1^2 + w_+ w_-\right)\right)}{2\sqrt{w_+\, w_-\, (w_+ + 2H_1 + A_{zz})\,(w_- + 2H_1 - A_{zz})}} \tag{4.10}$$

and

$$j^{(2)} = \frac{\left(\frac{J_{pp}^3\, h_{12}\, h_{34}^2}{2\, H_1\, H_2^3} + \frac{2\, J_{pp}^2\, h_{34}}{H_2} - \frac{J_{pp}\, h_{12}}{2\, H_1\, H_2}\left(2H_1(w_+ - w_-) + 4H_1^2 - w_+ w_-\right)\right)}{2\sqrt{w_+\, w_-\, (w_+ + 2H_1 + A_{zz})\,(w_- - 2H_1 - A_{zz})}}, \tag{4.11}$$

where we use the on-site field h_{34} of the respective transition: $h_{34} = h^{(i)}$.

We approximate Equation (4.5) for large and small values of J_{pp} in Appendix A.4.2. Moreover, we examine the case of a weak pair, that controls the resonance condition of a strong pair, in Appendix A.4.3.

4.1.2 "Weak" pair coupled to more than one strong pair

In the last subsection, we investigated the presence of resonant transitions for a system of two pairs. We found, that there exist four transitions, which lead to a new resonance condition

$$|h_{34} \pm h^{(i)}| < |j^{(i)} \cdot \frac{1}{4}\, J_{34}| \tag{4.12}$$

of the weak pair.

This procedure can be generalized to an arbitrary number of strong pairs acting on the same weak pair $(3, 4)$. For each strong pair s, we obtain energy shifts $h_s^{(i)}$ and transition amplitudes $j_s^{(i)}$ as discussed in Section 4.1: The shifts are calculated using Equation (4.5) and the transition amplitudes are obtained from Equation (4.10) and Equation (4.11).

For each strong pair, we obtain four possible transitions. Hence, n strong pairs lead to 4^n possible transitions of the weak pair. We add the respective shifts $h_s^{(i)}$ for different s to determine the value of h_{34}, at which the resonant transition occurs. The transition amplitude is suppressed by each involved

strong pair by $j_s^{(i)} \in [0,1]$. In order to obtain the full transition amplitude, we multiply all values of $j_s^{(i)}$. The resulting condition

$$\left| h_{34} - \sum_{\pm,s,i} \pm h_s^{(i)} \right| < \left| J_{34} \cdot \prod_{s,i} j_s^{(i)} \right| \tag{4.13}$$

is called advanced resonance condition. We test this formula for a system consisting of three pairs in Appendix A.5.

If one of the conditions (4.13) holds true, there exists a many particle state, such that every combination of the weak and a strong pair is in resonance at once. In this case, the weak pair is resonant and it is coupled to every strong pair. If no condition (4.13) is satisfied, the weak pair is not resonant. Furthermore, the weak pair is not coupled to any strong pair.

The notion of weak and strong pairs is relative to the interactions of the two pairs involved. A pair 1 with interaction J_1 adopts the role of a weak pair in the interaction with a pair 2, if $J_1 < J_2$ holds. The same pair is regarded as strong pair in the interaction with a third pair 3, when $J_2 > J_3$. In this situation, the second pair can be linked to both first and third pair. These links represent interactions of four spin systems and can be the source of spin diffusion. In contrast to the concept of resonant pairs, links do not create closed groups of four spins, but can connect many spin pairs at once.

Moreover, a strong pair can be coupled to several weak pairs. We treat the interaction of the strong pair with each of its weak pairs separately.

4.2 Forming "resonant cluster" by the links between spin pairs

In the last section, we derived the advanced resonance condition (4.13), which determines the resonance of a weak pair coupled to several strong pairs. In the following, we describe, how this condition is used to identify interacting spin pairs.

4.2.1 Defining links

In the following, we consider a spin pair (i,j) with interaction J_{ij} and look for pairs (k,l), that interact strongly with this pair. We refer to the analysis of Section 3.3, where a weak pair controls the resonance of a strong pair. Hence, we require

$$|J_{ij}| < |J_{kl}| \,. \tag{4.14}$$

Since we vary both pairs under all possible spin pairs, we obtain each combination of two pairs exactly once.

The following concept arises from the notion of fluctuating pairs, which was discussed in Section 3.2.4, and the discussion of the blocking of pairs from Section 3.3.

We define, that the pair (k, l) interacts strongly with the pair (i, j), if a flip of the second pair would change the resonance state of the original pair. This condition reads as

$$|J_{pp}| > |S_{ij}|\,, \tag{4.15}$$

where the resonance range $S_{ij} = J_{ij} - h_{ij}$ was introduced in Equation (2.9) and the pair-pair interaction in Equation (2.35). Additionally, we require, that the pair-pair interaction is at least of the same order as the internal interaction J_{ij} of the pair:

$$|J_{pp}| > 0.5\,|J_{ij}|\,, \tag{4.16}$$

where the factor 0.5 was chosen from Figure 2.1. This condition ensures, that the eigenvector decomposition of the pair is changed by a sufficient amount. Otherwise, pairs with a small absolute value of S_{ij} would be coupled to any other pair.

Pairs, that satisfy conditions (4.14) to (4.16), are called *potential weak pairs* of the spin pair (i, j). Let us consider one of these potential weak pairs, label it as (k, l), and neglect all other pairs for simplicity. As discussed in Section 4.1, the two pair system consisting of (i, j) and (k, l) is in resonance, if one of the advanced resonance conditions (4.12) of the weak pair (k, l) holds. In this case, we put a *link* between pairs (i, j) and (k, l). This link connects the four spins i, j, k, l.

In general, a given pair can be considered as "weak" for several different "strong" pairs. In this case, we use the generalized advanced resonance condition of Equation (4.13) for the weak pair. If one of these conditions is satisfied, we link the weak pair to all its strong partners.

As a next step, we translate the concept of links between pairs into an algorithm. A vital aspect of this routine is the use of the list of spin pairs (i, j), which is ordered with respect to their internal interactions J_{ij}. We start at the top of the list and execute two main steps:

- First, we determine the resonance of the pair (i, j). If (i, j) is potential weak pair of one or many other pairs, we use the advanced resonance condition (4.13). Else, the routine uses the classical condition (2.21).

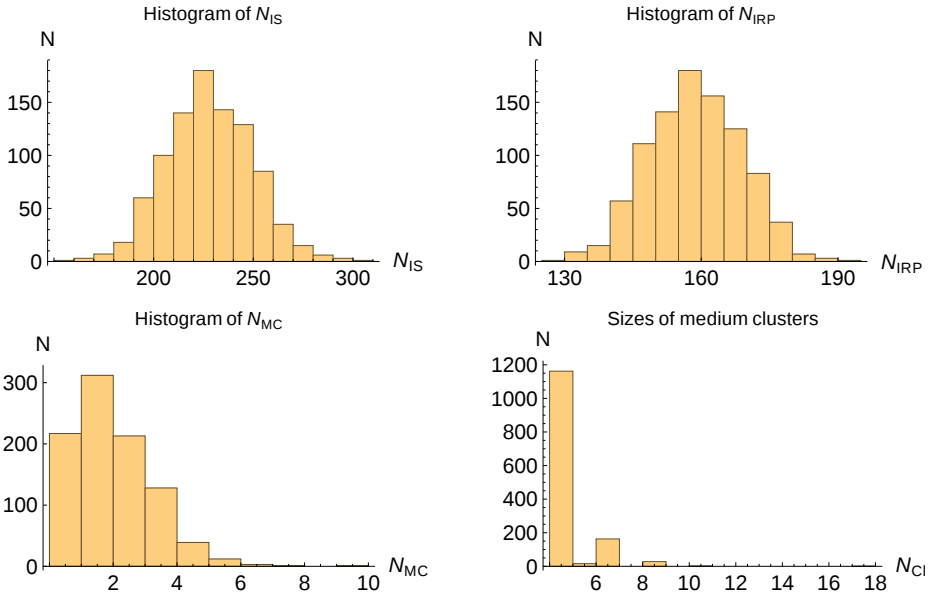

Figure 4.3: Histogram of the number of cluster of one of the three categories: Independent spins (N_{IS}, top left histogram), Independent resonant pairs (N_{IRP}, top right) and medium cluster (N_{MC}, bottom left). Additionally we present a histogram of the sizes of medium clusters (bottom right). We used 936 different initial configuration of spins with a disorder of $\varepsilon = 10$.

- Second, we identify all potential weak pairs of the pair (i, j). Since these pairs have a smaller interaction, their resonance condition was not yet examined.

The order of the list ensures, that all potential strong pairs of (i, j) already identified (i, j) as potential weak pair. One complete examination of the list of spin pairs investigates each pair-pair combination exactly once.

As for the algorithm of Chapter 3, we allow only one resonant partner for every spin. This was discussed in Section 2.2. This condition extends to the concept of the advanced resonant condition.

A complete and detailed description of the linking algorithm can be found in Appendix B.3. There, the search for potential weak pairs is separated into to subroutines: First, we identify all spins s, that would modify the resonance condition of a strong pair. Then, we consider all pairs, which include spin s, and check the conditions (4.14) to (4.16).

4.2.2 Preliminary investigation of resonant cluster

As the algorithm puts links between spin pairs, resonant cluster evolve. We define a cluster as a set of spins, where each spin is connected to all other elements of of the same cluster via arbitrary many other spins (that are also part of the same cluster). After we analyzed all spin pairs, we obtain four different types of cluster:

1. Independent spins, which form cluster of size 1. These spins are not linked to any other spin and not part of a resonant pair.
2. Independent resonant pairs, which form cluster of size 2. Here, spins are part of a resonant pair, but this pair is not linked to any other pair.
3. The largest cluster. This is the cluster with largest size. The results indicate, that there is always one cluster, which is considerably larger than all other cluster.
4. Medium cluster. All cluster, that are not part of one of the first three categories, are denoted as a medium cluster. The word 'medium' refers to the medium size of these cluster.

Figure 4.3 presents histograms of the number of clusters of each of the categories. As one can see, both the number and the size of medium cluster are very small (which is true for all disorder values). Hence, these cluster are not important for the dynamics of the system and are neglected in the following analysis.

Both, the mean number N_{IRP} of independent resonant pairs, and the size N_{MCL} of the largest cluster, depend on the value of the disorder ε. We present a plot of this dependence in Figure 4.4.

At disorder values around $\varepsilon \approx 1000$, no resonant cluster forms (except of a few resonant pairs). If we decrease the disorder value, the size of the maximum cluster increases. The number of independent resonant pairs increases as well, but much slower. However, at a value of $\varepsilon \approx 20$, the maximum cluster size has a maximum and drops if we further decrease the disorder. We can explain this effect only partly by the sharp rise of the number of independent resonant pairs. Figure 4.4 shows the number of spins that are part of independent resonant pairs or the maximum cluster as green dots. We see, that this curve has a maximum at $\varepsilon \approx 20$ as well. The number of spins participating in a medium cluster is about constant and its mean is always smaller than 10.

This result agrees with the results of Section 3.2.4, which obtains the same marginal value $\varepsilon = 20$.

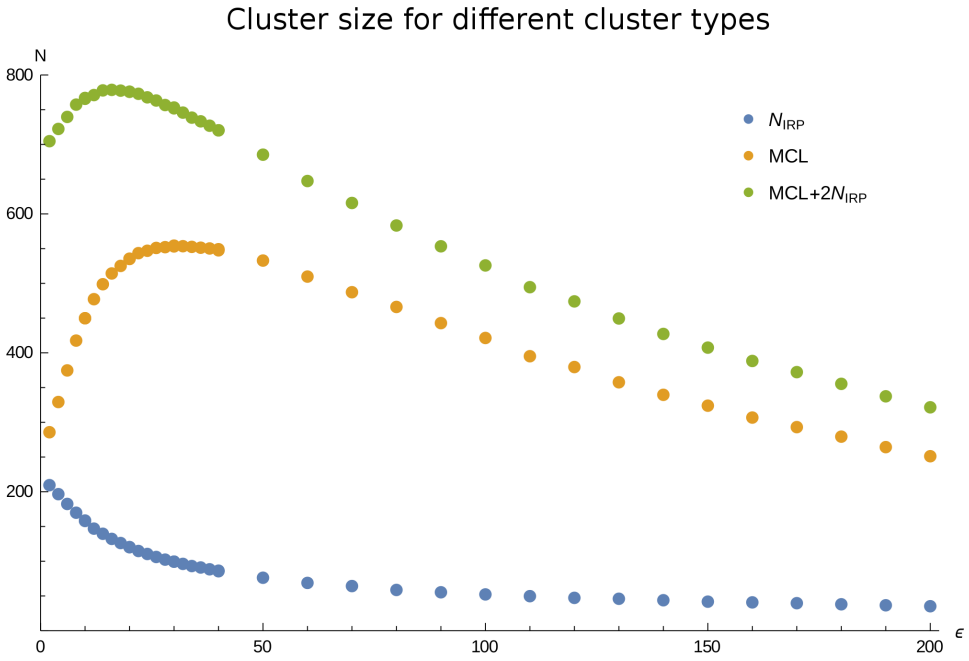

Figure 4.4: Mean numbers of the maximum cluster size μ_{MCL} and the number of independent resonant pairs μ_{NIRP}. Additionally we show the number of all spins, that are either part of of an independent resonant pair or of the maximum cluster.

4.2.3 Using the inverse participation ratio to detect and characterize the formation of a resonant cluster

We calculate the inverse participation ratio I as

$$I = \frac{1}{N_{\mathrm{Spins}}^2} \sum_i N_{\mathrm{cl},i}^2 \,, \tag{4.17}$$

where $N_{\mathrm{cl},i}$ denotes the size of cluster i. If a spin is not connected to any other spin, it is regarded as a cluster of size 1.

A system consisting of $N_{\mathrm{Spins}} = 1000$ spins without any connections has an IPR value $I = 0.001$. If we increase the number of connections, the cluster size grows and the value of I increases. If all spins are connected, we obtain $I = 1$. Since $N_{\mathrm{cl},i}$ appears as a square in Equation (4.17), a single large cluster increases the value of I more than many small clusters.

As an example, let us consider a system, which consists entirely of resonant pairs without links. In this case, we obtain $I = 0.002$, which is hardly larger than the minimum IPR value of 0.001. On the other hand, a system

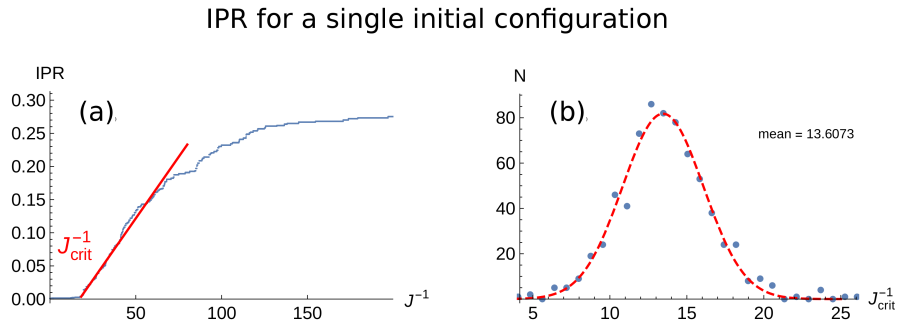

Figure 4.5: In figure (a), we present the IPR function defined in (4.17) for $\varepsilon = 40$. As described in the main text, we fit a line for $J^{-1} \in [0.004, 0.3 \cdot \text{max} = 0.09]$ and obtain the red line as a fit. The intersection of this line with the x-axis is labeled as J^{-1}_{crit}. Figure (b) shows a histogram of the values of J^{-1}_{crit} obtained from $\varepsilon = 40$ and 703 different initial configurations. The Gaussian fit (red dashed line) has a standard deviation of $s = 2.6$.

consisting of 900 independent spins and one cluster of size 100 would already lead to $I = 0.01$. As a result, the value of I is mainly determined by the size of the largest cluster:

$$I = \frac{1}{N^2_{\text{Spins}}} \sum_i N^2_{\text{cl},i} \approx \frac{N^2_{\text{Mcl}}}{N^2_{\text{Spins}}} \sim N^2_{\text{Mcl}} \tag{4.18}$$

In order to investigate the composition of different cluster, the algorithm monitors the value of I, while it works through the list of spin pairs to determine their resonance state (see Section B.1). Since this list is ordered with respect to the pair interactions J, we obtain I as function of the interaction.

Since the probability density function scales as J^{-2}, the mean number of pairs is not constant for any range of interactions. This complicates the analysis of the IPR as function of the interaction. In order to solve this problem, we transform the interaction J to its inverse J^{-1} and determine I as function of J^{-1}. As shown in Section 2.5.1, the probability distribution for J^{-1} is constant in the interval $[0, 62.5]$.

A plot of the IPR function in dependence of J^{-1} for one initial configuration of spins and disorder $\varepsilon = 40$ can be found in the left plot of Figure 4.5. A main feature of this plot is the flat region up to a certain value $J^{-1} = J^{-1}_{\text{crit}}$. We obtain this value by fitting a straight line in the range defined by $I > 0.004$ and $I < 0.3 \cdot I_{\text{max}}$, where I_{max} denotes the maximum IPR value. The right plot in Figure 4.5 shows a histogram of the critical points J^{-1}_{crit} for 703 different initial configurations and $\varepsilon = 40$.

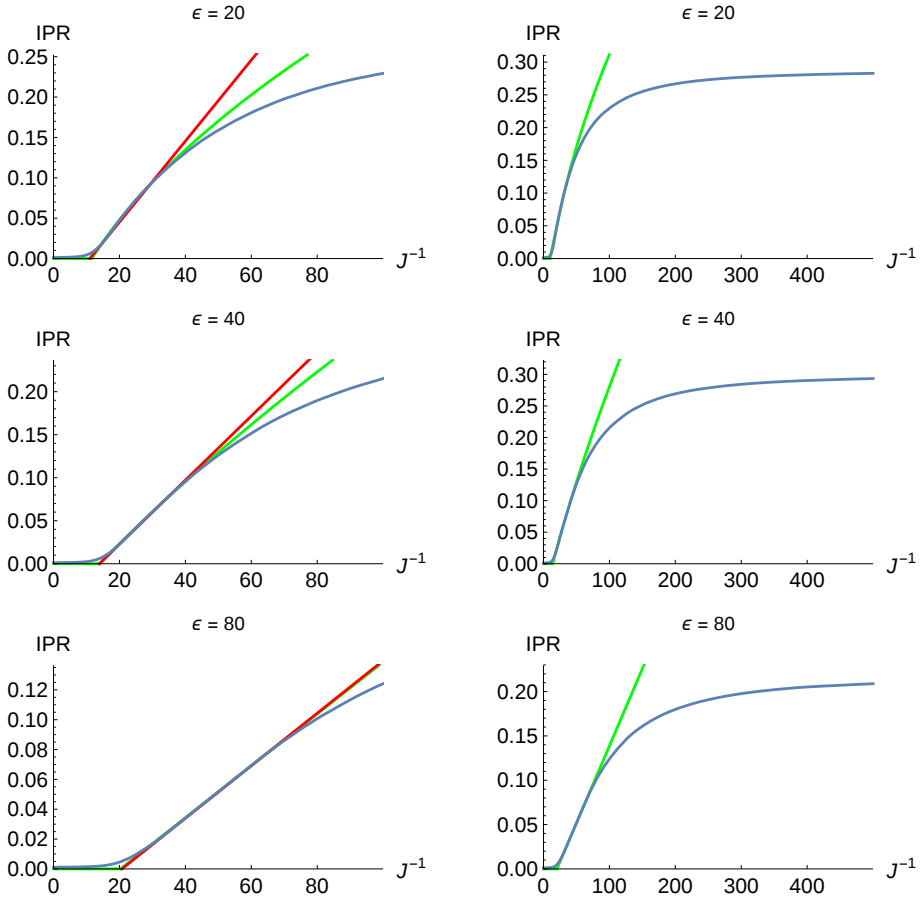

Figure 4.6: In these six plots we present the averaged IPR function defined in (4.17) for the three disorder values $\varepsilon = 20, 40, 80$. For each disorder value we show a small scale ($J^{-1} \in [0, 100]$, left column) and a larger scale ($J^{-1} \in [0, 500]$, right column). The two fits represent a straight line fitted at J_{ip}^{-1} (red line) and a square root function (green line). Each plot was obtained by averaging over about 700 initial configurations.

4.2.4 Averaging over initial configurations

The evolution of the spin system depends on the actual positions and on the local fields h_i of spins. Therefore, we average the IPR function over about 700 different initial configurations to balance this dependence. This leads to a smooth plot of the IPR, as presented in Figure 4.6. In this figure, we present IPR plots for different disorder values. We identify four different ranges for the IPR as a function of J^{-1}:

- For very small values of J^{-1}, the plot of the averaged function is relatively flat. This is due to the initial flat behaviour of the individual IPR function (see Figure 4.5).

- At a certain value J_s^{-1} of J^{-1}, the averaged IPR starts to increase significantly. Thereby, the second derivative of I is positive, but decreases. Since the value of J_{crit}^{-1} varies for different initial configurations (right plot of Figure 4.5), there is no clear cutoff point for the average IPR function, but a region where it slopes up slowly compared to the behaviour for larger J^{-1}.

- At a value J_{ip}^{-1}, the function has an inflection point.

- For large values of J^{-1}, the IPR function is nearly flat again. It approaches a final inverse participation ratio.

To understand this behaviour, we use the distribution of J^{-1} from Figure 2.4. The density function of J^{-1} is constant up to $J^{-1} = 62.5$. For larger values, it decreases due to finite size effects. This explains the negative second derivative for $J^{-1} > 62.5$ and the slow approach to some final value of IPR. However, for small values $J^{-1} < 62.5$, the routine exhibits no finite size effects.

4.3 Results for the inverse participation ratio

As a next step, we compare the IPR plots for different disorder values in Figure 4.6.

- The final value of the IPR does not change much for $\varepsilon = 20, 40$. This is due to the fact, that the size of the maximum cluster is nearly constant in this range (figure 4.4). For $\varepsilon > 40$, the size decreases faster, as does the value of IPR.

- The width of initial flat range increases, if we increase the disorder. Both, the onset J_s^{-1} of the rise of I and the inflection point J_{ip}^{-1} increase. Both values were introduced in the last subsection.

- The initial slope of the IPR changes with disorder.

Whereas the first and last point can be explained qualitatively with the different sizes of the maximum cluster, the extended range of the flat region and its dependence on ε was not expected by us. To investigate this behaviour, we used three different fitting routines to obtain values for J_s^{-1} and J_{ip}^{-1}.

The first fit is a straight line fitted to the inflection point J_{ip}^{-1} of the averaged IPR function. The second fit is a square root function fitted to the averaged IPR function. Since both fits use the already averaged IPR function, it is difficult to obtain error estimates. For that reason, we introduced a third fit, which fits a straight line to every individual IPR plot (no averaging). This

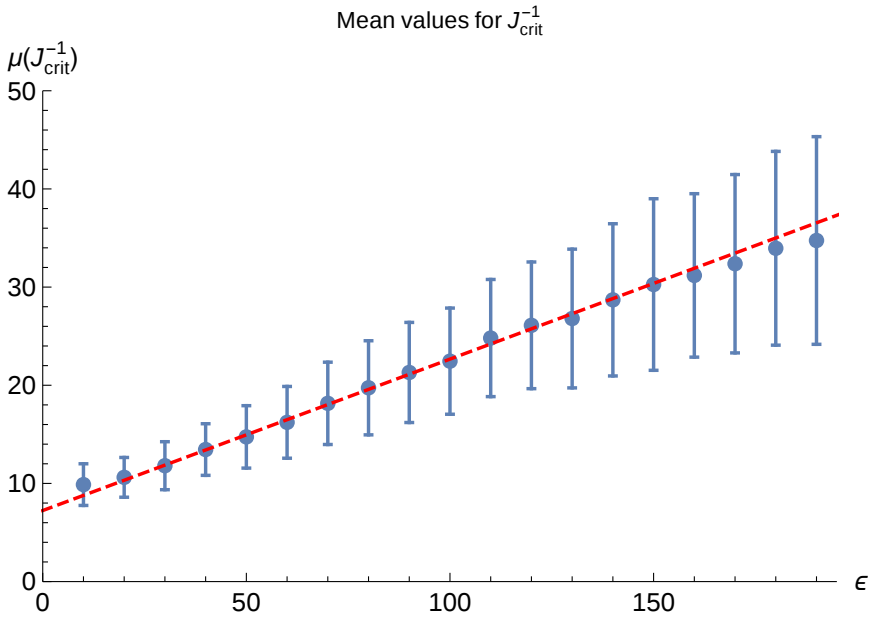

Figure 4.7: The plot shows mean values of J_{crit}^{-1} for large disorder. For each point, we calculated a histogram of J_{crit}^{-1} as shown in the right plot of Figure 4.5 and obtained mean μ and standard deviation σ. This determines a point as $\mu \pm \sigma$. Each point was obtained using a histogram with about 700 initial configurations.

fit is represented by a red line in the left plot of Figure 4.5. The resulting values of J_{crit}^{-1} are approximated well by a Gaussian distribution with clear maximum value μ, which is indicated as a red dashed line in the right plot of Figure 4.5.

Figure 4.7 shows the dependence of μ on the disorder, where the error bar is given by the width of the Gaussian distribution. Both, the mean and the width, increase for increasing disorder value ε. The main reason for the latter behaviour is the fitting routine: We fit in the range of a minimum value of 0.004 and a fraction of the maximum IPR value. This fraction is 0.3 for $\varepsilon < 100$ and 0.4 for $100 < \varepsilon < 200$. For growing disorder values, the maximum IPR decreases fast and we obtain a smaller fitting range. Therefore, there exists a larger variation of fits and the standard deviation increases. However, the error is always considerably smaller than the mean value.

We optimized this routine by fitting a line to a larger range of IPR values, but the standard deviation did not change. We deduce, that for larger disorder, the dependence on initial configuration of spins is larger than for smaller disorder values.

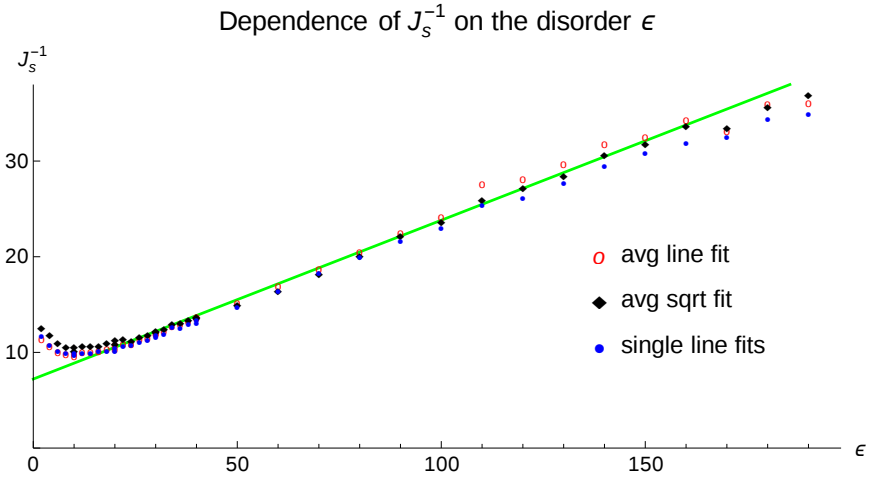

Figure 4.8: The plot estimates J_s^{-1} for different disorder values ε. We used the three different fitting routines described in the text. Each point was obtained using a histogram with about 700 initial configurations. The green line $f(x) = 0.166\,x + 7.215$ is a fit of the average of all three routines.

4.3.1 Investigation of the marginal value J_s^{-1}

In the last passage we mentioned three routines that estimate the value of J_s^{-1} for a fixed disorder value ε:

First, the individual line approximation, which was introduced in the last subsection.

Second, the average line approximation. This routine determines the inflection point of the averaged IPR function and fits a tangent to this point. The intersection of this tangent with the x-axis gives the value for J_s^{-1}.

Third, the average square root approximation. This routine fits $a_1x^2+a_2x+a_3$ to the inverse of the averaged IPR function. In this way we obtain J_s^{-1} as the coefficient a_3 of the fit.

We denote these routines as individual line routine (ind line), average line routine (avg line) and average square root routine (avg sqrt).

To deduce the dependence of J_s^{-1} on ε, we use all three routines and compare the results. Figure 4.8 shows that the routines agree in the range $\varepsilon \in [0, 200]$ and indicate an increase of J_s^{-1} for increasing ε. We obtain linear

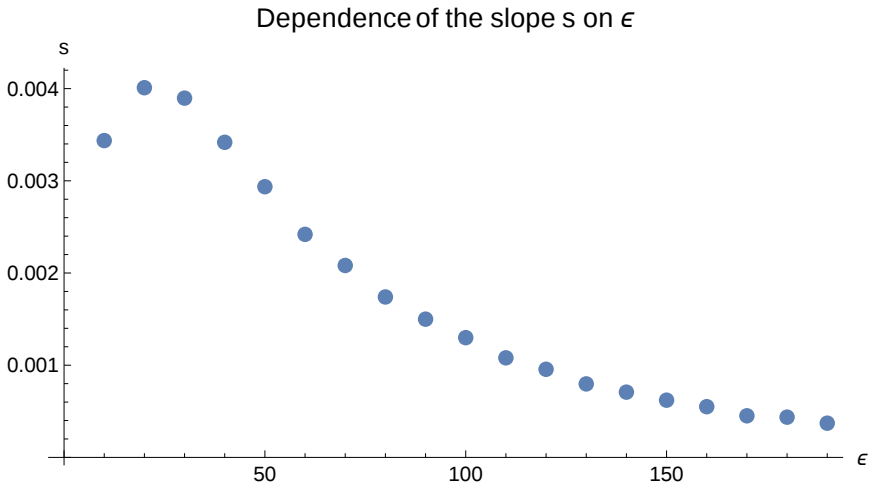

Figure 4.9: Dependence of the slope s from Equation (4.19) on disorder ε.

approximations

$$\begin{aligned} f_{\text{ind line}} &= 0.159\,\varepsilon + 7.24 \\ f_{\text{avg line}} &= 0.176\,\varepsilon + 6.93 \\ f_{\text{avg sqrt}} &= 0.164\,\varepsilon + 7.47\,. \end{aligned}$$

of J_s^{-1} for the three different fitting routines introduced in the last paragraph. In Figure 4.8, we indicate the average of all three fits $f(\varepsilon) = 0.166\,\varepsilon + 7.215$ as a solid green line. We observe that the fit approximates the data well for $20 < \varepsilon < 180$. For smaller disorder $\varepsilon < 20$, the function J_s^{-1} has a minimum and increases as we decrease ε. This behaviour is related to the decrease of the maximum cluster size for small disorder. Since we interpreted the latter effect as an artifact of the restriction of one resonant pair for each spin, the validity of the minimum of J_s^{-1} at small disorder remains at least questionable. However, the linear dependence of J_s^{-1} for $20 < \varepsilon < 180$ is not affected by this consideration.

Slope at takeoff point J_s^{-1}

Next to the position of the marginal value J_s^{-1}, we now examine the slope of the average square root fit at J_s^{-1}. We determine the slope s as

$$s = \frac{1}{\sqrt{a_2^2 + 8a_1a_3}}\,. \tag{4.19}$$

Figure 4.9 shows a plot of the slope dependent on ε. We experience a similar behaviour as for J_s^{-1}: For $\varepsilon > 20$, s decreases fast as ε grows.

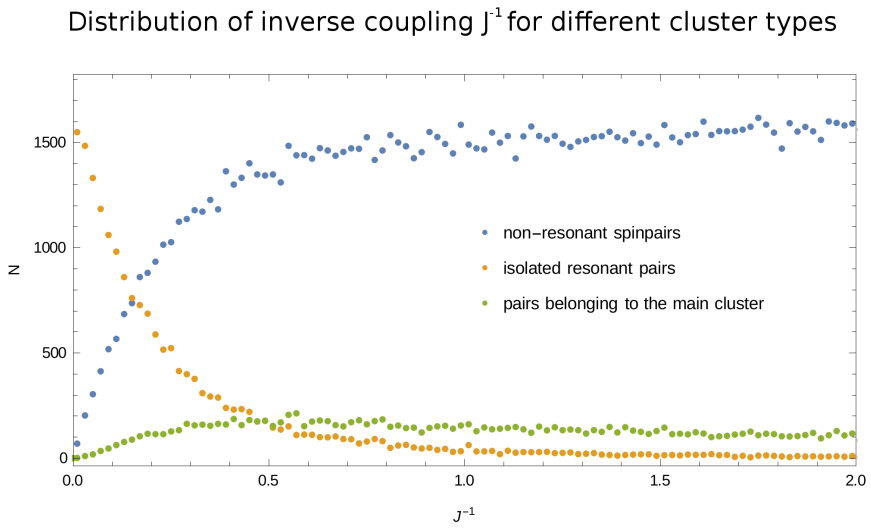

Figure 4.10: Distribution of inverse couplings J^{-1} for disorder $\varepsilon = 5$. Note, that the probability density function $p_{J^{-1}}(J^{-1})$ is constant.

The slope is an estimate for the speed of the growth of the largest cluster. Similar to the results of Section 3.2.4, the size of the resonant network exhibits a maximum at about $\varepsilon \approx 10$. In order to explain this behaviour, we investigate the distribution of coupling constants of the maximum cluster.

4.4 Further investigations

4.4.1 Distribution of spin pairs

In the last subsection, we classified the following types of spin pairs:

1. Pairs which belong to the maximum cluster.
2. Pairs which belong to a medium sized cluster.
3. Isolated resonant pairs.
4. Non-resonant pairs.

We found, that the number of pairs, which belong to a medium sized cluster, is very small. Therefore, we neglect these pairs in the following analysis. Figure 4.10 shows the magnitude of the remaining types as a function of J^{-1}.

For large interactions $J > 1$, most spin pairs belong to the group of isolated strong pairs and do not contribute to the largest cluster. In order to investigate this effect, we examine the distribution of J^{-1} for linked pairs of

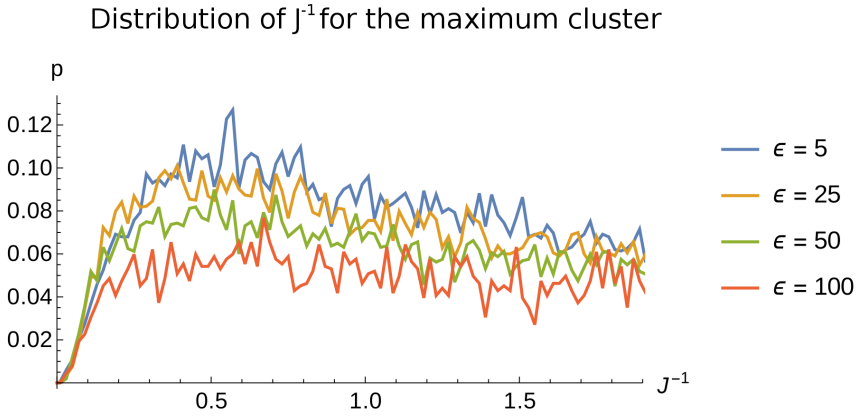

Figure 4.11: Distribution of inverse coupling constants J^{-1} in the maximum cluster for $\varepsilon = 5$.

the largest cluster in Figure 4.11. For large inverse interactions, the number of resonant pairs decreases and so does the number of spin pairs contributing to the maximum cluster. This behaviour reverses for $J^{-1} < 0.5$: The number of spin pairs increases with increasing inverse coupling constant and can be approximated by a straight line for $J^{-1} < 0.2$. The straight line is independent of the disorder value ε.

These results indicate, that pairs with large interactions have small probabilities of interacting with other pairs. In order to explain this fact, we examine the spin-pair interaction $J_{sp} = J_{il} - J_{jl}$ of a spin pair (i, j) and a spin l. It depends on the interaction J_{ij} of the pair. In the next subsection, we calculate this dependence analytically and deduce the probability for a link in dependence of the coupling constant J_{ij} of a pair.

4.4.2 Spin-pair interaction in dependence of the interaction of the strong pair

Let us consider three spins 1, 2 and 3, where spins 1 and 2 form a resonant pair and are separated by a distance $d = r_{ij}$ (see Figure 4.12). This distance is related to the pair interaction, which is denoted by J_s, by $J_s = d^{-3}$. The spin-pair interaction depends on the distances r_{il} as

$$J_{sp} = \frac{1}{r_{il}^3} - \frac{1}{r_{jl}^3} \,.$$

If we rotate the third spin l around the line that connects spins i and j, the distances r_{il} and r_{jl} do not change. Therefore, the problem of calculating J_{sp} has a radial symmetry around the z-axis, which we define by the line connecting spins i and j. The origin of the coordinate system is located in

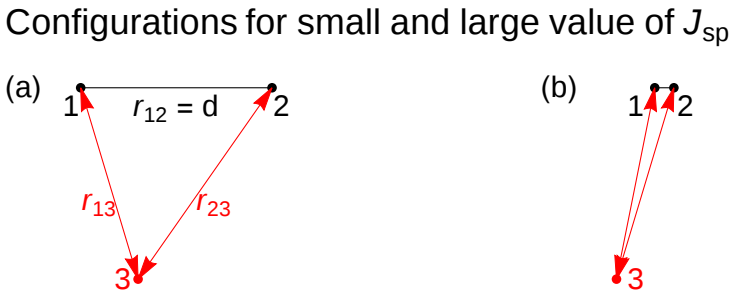

Figure 4.12: Two constellations of a three spin setup. Plot (a) shows a setup with a large distance $d = r_{12}$ and therefore small interaction $J_{12} = J_s$. In contrast, plot (b) depicts the situation for large J_s and small distance d. The difference of distances r_{13} and r_{23} is larger for the left setup, which results in a larger value of the spin-pair interaction J_{sp}.

the middle of the two spins.

If we fix a value of J_{sp} at J_{sp}^{fixed}, all positions of the remote spin j that reproduce this value for a given pair (i, j) are located on the surface of sphere-like bodies around spins i and j. Figure 4.13 depicts a slice of these equipotential areas for $y = 0$ and different values of J_{sp}.

The interior of these bodies represents all possible positions of the third spin, where $J_{sp} > J_{sp}^{\text{fixed}}$ holds. Their volume V is proportional to the probability P, that a given spin pair finds a third spin such that J_{sp} exceeds a certain value J_{sp}^{fixed}:

$$P_{J_{sp}>J_{sp}^{\text{fixed}}}(d, J_{sp}^{\text{fixed}}) = \frac{V}{V_{\text{full}}}\,, \tag{4.20}$$

where the third spin is sampled in a cube with volume $V_{\text{full}} = 1000$.

As a next step, we determine the dependence of $P_{J_{sp}>J_{sp}^{\text{fixed}}}(d, J_{sp}^{\text{fixed}})$ on the distance d and thus on the interaction $J_s = d^{-3}$ of the spin pair. Figure 4.14 shows the dependence of $P_{J_{sp}>J_{sp}^{\text{fixed}}}$ on J_s for different values of J_{sp}^{fixed} in a double-logarithmic plot. The straight line indicates a power law dependence for $P_{J_{sp}>J_{sp}^{\text{fixed}}} \sim J_s^{0.25}$.

In Appendix A.8, we use geometric arguments to derive the probability density function $p_{Jsp}(J_{sp})$ analytically. We obtain

$$p_{J_{sp}}(J_{sp}) = 0.015\ J_{sp}^{-7/4}\ J_s^{-1/4}\,,$$

which is equivalent to the power law dependence of $P_{J_{sp}>J_{sp}^{\text{fixed}}}$ and agrees with numerical data (Figure C.20 in Appendix C).

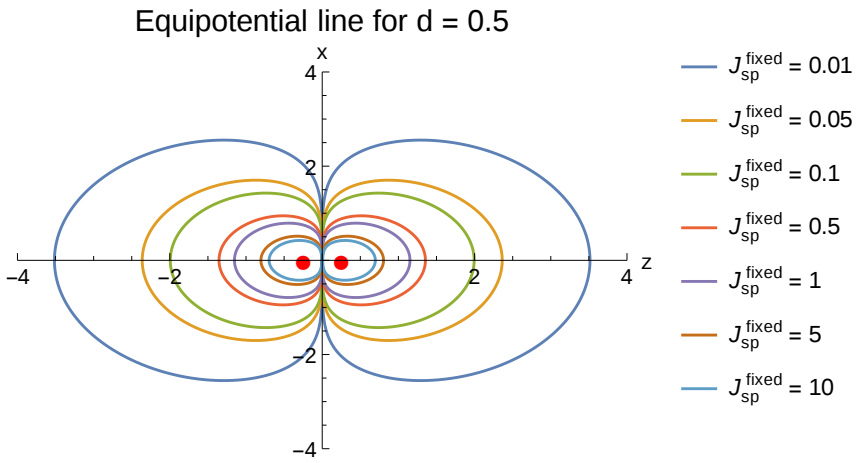

Figure 4.13: Plot of lines with a fixed value of J_{sp}. The two spins of the spin pair are fixed on the positions $z = \pm 0.25$.

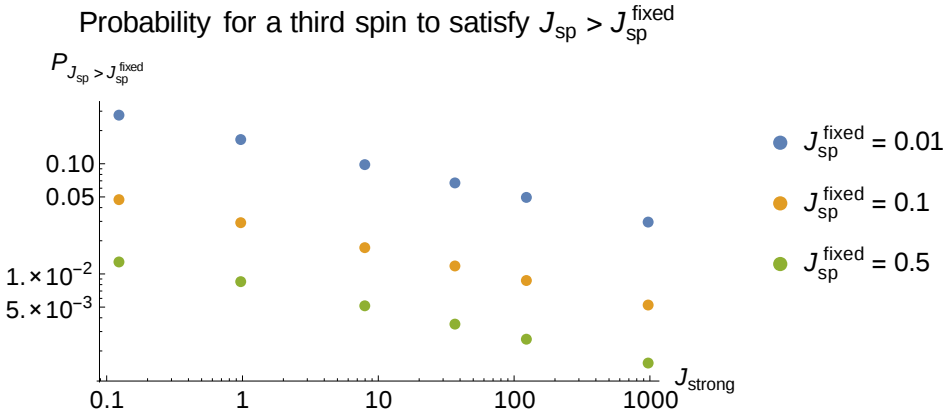

Figure 4.14: Plot of $P_{J_{sp}>J_{sp}^{\text{fixed}}}$ from Equation (4.20) over the interaction J_s of the spin pair. Data sets distinguish in the choice of J_{sp}^{fixed}.

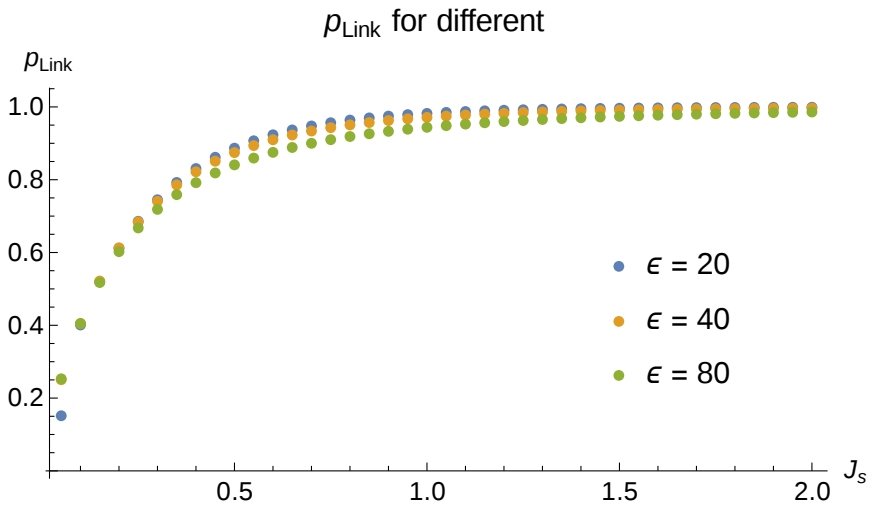

Figure 4.15: Probability p_{Link} for a link between two pairs in dependence of the interaction of the strong pair for different disorder values ε. The numerical integration has a large error for first point of $\varepsilon = 20$ (blue).

4.4.3 Probability of a link in dependence of the interaction of the strong pair

Now, we estimate the probability p_{link}, that a given pair with interaction J_s links to another pair. The derivation of this function is presented in Appendix B.3. Figure 4.15 shows the dependence of p_{link} on the interaction J_s. It indicates, that pairs with large interaction ($J_s > 1$) are less likely to produce a link between spin pairs. This behaviour explains the distribution of inverse couplings J^{-1} in Figure 4.11. Moreover, Figure 4.15 indicates, that p_{link} is independent of the disorder value ε.

4.5 Spins on a simple cubic lattice

In the last section, we investigated a system with random placement of spins. In this section, we will shortly introduce a lattice simulation and compare the results of this simulation with the results from random placement.

Implementation

We kept the number of spins and the size of the box constant. Hence, we obtain a simple cubic lattice, where the nearest-neighbour distance is 1. After we set the coordinates of spins, we sample their on-site fields by a uniform distribution in $[0, \varepsilon]$. The spins are aligned in x-y and z direction, which is important for the θ dependence of the interaction.

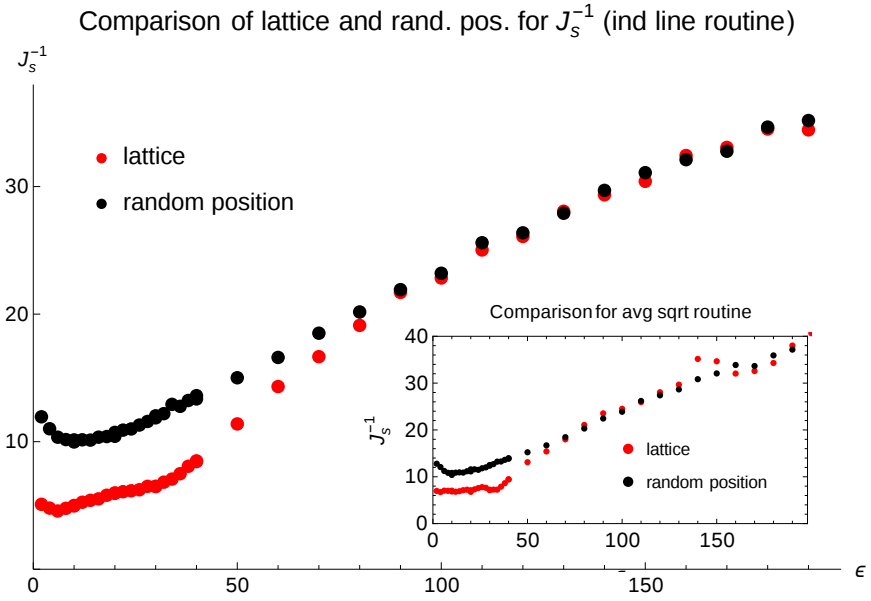

Figure 4.16: The plot shows mean values of J_s^{-1} for the average square root and individual line routine. The latter determines J_s^{-1} from the distribution of J_{crit}^{-1}, we obtain an error by using the standard deviation σ of this distribution. This determines a point as $\mu \pm \sigma$. Each point was obtained using about 500 initial configurations.

In contrary to random placement of spins, the parameter range for the interaction J_{ij} of spins on a lattice is not continuous anymore. The same is true for values of J^{-1}. This property destroys the smoothness of the IPR function, which affects the routines to determine the value of J_s^{-1}. Since it is difficult to compute the inflection point automatically, the errors of the average line routine increase. Therefore we restrict the analysis of J_s^{-1} on the other two algorithms: The individual line routine and the average square root routine.

IPR results

Figure C.21 in Appendix C shows a collection of average plots as well as an individual IPR plot for spins on a lattice. In comparison to Figures 4.5 and 4.6, the shape of the function did not change much.

Analogous to the last section, we determine the takeoff point J_s^{-1} and investigate its dependence on the disorder ε. The results are shown in Figure 4.16 together with the previous results for random placement of spins. The characteristics of the function are the same as for random placement of spins, namely:

- There is a flat region for small disorder $\varepsilon < 30$.
- For $\varepsilon > 30$ value J_s^{-1} increases. In contrary to J_s^{-1} for random placement of spins, a line is not a good approximation to $J_s^{-1}(\varepsilon)$.
- The errors of the individual line routine increase for increasing value of ε (see Figure C.21 in Appendix C).
- Both functions $J_s^{-1}(\varepsilon)$ agree for large disorder ($\varepsilon > 90$).

The disagreement for small and medium disorder values is interesting and indicates a different composition of the resonant cluster for lattice and random positions. We can interpret the value of J_s^{-1} as the time scale of the dynamics of the system. Figure 4.16 shows, that the values of J_s^{-1} differ by a factor of two for small disorder values $\varepsilon < 40$. Hence, we expect a significant difference in the time scale of the dynamics in the two setups.

Chapter 5

Summary and discussion

5.1 Summary of results

The previous chapters described a hybrid quantum classical simulation, which allows us to study a medium of TLS with dipolar interaction and energy disorder. We investigated the dynamics as function of disorder and deduced a time scale for the energy transport.

Chapter 3 and 4 present two routines, which investigate the dynamics of the spin system. Both rely on the concept of resonant pairs, but differ in their treatment of pair-pair interaction.

The routine of Chapter 3 generates a time evolution of the system. This evolution is studied by an analysis of correlations. Up to large disorder values, the correlations decay to 5% of their initial value. This indicates, that the system is delocalized. Even though a transition to the localized regime appears at large disorder values, we presume, that this transition is strongly influenced by the finite size of the system and is irrelevant for experimental setups. However, this remains to be proven by experiments or by an investigation of larger systems.

In the delocalized regime, even for systems with no disorder of their on-site fields, some spins remain isolated from the dynamics. Figures 3.2 and 3.6 indicate, that the number of isolated spins is independent of the disorder. This effect is caused by interactions originating from $S_i^z S_j^z$ terms of the Hamiltonian.

Moreover, we studied the decay rate of the correlations. For disorder values larger than a marginal value $\varepsilon = 20$, the rate decreases significantly for increasing disorder. For smaller disorder values, this intuitive relation is not satisfied: Figure 3.9 indicates a maximum for the decay rate around $\varepsilon \approx 10$.

In contrast to the algorithm of Chapter 3, the algorithm of Chapter 4 includes the full interaction of two spin pairs. Investigation of this interaction leads to a modification of the resonance condition. For this complicated system, a calculation of the time evolution is not possible. Instead, we determine cluster of connected spins. We believe that these cluster are essential for energy transport.

The analysis of these clusters indicates, that pairs with large couplings alone do not suffice to form large connected clusters, which lead to considerable energy transport in the system. Only by adding spin pairs with smaller interaction, such a cluster evolves. The marginal interaction J_s^{-1}, which leads to a formation of a large cluster, corresponds to the time scale of energy transport. Similar to the examination of the decay rate, we observe two regimes for the dependence of the time scale on ε, namely: A linear dependence of the time scale for disorders larger than the marginal value $\varepsilon = 20$ (Figure 4.8), and, for smaller values, a dependence which is dominated by a minimum around $\varepsilon \approx 10$. However, the treatment of conflicts is questionable for these disorder values and one might be skeptical, if this effect can be verified experimentally.

In order to analyze this effect further, we examine the distribution of pair couplings of the main cluster (Figure 4.11). It indicates, that pairs with couplings $J > 2$ are not part of the main cluster, but form isolated clusters of size 2. We show, that this effect can be explained by the dependence of the spin-pair coupling on the internal pair coupling.

In addition to the system with random positions, we studied a system with spins on a simple cubic lattice. Figure 4.16 compares the dependence of the time scale of energy transport for a cubic lattice and random positions. We see, that both values agree for large disorder value $\varepsilon > 90$. For smaller disorder, the time scale is shorter for the lattice. This result indicates, that for small energy disorder, the dynamics on lattices is considerably faster than the dynamics in systems with random positions of TLS. This result, and the explicit dependence of the time scale on the disorder of Figure 4.16, could be studied experimentally.

5.1.1 Outlook

As a possible next step to improve results, we would study the influence of the two main approximations of the model on the results, namely: The finite size effect and the restriction, that each spin can only be part of one resonant pair.

The finite size influences especially the localization-delocalization transition for large disorder values and the explicit percentage of isolated spins.

The restriction to one resonant pair is problematic for small disorder values. We assume, that this approximation causes the anomalous behaviour below the marginal value $\varepsilon = 20$. Therefore, it would be interesting to modify the algorithm such, that it allows multiple resonances for every spin. However, this would change the model significantly.

Appendix A

Derivations

A.1 Selection of a basis

The basis states are aligned parallel to the quantization axis. We use the standard convention of denoting the 1-spin basis as $\{|\uparrow\rangle, |\downarrow\rangle\}$. For N spins, we obtain the basis vector $e_i^{(N)}$ by taking the Kronecker product $\otimes$ of the 1-spin basis states $e_i^{(1)}$ as

$$e_i^{(N)} = e_{i_1}^{(1)} \otimes e_{i_2}^{(1)} \otimes \cdots \otimes e_{i_N}^{(1)}. \tag{A.1}$$

In the next sections, we often regard two spin systems. We can obtain the first basis vector $|\uparrow\uparrow\rangle$ by using Equation (A.1) as

$$|\uparrow\uparrow\rangle = |\uparrow\rangle \otimes |\uparrow\rangle = \begin{pmatrix} 1 \\ 0 \end{pmatrix} \otimes \begin{pmatrix} 1 \\ 0 \end{pmatrix} = \begin{pmatrix} 1 \\ 0 \\ 0 \\ 0 \end{pmatrix}. \tag{A.2}$$

In this way, the full basis is determined as

$$\mathbb{E}_{\text{full}} = \{|\uparrow\uparrow\rangle, |\uparrow\downarrow\rangle, |\downarrow\uparrow\rangle, |\downarrow\downarrow\rangle\}. \tag{A.3}$$

As discussed in Section A.3, we truncate this basis to

$$\mathbb{E} = \{|\uparrow\downarrow\rangle, |\downarrow\uparrow\rangle\}, \tag{A.4}$$

which is equivalent to identifying the states $\{(0,1,0,0),(0,0,1,0)\}$ with the two-dimensional standard basis $\{(1,0),(0,1)\}$. Because of its origin from the Kronecker product $\otimes$, we denote $\mathbb{E}$ as *product basis* of the two spin system. In contrast, the eigenbasis of the two spin system is labeled as *diagonal basis*.

A.2 Operators of N-spin systems

In this section, we consider operators of a resonant two level system, which consists of an arbitrary number of spins. We obtain their matrix representation using the basis of Appendix A.1.

For a system consisting of only one spin, the matrix representation of the spin operators I^α is obtained as

$$I^\alpha = \frac{1}{2}\sigma_\alpha, \tag{A.5}$$

where σ_α denotes the Pauli matrices

$$\sigma_x = \begin{pmatrix} 0 & 1 \\ 1 & 0 \end{pmatrix},\ \sigma_y = \begin{pmatrix} 0 & -i \\ i & 0 \end{pmatrix},\ \sigma_z = \begin{pmatrix} 1 & 0 \\ 0 & -1 \end{pmatrix} \tag{A.6}$$

and the unity matrix σ_0. For a system consisting of N spins, the operator I_i^α of spin i is defined by the Kronecker product of Pauli matrices:

$$I_i^\alpha = \sigma_0 \otimes \ldots \otimes \sigma_0 \otimes \frac{1}{2}\sigma_\alpha \otimes \sigma_0 \otimes \ldots \otimes \sigma_0, \tag{A.7}$$

where σ_α appears on the i-th place of this product. Of special interest is the system consisting of two spins. As an example, we derive the operator I_1^z of the first spin as

$$I_1^z = \frac{1}{2}\sigma_\alpha \otimes \sigma_0 = \frac{1}{2}\begin{pmatrix} 1 & 0 & 0 & 0 \\ 0 & 1 & 0 & 0 \\ 0 & 0 & -1 & 0 \\ 0 & 0 & 0 & -1 \end{pmatrix}.$$

As discussed in Section A.1, we obtain the product states of a spin pair as $|\uparrow\downarrow\rangle = (0,1,0,0)$ and $|\downarrow\uparrow\rangle = (0,0,1,0)$. Since we reduce the basis to these two states, the vectors are transformed to $(1,0)$ and $(0,1)$ and I_1^z becomes:

$$I_1^z = \frac{1}{2}\begin{pmatrix} 1 & 0 \\ 0 & -1 \end{pmatrix}.$$

Similar to this calculation, we obtain the pair operators $I_{1,2}$ in a system consisting of four spins, and thus two pairs, as

$$\begin{aligned} I_1^z &= \frac{1}{2}\begin{pmatrix} 1 & 0 & 0 & 0 \\ 0 & 1 & 0 & 0 \\ 0 & 0 & -1 & 0 \\ 0 & 0 & 0 & -1 \end{pmatrix},\ I_1^x = \frac{1}{2}\begin{pmatrix} 0 & 1 & 0 & 0 \\ 1 & 0 & 0 & 0 \\ 0 & 0 & 0 & 1 \\ 0 & 0 & 1 & 0 \end{pmatrix}, \\ I_2^z &= \frac{1}{2}\begin{pmatrix} 1 & 0 & 0 & 0 \\ 0 & -1 & 0 & 0 \\ 0 & 0 & 1 & 0 \\ 0 & 0 & 0 & -1 \end{pmatrix},\ I_2^x = \frac{1}{2}\begin{pmatrix} 0 & 0 & 1 & 0 \\ 0 & 0 & 0 & 1 \\ 1 & 0 & 0 & 0 \\ 0 & 1 & 0 & 0 \end{pmatrix}. \end{aligned}$$

Obtaining Prefactors of the Hamiltonian

The next paragraph introduces properties of the trace of σ_α. The two relations $\operatorname{tr}\sigma_\alpha = 0$ for $\alpha = x, y, z$, and

$$\sigma_\alpha \sigma_\beta = \delta_{\alpha\beta}\sigma_0 + i\sum_{\gamma=1}^{3} \epsilon_{\alpha\beta\gamma}\sigma_\gamma \tag{A.8}$$

can be proven by direct calculation using the matrix representation from above. Note that the trace is independent of the choice of basis. From (A.8), we deduce $\operatorname{tr}(\sigma_\alpha\sigma_\beta)$ as

$$\operatorname{tr}(\sigma_\alpha\sigma_\beta) = 2\delta_{\alpha\beta}\,. \tag{A.9}$$

Additionally, we use the following two properties of the Kronecker product $\otimes$:

$$(A\otimes B)(C\otimes D) = AC\otimes BD \tag{A.10}$$

and

$$\operatorname{tr}(A\otimes B) = \operatorname{tr}A\cdot\operatorname{tr}B\,. \tag{A.11}$$

Equation (A.11) yields the trace of a single operator I_k^α as

$$\operatorname{tr} I_k^\alpha = \operatorname{tr}\left(\sigma_0\otimes\ldots\otimes\frac{1}{2}\sigma_\alpha\otimes\ldots\otimes\sigma_0\right) = \frac{1}{2}\operatorname{tr}\sigma_\alpha\cdot 2^{(N-1)} = 0\,, \tag{A.12}$$

where N is the number of spins. For the trace of the mixed product $I_1^\alpha I_2^\beta$, we obtain

$$\begin{aligned}\operatorname{tr}\left(I_1^\alpha I_2^\beta\right) &= \frac{1}{4}\operatorname{tr}\left((\sigma_\alpha\otimes\sigma_0)(\sigma_0\otimes\sigma_\beta)\right)\\ &= \frac{1}{4}\operatorname{tr}(\sigma_\alpha\sigma_0\otimes\sigma_0\sigma_\beta) = \frac{1}{4}\operatorname{tr}\sigma_\alpha\operatorname{tr}\sigma_\beta = 0\,,\end{aligned}$$

whereas the product of two operators of the same entity is transformed to

$$\begin{aligned}\operatorname{tr}\left(I_1^\alpha I_1^\beta\right) &= \frac{1}{4}\operatorname{tr}\left((\sigma_\alpha\otimes\sigma_0)(\sigma_\beta\otimes\sigma_0)\right)\\ &= \frac{1}{4}\operatorname{tr}(\sigma_\alpha\sigma_\beta\otimes\sigma_0\sigma_0) = \frac{1}{4}\operatorname{tr}(\sigma_\alpha\sigma_\beta)\operatorname{tr}\sigma_0 = \delta_{\alpha\beta}\,.\end{aligned}$$

For more than 2 spins, we can use Equation (A.10) to reduce $\operatorname{tr}\left(I_k^\alpha I_l^\beta\right)$ to the previous case. In this way we add a factor $\operatorname{tr}\sigma_0 = 2$ for each spin and obtain:

$$\operatorname{tr}\left(I_k^\alpha I_l^\beta\right) = 2^{N-2}\delta_{\alpha\beta}\delta_{kl} \tag{A.13}$$

This equation determines the trace of arbitrary product operators. In the following, we use Equation (A.13) to formulate a procedure, that determines the prefactors of an arbitrary operator in a given Hamiltonian $\mathcal{H}$. We assume, that this Hamiltonian has the form

$$\mathcal{H} = \sum_{i,\alpha} \lambda_{i,\alpha} I_i^\alpha \,, \tag{A.14}$$

where $\lambda_{i,\alpha}$ are scalar prefactors and I_i^α operators as described above. In the following, we consider the equation

$$\mathrm{tr}\left[\left(\mathcal{H} - \lambda I_k^\beta\right) \cdot I_k^\beta\right] = 0 \,. \tag{A.15}$$

Using Relations (A.12) to (A.13), we transform Equation (A.15) to

$$\begin{aligned} \mathrm{tr}\left[(\mathcal{H} - \lambda I) \cdot I\right] &= 0 \\ \Leftrightarrow \sum_{i\neq k,\alpha} \lambda_{i,\alpha} \,\mathrm{tr}\left(I_i^\alpha I_k^\beta\right) + \sum_{\alpha\neq\beta} \lambda_{k,\alpha} \,\mathrm{tr}\left(I_k^\alpha I_k^\beta\right) + (\lambda_{k,\beta} - \lambda)\,\mathrm{tr}\left(I_k^\beta I_k^\beta\right) &= 0 \\ \Leftrightarrow (\lambda_{k,\beta} - \lambda) &= 0 \,. \end{aligned}$$

Hence, the Equation (A.15) holds true if and only if λ is the correct prefactor of the operator I_k^β in $\mathcal{H}$. Now, we again consider Equation (A.15):

$$\begin{aligned} \mathrm{tr}\left[(\mathcal{H} - \lambda I) \cdot I\right] &= 0 \\ \Leftrightarrow \mathrm{tr}\left(\mathcal{H} \cdot I\right) - \lambda\,\mathrm{tr}\left(I \cdot I\right) &= 0 \\ \Leftrightarrow \lambda &= \frac{\mathrm{tr}\left(H \cdot I\right)}{\mathrm{tr}\, I^2} \,. \end{aligned}$$

By combining both derivations, we obtain

$$\lambda_{k,\beta} = \frac{\mathrm{tr}\left(H \cdot I\right)}{\mathrm{tr}\, I^2} \,. \tag{A.16}$$

This equation is independent of the basis of the matrix representations. We exploit this to obtain the prefactor of a given pair operator I: First, we determine the matrix representation of $\mathcal{H}$ in terms of spin operators. Then, we change the basis from the product basis to the diagonal basis of the pair. Finally, we determine the prefactors by using Equation (A.16) for the resulting representation for $\mathcal{H}$. Note, that both, the matrix representation of the operator I and the representation of $\mathcal{H}$, are written in terms of the diagonal basis of the respective pair.

A.3 Properties of a two-spin system

In this section, we investigate a system of two interacting spins. We use the results of this section in many parts of the thesis.

A.3.1 Hamiltonian and Basis

We use the truncated dipole Hamiltonian $\mathcal{H}$ from Equation (2.1). Reduced to two spins, $\mathcal{H}$ is determined as

$$\mathcal{H} = -h_1 S_1^z - h_2 S_2^z + J_{12}\left(S_1^z S_2^z - \frac{1}{4}\left(S_1^+ S_2^- + S_2^+ S_1^-\right)\right). \tag{A.17}$$

Each spin has basis states $|\uparrow\rangle$ and $|\downarrow\rangle$. We obtain the full basis $\mathbb{B}_{\text{full}}$ for the two-spin system as

$$\mathbb{B}_{\text{full}} = \{|\uparrow\uparrow\rangle, |\uparrow\downarrow\rangle, |\downarrow\uparrow\rangle, |\downarrow\downarrow\rangle\}. \tag{A.18}$$

The matrix elements of $\mathcal{H}$ written in $\mathbb{B}_{\text{full}}$ are calculated as

$$\mathcal{H} = \frac{1}{2}\begin{pmatrix} -h_1 - h_2 + \frac{1}{2}J_{12}^z & 0 & 0 & 0 \\ 0 & h_1 + h_2 + \frac{1}{2}J_{12}^z & 0 & 0 \\ 0 & 0 & -h_1 + h_2 - \frac{1}{2}J_{12}^z & -\frac{1}{4}J_{12} \\ 0 & 0 & -\frac{1}{4}J_{12} & h_1 - h_2 - \frac{1}{2}J_{12}^z \end{pmatrix}.$$

Only the coupling between states $|\uparrow\downarrow\rangle$ and $|\downarrow\uparrow\rangle$ does not vanish. Therefore, truncate the basis $\mathbb{B}$ to

$$\mathbb{B} = \{|\uparrow\downarrow\rangle, |\downarrow\uparrow\rangle\}. \tag{A.19}$$

The basis $\mathbb{B}$ is called *product basis* of the spin pair. Using $\mathbb{B}$, the matrix representation of $\mathcal{H}$ is obtained as

$$\mathcal{H}_D = \frac{1}{2}\begin{pmatrix} -h_{12} - \frac{1}{2}J_{12} & -\frac{1}{4}J_{12} \\ -\frac{1}{4}J_{12} & -h_{12} - \frac{1}{2}J_{12} \end{pmatrix},$$

where $h_{12} = h_1 - h_2$ is the local field of the spin pair.

A.3.2 Diagonalization

We diagonalize $\mathcal{H}$ via

$$\mathcal{H} = U^\top \mathcal{D}\, U, \tag{A.20}$$

using the change-of-basis matrix

$$U = \frac{1}{\sqrt{2}}\begin{pmatrix} \left(1 + \frac{h_{12}}{H}\right)^{\frac{1}{2}} & \left(1 - \frac{h_{12}}{H}\right)^{\frac{1}{2}} \\ -\left(1 - \frac{h_{12}}{H}\right)^{\frac{1}{2}} & \left(1 + \frac{h_{12}}{H}\right)^{\frac{1}{2}} \end{pmatrix} = \frac{1}{\sqrt{2}}\begin{pmatrix} c^+ & c^- \\ -c^- & c^+ \end{pmatrix}, \tag{A.21}$$

where

$$c^\pm = \left(1 \pm \frac{h_{12}}{H}\right)^{\frac{1}{2}}. \tag{A.22}$$

Since U is unitary, we determine its inverse U^{-1} by transposing U:

$$U^{-1} = U^\top = \frac{1}{\sqrt{2}} \begin{pmatrix} c^+ & -c^- \\ c^- & c^+ \end{pmatrix} \tag{A.23}$$

The diagonal matrix $\mathcal{D}$ in (A.20) consists of the two eigenvalues $\lambda_{1,2}$ of $\mathcal{H}$. We obtain $\lambda_{1,2}$ as

$$\lambda_{1,2} = \pm\frac{1}{2}\sqrt{h_{12} + \frac{1}{4}J_{12}} = \pm\frac{1}{2}H, \tag{A.24}$$

where $H = \sqrt{h_{12}^2 + \frac{1}{4}J_{12}^2}$ is denoted as energy of the spin pair $(1, 2)$.

The eigenvectors of the two-spin system are denoted as $|\Uparrow\rangle$ and $|\Downarrow\rangle$. We often refer to the basis $\mathbb{E} = \{|\Uparrow\rangle, |\Downarrow\rangle\}$ as *diagonal basis* of the spin pair.

Using $U^\top$, the eigenvectors are calculated as

$$|\Uparrow\rangle = c^+|\uparrow\downarrow\rangle - c^-|\downarrow\uparrow\rangle \tag{A.25}$$
$$|\Downarrow\rangle = c^-|\uparrow\downarrow\rangle + c^+|\downarrow\uparrow\rangle \tag{A.26}$$

A.3.3 Time evolution

We determine the time evolution of a wave function ψ as

$$\psi(t, x) = e^{-i\mathcal{H}t}\ \psi(0, x)\,. \tag{A.27}$$

By using the decomposition $\mathcal{H} = U^\top \mathcal{D}\ U$ from Equation (A.20), we obtain

$$\psi(t, x) = U^\top e^{-i\mathcal{D}t}\ U\ \psi(0, x)\,, \tag{A.28}$$

where $\mathcal{D}$ consists of the eigenvalues $\lambda_i = \pm\frac{1}{2}H$.

If we decompose the initial wave function $\psi(0, x)$ in terms of the eigenstates of the two spin system as

$$\psi(0, x) = c_1\ |\Uparrow\rangle + c_2\ |\Downarrow\rangle\,, \tag{A.29}$$

the time evolved wave function $\psi(t, x)$ is determined as

$$\psi(t, x) = c_1\ e^{-i\lambda_1 t}\ |\Uparrow\rangle + c_2\ e^{-i\lambda_2 t}\ |\Downarrow\rangle\,. \tag{A.30}$$

The probability to measure $\psi(t, x)$ in eigenstate $|\Uparrow\rangle$ is constant:

$$|\langle\Uparrow\ |\psi(t, x)\rangle|^2 = |c_1|^2\,, \tag{A.31}$$

but the probability to measure $\psi(t,x)$ in its initial state $\psi(0,x)$ typically oscillates in time:

$$|\langle\psi(0,x)|\psi(t,x)\rangle|^2 = |c_1|^4 + |c_2|^4 + 2|c_1|^2|c_2|^2 \cos\left((\lambda_1 - \lambda_2)\ t\right) . \quad \text{(A.32)}$$

We simplify this equation using $|c_1|^2 + |c_2|^2 = 1$ and $\omega = \lambda_1 - \lambda_2 = H$ to

$$|\langle\psi(0,x)|\psi(t,x)\rangle|^2 = 1 - 2|c_1|^2|c_2|^2 \left(1 - \cos\left(\omega t\right)\right) \quad \text{(A.33)}$$

and finally obtain

$$|\langle\psi(0,x)|\psi(t,x)\rangle|^2 = 1 - 4|c_1|^2|c_2|^2 \sin^2\left(\frac{\omega}{2}t\right) . \quad \text{(A.34)}$$

If the initial state is one of the product states, the wave function $\psi(t,x)$ oscillates between these states. We determine the period T of the oscillation from Equation (A.33) as

$$T = \frac{2\pi}{H} = 2\pi H^{-1} . \quad \text{(A.35)}$$

The value of the delay time of Eq. (2.18) is defined as one quarter of this period.

Finally, we determine the probability, that transition between the two product states occurs at time t_1, as

$$p_{\text{switch}} = \frac{1}{2}\ \frac{\frac{1}{4}J_{ij}^2}{H^2}\left(1 - \cos\left(Ht\right)\right) , \quad \text{(A.36)}$$

where we used $c_1 = c^+$ and $c_2 = c^-$, as well as Equation (A.22).

A.3.4 Resonance condition

In many parts of the thesis, we refer to *resonant pair*. The notion of a resonant pair is motivated by the consideration of two different cases for the parameter J_{12} and h_{12} of a spin pair.

- If J_{12} is small in comparison to h_{12}, the matrix $\mathcal{H}$ is similar to a diagonal matrix and the eigenstates are close to the original basis $\mathbb{E}$.
- If the opposite is true, the eigenstates are close to a mixed basis $\mathbb{E}' = \{\frac{1}{2}\left(|\uparrow\downarrow\rangle + |\downarrow\uparrow\rangle\ \right), \frac{1}{2}\left(|\uparrow\downarrow\rangle - |\downarrow\uparrow\rangle\right)\}$

In the latter case, we denote the spin pair as 'resonant pair', in the first case as 'non-resonant pair'. This motivates the condition

$$|h_1 - h_2| < |J_{12}| , \quad \text{(A.37)}$$

which determines the resonance state of a pair.

A.3.5 Derivation of the probability distribution of the resonance range S_{ij}

We can transform the resonance condition (A.37) to

$$S_{12} \equiv |J_{12}| - |h_{12}| > 0, \tag{A.38}$$

where S_{12} is called resonance range. Its probability distribution $p_{\mathrm{S}}(S)$ is derived from Equation (2.9) and (A.94) as

$$p_{\mathrm{S}}(S) = \int_{J_{\min}}^{\infty} p_J(J)\, p_{\Delta \mathrm{E}}(J - S)\, \mathrm{d}J, \tag{A.39}$$

where $p_{\Delta \mathrm{E}}(x) > 0$ for $0 \leq x \leq \varepsilon$. As a next step, we determine the domain of integration D. It is suitable to do a distinction of cases for S:

1. $S \geq J_{\min}$ where $D = [S, \varepsilon + S]$,
2. $S \leq J_{\min}$ and $S + \varepsilon \geq J_{\min}$ where $D = [J_{\min}, S + \varepsilon]$, and
3. $S + \varepsilon \geq J_{\min}$ where D is empty.

We will calculate p_{SR} for each case separately. First, we consider $D = [S, \varepsilon + S]$:

$$\begin{aligned} p_{\mathrm{S}}^{(1)}(S) &= \int_{S}^{\varepsilon+S} p_J(J)\, p_{\Delta E}(J - S)\, \mathrm{d}J \\ &= \frac{2J_{\min}}{\varepsilon^2} \int_{S}^{\varepsilon+S} \left(\frac{\varepsilon + S}{J^2} - \frac{1}{J} \right) \mathrm{d}J \\ &= \frac{2J_{\min}}{\varepsilon^2} \left[\frac{\varepsilon}{S} - \ln\left(\frac{\varepsilon + S}{S} \right) \right]. \end{aligned}$$

Then, $D = [J_{\min}, S + \varepsilon]$:

$$\begin{aligned} p_{\mathrm{S}}^{(2)}(S) &= \int_{J_{\min}}^{\varepsilon+S} p_J(J)\, p_{\Delta E}(J - S)\, \mathrm{d}J \\ &= \frac{2J_{\min}}{\varepsilon^2} \left[\frac{\varepsilon + S}{J_{\min}} - 1 - \ln\left(\frac{\varepsilon + S}{J_{\min}} \right) \right]. \end{aligned}$$

As a final result, we obtain

$$p_{\mathrm{S}}(S) = \begin{cases} 0 & : S \in (-\infty, J_{\min} - \varepsilon] \\ \frac{2J_{\min}}{\varepsilon^2} \left(\frac{\varepsilon+S}{J_{\min}} - 1 - \ln\left(\frac{\varepsilon+S}{J_{\min}} \right) \right) & : S \in [J_{\min} - \varepsilon, J_{\min}] \\ \frac{2J_{\min}}{\varepsilon^2} \left(\frac{\varepsilon}{S} - \ln\left(\frac{\varepsilon+S}{S} \right) \right) & : S \in [J_{\min}, \infty) \end{cases}.$$

A.3.6 Derivation of resonance probability without J^z fields

We use the probability distribution of the resonance range S_{ij} from the last subsection to derive a formula for the probability of a random pair to be resonant. Here, we neglect the presence of J^z fields. We will first calculate the probability $P_{\overline{\mathrm{RP}}}$ that a pair is non-resonant, namely

$$\begin{aligned} P_{\overline{\mathrm{RP}}} &= \int_{-\infty}^{0} p_{SR}(S)\,\mathrm{d}S = \int_{J_{\min}-\varepsilon}^{0} p_{SR}^{(2)}(S)\,\mathrm{d}S \\ &= \frac{2J_{\min}}{\varepsilon^2} \int_{J_{\min}-\varepsilon}^{0} \left[\frac{\varepsilon+S}{J_{\min}} - 1 - \ln\left(\frac{\varepsilon+S}{J_{\min}}\right)\right] \mathrm{d}S \\ &= 1 - \frac{J_{\min}^2}{\varepsilon^2} - \frac{2J_{\min}}{\varepsilon} \ln\left(\frac{\varepsilon}{J_{\min}}\right). \end{aligned}$$

The probability that a spin pair is resonant evaluates to

$$P_{\mathrm{RP}} = 1 - P_{\overline{\mathrm{RP}}} = \frac{J_{\min}^2}{\varepsilon^2} + \frac{2J_{\min}}{\varepsilon} \ln\left(\frac{\varepsilon}{J_{\min}}\right). \tag{A.40}$$

Next, we compare P_{RP} to the widely-used formula (2.12) [8, 10], which describes the probability p_{RP} for a spin to find a resonant partner in a sphere with radius R. Since P_{RP} represents the resonance probability for a given pair, we multiply it by the number of spins in this sphere:

$$p'_{RP} = \rho_{\mathrm{Spins}} \cdot \frac{4\pi}{3} R^3 \cdot P_{\mathrm{RP}} \approx 8\pi\rho_{\mathrm{Spins}} \frac{u_0}{\varepsilon} \log\left(\frac{R}{(u_0/\varepsilon)^{1/3}}\right), \tag{A.41}$$

neglecting the term proportional in ε^{-2} and using $J_{\min} = \frac{u_0}{R^3}$ from Equation (2.39). The derivation of (2.39) is only valid, if $J \ll \varepsilon$. Therefore, we can estimate the minimum distance, for which this equation holds, by the equation $J = \varepsilon$. This yields $R_{\min} = (u_0/\varepsilon)^{1/3}$.

Substituting $R_{\min}$ for $(u_0/\varepsilon)^{1/3}$ in Equation (A.41) gives

$$p'_{RP} \approx 8\pi\rho_{\mathrm{Spins}} \frac{u_0}{\varepsilon} \log\left(\frac{R}{R_{\min}}\right), \tag{A.42}$$

which reproduces Equation (2.12).

A.3.7 Transition probabilities for resonant pairs

As discussed in Section 2.2.2, the state of a spin pair is projected on states of a different basis if its resonance is changed. In the following subsection

we explain this projection and derive the probabilities for all possible transitions. First, we use the example of an non-resonant pair becoming resonant.

We consider an non-resonant spin pair (i,j) which has initial state $\psi_0 = |\uparrow\downarrow\rangle$. By a change of fields, its resonant condition is modified such that $|h'_{ij}| < J_{ij}$ holds. Hence, at the next time step, the pair (i,j) is identified as a resonant pair and after I_d time steps (delay time) its new state is chosen from $\{|\Uparrow\rangle, |\Downarrow\rangle\}$. We use the decomposition $|\uparrow\downarrow\rangle = c^+|\Uparrow\rangle + c^-|\Downarrow\rangle$ and obtain a probability $p_- = |c^-|^2$ for the transition $|\uparrow\downarrow\rangle \rightarrow |\Uparrow\rangle$ and a probability $p_+ = |c^+|^2$ for the transition $|\uparrow\downarrow\rangle \rightarrow |\Downarrow\rangle$. The coefficients $c^\pm$ of these projections are determined in Equation (2.13). In summary, the transition probabilities are determined as

$$\begin{aligned} p_{(\uparrow\downarrow \rightarrow \Uparrow)} &= p_{(\downarrow\uparrow \rightarrow \Downarrow)} = p_+ \\ p_{(\uparrow\downarrow \rightarrow \Downarrow)} &= p_{(\downarrow\uparrow \rightarrow \Uparrow)} = p_-, \end{aligned}$$

where

$$p_\pm = |c^\pm|^2 = \frac{1}{2}\left(1 \pm \frac{h_{ij}}{H}\right). \tag{A.43}$$

We obtain similar probabilities for the transitions from resonant to product states:

$$p_{(\Uparrow \rightarrow \uparrow\downarrow)} = p_{(\uparrow\downarrow \rightarrow \Uparrow)} = p_+ = \frac{1}{2}\left(1 + \frac{h_{ij}}{H}\right) \tag{A.44}$$

and likewise for the transitions $(\Uparrow \rightarrow \downarrow\uparrow)$, $(\Downarrow \rightarrow \uparrow\downarrow)$, $(\Downarrow \rightarrow \downarrow\uparrow)$.

If $h_{ij} \ll J_{ij}$ holds, the probabilities p_- and p_+ are equal: $p_+ = p_- = \frac{1}{2}$. This case corresponds to a resonant pair. Else, ff $h_{ij} \gg J_{ij}$, we obtain $p_+ = 1$ and $p_- = 0$ (in this case pair states and product states are exactly the same). This case corresponds to a non-resonant pair.

A.3.8 Correction of a spin pair (i,j) due to $S_i^z S_j^z$

This subsection is related to the calculation of J^z fields. This concept is discussed in Section 2.2.

In the following, we consider a spin pair (i,j) consisting of spins i and j and examine the effect of the product operator $S_i^z S_j^z$ on the resonance condition of (i,j). Since the respective fields f_i and f_j include the fields of all spins of the spin system, they include the field of their respective pair partner as well:

$$\begin{aligned} f_i &= f'_i - J_{ij} S_j^z \\ f_j &= f'_j - J_{ij} S_i^z, \end{aligned}$$

where we put the fields of all other spins and pairs to the variable f_i'. The resonance condition (2.20) contains the difference of fields $f_i - f_j$. Since a pair is always in one of the asymmetric states $|\uparrow\downarrow\rangle$ or $|\downarrow\uparrow\rangle$, we obtain

$$f_i - f_j = f_i' - f_j' - \sigma J_{ij} \tag{A.45}$$

where $\sigma \in \{\pm 1\}$ depends on the state of the spin pair. On the other hand, in the Hamiltonian of a two spin problem this term appears as a constant $-\frac{1}{4}J_{ij}$ and does not contribute to the resonance of i, j (see Appendix A.3). Therefore, we neglect it for the resonance condition by introducing a correction κ as

$$\kappa = \sigma J_{ij}, \tag{A.46}$$

where $\sigma = -1$ for the state $|\uparrow\downarrow\rangle$ and $\sigma = 1$ for $|\downarrow\uparrow\rangle$.

A.4 Investigation of a system consisting of four spins

In this section, we present a detailed study of the two-pair system. This system was introduced in Section 4.1.

A.4.1 Derivation of shifts and transition amplitudes

In the following, we derive equations for the shifts $h^{(i)}$ and their coupling elements $J^{(i)}$. Since the eigenvalues are symmetric in h_{34}, it suffices to calculate the two positive values of $h^{(i)}$. We will denote the smaller value $h^{(1)}$ as first shift, and the larger value $h^{(2)}$ as second shift.

We will first separate the Hamiltonian $\mathcal{H}$ into two parts $\mathcal{H} = \mathcal{H}_0 + d\mathcal{H}$. Then we will find the value of h_{34}, where two eigenvalues λ_i and λ_j of $\mathcal{H}_0$ cross: $\lambda_i = \lambda_j$. Next we will calculate the normalized eigenvectors v_i and v_j (related to λ_i and λ_j) for this specific value of h_{34} and obtain the coupling as $\langle v_i|H|v_j\rangle$.

We consider the same two pair setup as in the Section 4.1. Additionally, we require that the approximation

$$J_{34} \ll h_{34} \sim h_{12} \sim J_{12} \sim J_{pp} \tag{A.47}$$

holds. As discussed in Section 4.1, this approximation is good for $h_{34} \ll J_{34}$, which implies

$$h_{34} \approx H_2\,. \tag{A.48}$$

From the definitions of $A_{xx}, A_{zz}, A_{xz}, A_{zx}$ in Equation (2.34), we deduce

$$A_{xx} \sim J_{pp} \cdot \frac{J_{34}}{h_{34}}, \qquad A_{zx} \sim J_{pp} \cdot \frac{J_{34}}{h_{34}}$$
$$A_{zz} \sim J_{pp} \cdot 1, \qquad A_{xz} \sim J_{pp} \cdot 1\,.$$

We use these approximations to separate the pair-pair Hamiltonian $\mathcal{H}$ (Equation (2.30)) as $\mathcal{H} = \mathcal{H}_0 + \delta\mathcal{H}$, where

$$\mathcal{H}_0 = -H_1 I_1^z - H_2 I_2^z + A_{zz} I_1^z I_2^z + A_{xz} I_1^x I_2^z \tag{A.49}$$

and

$$\delta\mathcal{H} = A_{zx} I_1^z I_2^x + A_{xx} I_1^x I_2^x \,. \tag{A.50}$$

Note, that $\delta\mathcal{H}$ has no diagonal elements.

The eigenvalues of $\mathcal{H}_0$ are calculated as

$$\begin{aligned}
\lambda_1 &= -\frac{1}{4}\sqrt{(4H_1 + A_{zz})^2 + A_{xz}^2} + \frac{1}{2}H_2 \\
\lambda_2 &= \frac{1}{4}\sqrt{(4H_1 + A_{zz})^2 + A_{xz}^2} + \frac{1}{2}H_2 \\
\lambda_3 &= -\frac{1}{4}\sqrt{(4H_1 - A_{zz})^2 + A_{xz}^2} - \frac{1}{2}H_2 \\
\lambda_4 &= \frac{1}{4}\sqrt{(4H_1 - A_{zz})^2 + A_{xz}^2} - \frac{1}{2}H_2 \,.
\end{aligned}$$

The two square roots will appear more often and will be denoted as w_+ and w_-:

$$w_+ = \sqrt{(2H_1 + A_{zz})^2 + A_{xz}^2} \tag{A.51}$$

$$w_- = \sqrt{(2H_1 - A_{zz})^2 + A_{xz}^2} \,. \tag{A.52}$$

In order to obtain the two avoided crossings, we vary the value of $h_{34} \sim H_2$. A plot of the behaviour of λ_i can be found in Figure 4.2.

The first shift is obtained from $\lambda_1 = \lambda_3$:

$$H_2^{(1)} = \frac{1}{4}(w_+ - w_-) \,. \tag{A.53}$$

Analogous, the second shift is defined by $\lambda_1 = \lambda_4$ and results in

$$H_2^{(2)} = \frac{1}{4}(w_+ + w_-) \,. \tag{A.54}$$

Condition (A.48) yields

$$h^{(1)} = \frac{1}{4}(w_+ - w_-) \tag{A.55}$$

and

$$h^{(2)} = \frac{1}{4}(w_+ + w_-) \,. \tag{A.56}$$

Next, we derive the coupling amplitudes as $\langle v_i|H|v_j\rangle$. First, we obtain the eigenvectors of $\mathcal{H}_0$ as

$$v_1 = \begin{pmatrix} 0 \\ A_{zz}+2H_1+w_+ \\ 0 \\ A_{xz} \end{pmatrix}, \quad v_2 = \begin{pmatrix} 0 \\ A_{zz}+2H_1-w_+ \\ 0 \\ A_{xz} \end{pmatrix}, \tag{A.57}$$

$$v_3 = \begin{pmatrix} A_{zz}-2H_1-w_- \\ 0 \\ A_{xz} \\ 0 \end{pmatrix}, \quad v_4 = \begin{pmatrix} A_{zz}-2H_1+w_- \\ 0 \\ A_{xz} \\ 0 \end{pmatrix}. \tag{A.58}$$

As a next step, we normalize v_1,v_3,v_4. We derive $\langle v_i|v_i\rangle$ using the definitions (A.51) and (A.52) of w_+ and w_- as

$$\begin{aligned} \langle v_1|v_1\rangle &= 2w_+\,(w_+ + 2H_1 + A_{zz}) \\ \langle v_3|v_3\rangle &= 2w_-\,(w_- + 2H_1 - A_{zz}) \\ \langle v_4|v_4\rangle &= 2w_-\,(w_- - 2H_1 + A_{zz})\ . \end{aligned}$$

Hence, the coupling elements are determined as

$$J^{(1)} = \frac{\langle v_1|d\mathcal{H}|v_3\rangle}{\sqrt{\langle v_1|v_1\rangle}\cdot\sqrt{\langle v_3|v_3\rangle}} =: \frac{Z^{(1)}}{N^{(1)}} \tag{A.59}$$

and

$$J^{(2)} = \frac{\langle v_1|d\mathcal{H}|v_4\rangle}{\sqrt{\langle v_1|v_1\rangle}\cdot\sqrt{\langle v_4|v_4\rangle}} =: \frac{Z^{(2)}}{N^{(2)}}\,. \tag{A.60}$$

Using the definitions of the pair operators from Equation (2.34), $Z^{(i)}$ is obtained as

$$Z^{(1)} = \frac{J_{34}}{4}\left(\frac{J_{pp}^3\,h_{12}\,h_{34}^2}{2\,H_1\,H_2^3} + \frac{2\,J_{pp}^2\,h_{34}}{H_2} - \frac{J_{pp}\,h_{12}}{2\,H_1\,H_2}\left(2H_1(w_+ + w_-) + 4H_1^2 + w_+w_-\right)\right) \tag{A.61}$$

and

$$Z^{(2)} = \frac{J_{34}}{4}\left(\frac{J_{pp}^3\,h_{12}\,h_{34}^2}{2\,H_1\,H_2^3} + \frac{2\,J_{pp}^2\,h_{34}}{H_2} - \frac{J_{pp}\,h_{12}}{2\,H_1\,H_2}\left(2H_1(w_+ - w_-) + 4H_1^2 - w_+w_-\right)\right). \tag{A.62}$$

The normalization factors $N^{(i)}$ are calculated as

$$N^{(1)} = 2\sqrt{w_+\,w_-\,(w_+ + 2H_1 + A_{zz})\,(w_- + 2H_1 - A_{zz})} \tag{A.63}$$

and

$$N^{(2)} = 2\sqrt{w_+\,w_-\,(w_+ + 2H_1 + A_{zz})\,(w_- - 2H_1 + A_{zz})}. \tag{A.64}$$

Note, that the expressions w_- and w_+ still depend on operators A and therefore on the basic parameter h_{ij} and J_{ij}. The Equations (A.59) to (A.64) enable us to calculate the shift and the coupling elements of all transitions analytically.

A.4.2 Approximation for large and small value of J_{pp}

For a better physical intuition, we derive an approximation of Equations (A.59) to (A.64) for large values of J_{pp}. First, we will approximate the shifts $h^{(i)}$ and then their respective coupling amplitudes $J^{(i)}$.

For large value of J_{pp} we see that

$$\sqrt{A_{zz}^2 + A_{xz}^2} = \frac{J_{pp}}{H_1}\,\frac{h_{34}}{H_2}\sqrt{\frac{1}{4}J_{12}^2 + h_{12}^2} \approx J_{pp}\,, \tag{A.65}$$

where we use $H_1 = -\sqrt{h_{12}^2 + 0.25J_{12}^2}$. Taylor expansion of $w_\pm$ gives

$$\begin{aligned} w_\pm &= \left(A_{zz}^2 + A_{xz}^2\right) \pm \frac{2\,A_{zz}\,H_1}{\sqrt{A_{zz}^2 + A_{xz}^2}} + \frac{2A_{xz}^2\,H_1^2}{\sqrt{A_{zz}^2 + A_{xz}^2}^3} \\ &\approx J_{pp} \pm \frac{2\,A_{zz}\,H_1}{J_{pp}} + \frac{2A_{xz}^2\,H_1^2}{J_{pp}^3}. \end{aligned}$$

We approximate the shifts as

$$h^{(1)} = \frac{1}{4}(w_+ - w_-) = \frac{A_{zz}\,H_1}{J_{pp}} = h_{12}\,\frac{h_{34}}{H_2} \approx \frac{1}{2}J_{pp} + \mathcal{O}(J_{pp}^{-2}) \tag{A.66}$$

and

$$h^{(2)} = \frac{1}{4}(w_- + w_+) \approx \frac{1}{2}J_{pp} + \mathcal{O}(J_{pp}^{-1}) \tag{A.67}$$

For small J_{pp}, our basic assumption of $J_{34} \ll J_{pp}$ is violated and we cannot deduct approximations from the expressions of $h^{(i)}$ and $J^{(i)}$ from above. However, for the special case of $J_{pp} = 0$ the full diagonalization of $\mathcal{H}$ is trivial since all pair operators vanish. The first transition becomes the unperturbed resonant transition of the second pair at $h^{(1)} = 0$ with a coupling element $J^{(1)} = \frac{1}{4}J_{34}$, whereas the second transition has a vanishing transition element $J^{(2)} = 0$ at $h_{34} = \sqrt{H_1^2 - 0.25J_{34}^2}$.

A.4.3 Case of blocking

As described in Section 3.3, the situation, that a pair with weak interaction affects the resonance condition of a pair with strong interaction, is of special interest. In the following, we derive approximations for $h^{(i)}$ and $J^{(i)}$ and interpret their physical meaning. In order for this configuration to occur, we require

$$h_{12} \approx \frac{1}{2}J_{pp}\,. \tag{A.68}$$

If this condition holds, the first pair is resonant for one state of the second pair, and not resonant for the other. Additionally, we assume that the pair-pair coupling J_{pp} is larger than the internal interactions J_{12} and J_{34}. Thus,

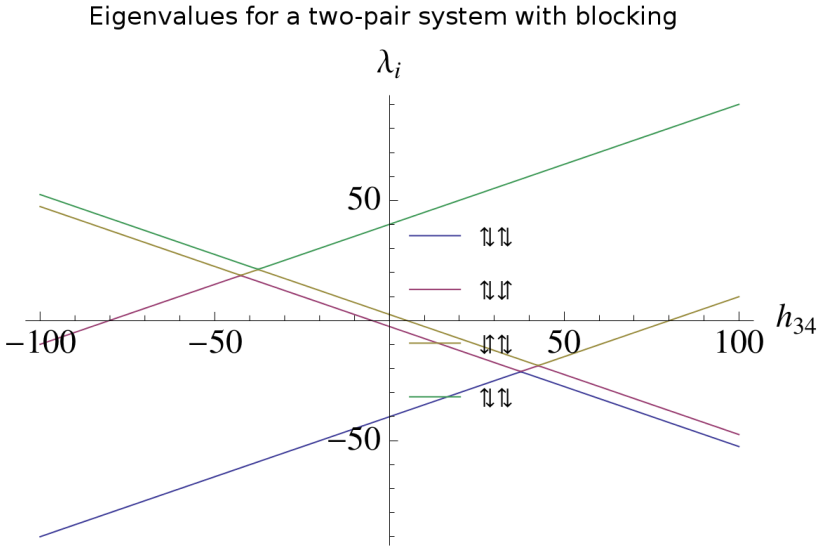

Figure A.1: Eigenvalues λ_i for $h_{12} = 42$, $J_{12} = 10$, $J_{pp} = 80$ and $J_{34} = 1$. There are two avoided crossings around $h_{34} \approx 40$.

$H_1 \approx h_{12}$ holds.

Figure A.1 shows one example of a setup with condition (A.68). We obtain two transitions at about $h_{34} \approx h_{12}$. Equation (4.4) and $H_1 \approx h_{12}$ yields

$$w_+ \approx 2h_{12} + J_{pp} \approx 4h_{12} \tag{A.69}$$

and

$$w_- \approx \frac{1}{2}\, J_{12}\, \frac{J_{pp}}{H_1} \approx J_{12}\,. \tag{A.70}$$

We substitute these approximations into Equation (4.5) and obtain

$$h^{(i)} = \frac{1}{4}(w_+ \pm w_-) = h_{12} \pm \frac{1}{4} J_{12}\,. \tag{A.71}$$

In the limit $h_{12} = \frac{1}{2}J_{pp}$, the two transitions occur at $h_{12} \pm \frac{1}{4}J_{12}$. Otherwise the shifts differ. Note that the resonance condition $h_{12} - \frac{1}{2}J_{pp} < J_{12}$ confines the deviation of h_{12} from $\frac{1}{2}J_{pp}$ to about J_{12}.

Next, we allow deviations of h_{12} from $\frac{1}{2}J_{pp}$ of the order of J_{12} (see Figure C.17). In this range, the value of $j^{(i)}$ can be approximated by

$$c^{\pm} = \frac{1}{\sqrt{2}} \left(1 \pm \frac{h_{12}}{H_1}\right)^{\frac{1}{2}}\,, \tag{A.72}$$

which were already observed in diagonalization the strong pair (section A.3.2). We see that the variables j and $c^{\pm}$ agree fairly well in Figure C.18.

The parameter $c^{\pm}$ represent the transition elements of the first pair from product to diagonal states:

$$\begin{aligned} c^{+} &= \langle \uparrow\downarrow | H | \Uparrow \rangle \\ c^{-} &= \langle \uparrow\downarrow | H | \Downarrow \rangle . \end{aligned}$$

Hence, the value of j is connected to the transition element of the first pair.

The transitions occur for $h_{34} \approx \pm h_{12}$, where the sign is determined by the state of the strong pair. This result agrees roughly with the algorithm of Chapter 3, where the J^z field of pair $(1,2)$ shift the resonance condition of pair $(3,4)$ by $A^{zz} \approx \frac{1}{2} J_{pp} = h_{12}$. However, instead of one resonance condition with transition element $\frac{1}{4} J_{34}$, we now obtain two conditions with reduced transition element $\frac{1}{4 \cdot \sqrt{2}} J_{34}$.

A.5 System of three pairs

In the following, we consider a system consisting of six spins, which are distributed on three pairs $p_1 = (1,2)$, $p_2 = (3,4)$ and $p_3 = (5,6)$. We assume that p_1 and p_3 are strong pairs of the weak pair p_2 and neglect the coupling between the strong pairs p_1 and p_3. This setup is depicted in Figure A.2.

If one of the parameter J_{23}, J_{45} vanishes, we obtain the standard situation of one weak and one strong pair. Now, we assign numbers to all parameter and determine the avoided level crossings of this system. We compare the shifts and transition amplitudes with the predictions we made earlier. As a parameter set, we chose:

$$h_{12} = 40, J_{12} = 20, h_{56} = 60, J_{56} = 30, J_{34} = 2, J_{23} = 80, J_{45} = 120 .$$

We obtain $2 \cdot h_{ij} = J_{pp}$ for both combination of pairs. From Section 4.1, we obtain the shifts $h^{(i)}$ for one strong/weak pair combination as:

$$h = h_{ij} \pm \frac{1}{4} J_{ij} , \tag{A.73}$$

where h_{ij}, J_{ij} are the parameter of the strong pair. We obtain these shifts in our six spin system by setting $J_{pp} = 0$ for the other strong pair. For $J_{23} = 0$, we obtain Figure A.3 and obtain the shifts of the two pair problem (p_2, p_3) as

$$h^{(3)} = 52.5 \tag{A.74}$$

$$h^{(4)} = 67.5. \tag{A.75}$$

Similar, we obtain the shifts

$$h^{(1)} = 35 \tag{A.76}$$

$$h^{(2)} = 45. \tag{A.77}$$

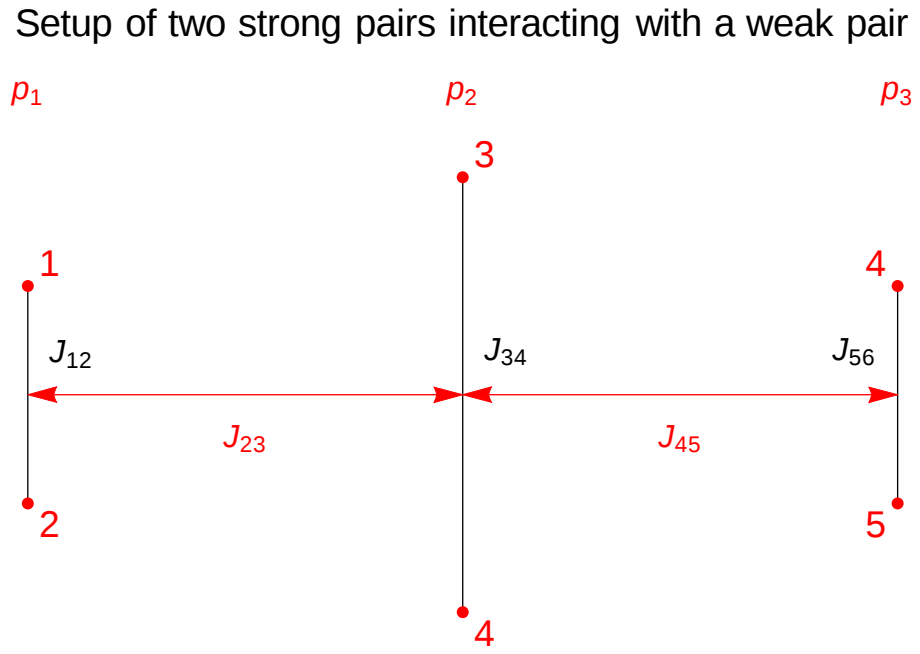

Figure A.2: Setup for a 6 spin system. Coupling is allowed in pairs p_1, p_2, p_3 and between the pairs p_1 and p_2, and p_2 and p_3.

of the two pair problem (p_1, p_2) from $J_{45} = 0$.

As a next step, we measure the distances d between the levels to determine the transition elements. We obtain

$$d^{(1)} = 0.75 \tag{A.78}$$
$$d^{(2)} = 0.65 \tag{A.79}$$
$$d^{(3)} = 0.75 \tag{A.80}$$
$$d^{(4)} = 0.65\,. \tag{A.81}$$

From $d = 2J$ and $J = \frac{1}{4} J_{34} j$ we deduce

$$d = \frac{1}{4} \cdot 2 \cdot 2 \cdot j \tag{A.82}$$

which implies $j = d$. This gives the transition amplitude prefactors $j^{(i)}$ directly as

$$j^{(1)} = 0.75 \tag{A.83}$$
$$j^{(2)} = 0.65 \tag{A.84}$$
$$j^{(3)} = 0.75 \tag{A.85}$$
$$j^{(4)} = 0.65\,. \tag{A.86}$$

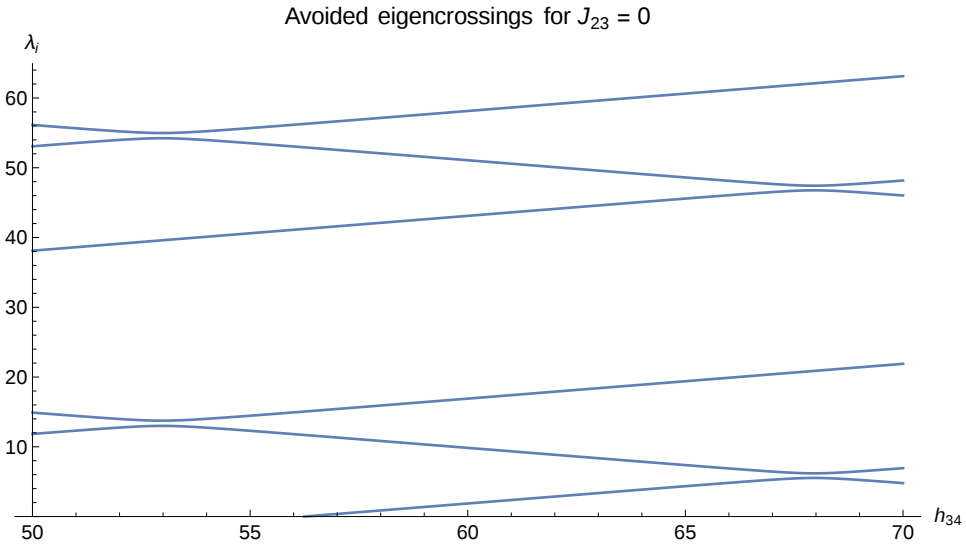

Figure A.3: Avoided level crossing of the eigenvalues λ_i for a six spin system. Since $J_{23} = 0$, only p_2 and p_3 are coupled and we obtain the shifts and transition amplitudes from the two pair problem. The shifts are at $h^{(3)} = 52.5$ and $h^{(4)} = 67.5$. For each shift value we see two transitions.

Now, we turn our attention to the fully interacting 6 spin system. A plot of the eigenvalues can be found in Figure A.4, where one group of four crossings is plotted in A.5. We see four groups of avoided crossings. We obtain the eight positive shifts h^A to h^H as

$$\begin{aligned} h^A &= 7.5 \\ h^B &= 17.5 \\ h^C &= 22.5 \\ h^D &= 32.5 \\ h^E &= 87.5 \\ h^F &= 97.5 \\ h^G &= 102.5 \\ h^H &= 112.5. \end{aligned}$$

In Section 4.2.1, we predicted, that each shift h^α of the 3-pair problem is a combination of the shifts $h^{(i)}$ obtained from the 2-pair interaction:

$$\forall \alpha \quad \exists i, j: \quad h^\alpha = h^{(i)} \pm h^{(j)} \tag{A.87}$$

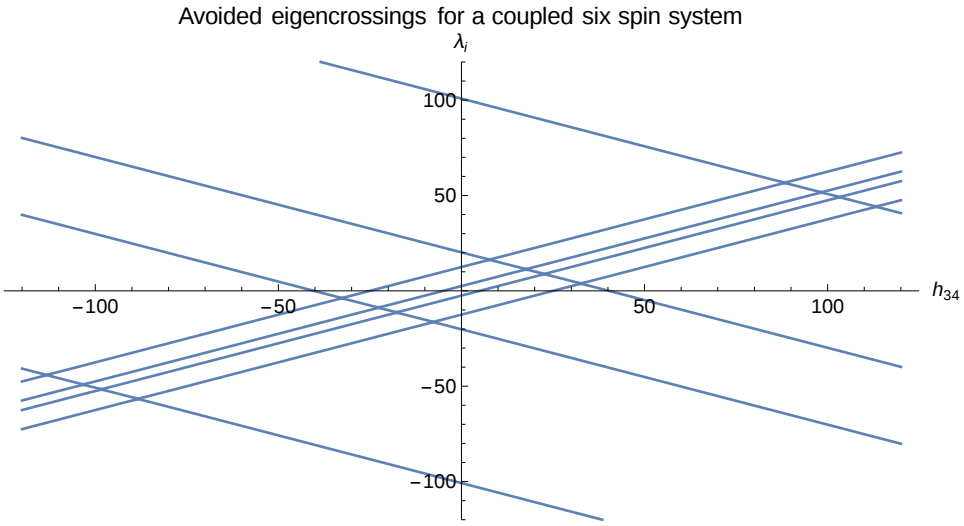

Figure A.4: Avoided level crossing of the eigenvalues λ_i for a six spin system with interactions $J_{23} = 80$ and $J_{45} = 120$. This implies, that the weak pair $p_2 = (3, 4)$ is coupled to the strong pair $p_1 = (1, 2)$ and the strong pair $p_3 = (56)$.

Indeed we find

$$\begin{aligned} h^A &= h^{(3)} - h^{(2)} \\ h^B &= h^{(3)} - h^{(1)} \\ h^C &= h^{(4)} - h^{(2)} \\ h^D &= h^{(4)} - h^{(1)} \\ h^E &= h^{(3)} + h^{(1)} \\ h^F &= h^{(3)} + h^{(2)} \\ h^G &= h^{(4)} + h^{(1)} \\ h^H &= h^{(4)} + h^{(2)}. \end{aligned}$$

As a next step, we obtain the transition amplitude factors j^α from the distances d^α between the levels. We obtain

$$\begin{aligned} j^A = d^A &= 0.5 \\ j^B = d^B &= 0.55 \\ j^C = d^C &= 0.45 \\ j^D = d^D &= 0.5 \\ j^E = d^E &= 0.55 \\ j^F = d^F &= 0.5 \\ j^G = d^G &= 0.5 \\ j^H = d^H &= 0.45 \end{aligned}$$

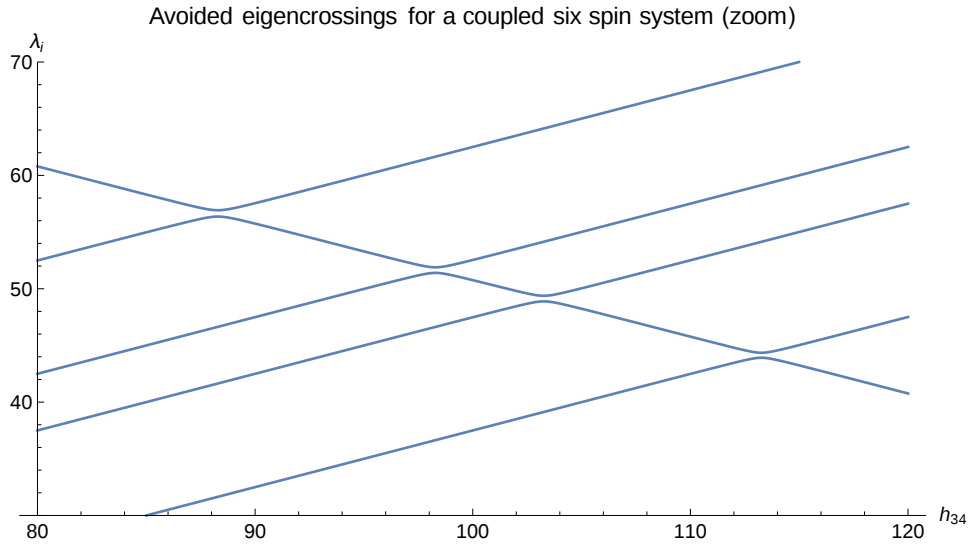

Figure A.5: We used the same setup as for Figure A.4, but chose the axis such, that we zoom into one group of four avoided crossings.

We expect from Equation (A.87), that

$$j^{\alpha} = j^{(i)} \cdot j^{(j)}\,, \tag{A.88}$$

where we determine i, j from identifying h^{α} in Equation (A.87). This yields

$$\begin{aligned}
j^{A} &= j^{(3)} \cdot j^{(2)} = 0.49 \\
j^{B} &= j^{(3)} \cdot j^{(1)} = 0.56 \\
j^{C} &= j^{(4)} \cdot j^{(2)} = 0.42 \\
j^{D} &= j^{(4)} \cdot j^{(1)} = 0.49 \\
j^{E} &= j^{(3)} \cdot j^{(1)} = 0.56 \\
j^{F} &= j^{(3)} \cdot j^{(2)} = 0.49 \\
j^{G} &= j^{(4)} \cdot j^{(1)} = 0.49 \\
j^{H} &= j^{(4)} \cdot j^{(2)} = 0.42
\end{aligned}$$

The predictions (A.87) and (A.88) agree fairly well with the values directly obtained from the simulation of the full three-pair system.

A.6 Techniques of Probability Theory

In Chapter 2.5, we derive probability distributions using properties of probability density functions. Hence, we shortly introduce density functions and describe some of their properties. The definitions and derivations can be

found in the book of Papoulis on Probability Theory [18].

A density function is defined such, that the integral over a certain range I gives the probability $P(x \in I)$ to measure $x \in I$:

$$P(x \in I) = \int_I p_x(x)\mathrm{d}x \tag{A.89}$$

A probability density function is strictly positive and its integral over the full space is 1. As a representative for many interesting features, we discuss a transformation from x to $y = y(x)$. In one dimension, $p_x(x)$ transforms as

$$p_y(y) = p_x(x)\left|\frac{\mathrm{d}x}{\mathrm{d}y}\right|, \tag{A.90}$$

where we have to substitute $y(x)$ on the right side of the equation to obtain $p_y(y)$ as a function of y. In n dimensions, the derivative $\frac{\mathrm{d}x}{\mathrm{d}y}$ is substituted by the Jacobian

$$J(\vec{x}) = \begin{pmatrix} \frac{\mathrm{d}y_1}{\mathrm{d}x_1} & \cdots & \frac{\mathrm{d}y_1}{\mathrm{d}x_n} \\ \vdots & \ddots & \vdots \\ \frac{\mathrm{d}y_n}{\mathrm{d}x_1} & \cdots & \frac{\mathrm{d}y_n}{\mathrm{d}x_n} \end{pmatrix}$$

and we obtain

$$p_{\vec{y}}(\vec{y}) = p_{\vec{x}}(\vec{x})\left|J^{-1}(\vec{x})\right|. \tag{A.91}$$

Following the lines of Papoulis, this equation determines the convolution of several different density functions to one combined density function [18]. As a standard example, we consider the sum $y = x_1 + x_2$ of two independent random variables x_1 and x_2 with arbitrary density functions $p_{x_1}(x_1)$ and $p_{x_2}(x_2)$.

In this case, the Jacobian of the transformation

$$\begin{aligned} y_1 &= x_1 \\ y_2 &= x_1 + x_2 \end{aligned}$$

evaluates to

$$|J(\vec{x})| = \begin{vmatrix} 1 & 0 \\ 1 & 1 \end{vmatrix} = 1\,.$$

By using Equation (A.91), the combined probability distribution is found to be

$$p_{\vec{y}}(\vec{y}) = p_{x_1}(y_1)p_{x_2}(y_2 - y_1). \tag{A.92}$$

In the specific example $y = x_1 + x_2$, we obtain

$$p_{x_1+x_2}(x_1 + x_2) = p_{y_2}(y_2) = \int p_{\vec{y}}(\vec{y})\mathrm{d}y_1 = \int p_{x_1}(x_1)p_{x_2}(y_2 - x_1)\mathrm{d}x_1, \tag{A.93}$$

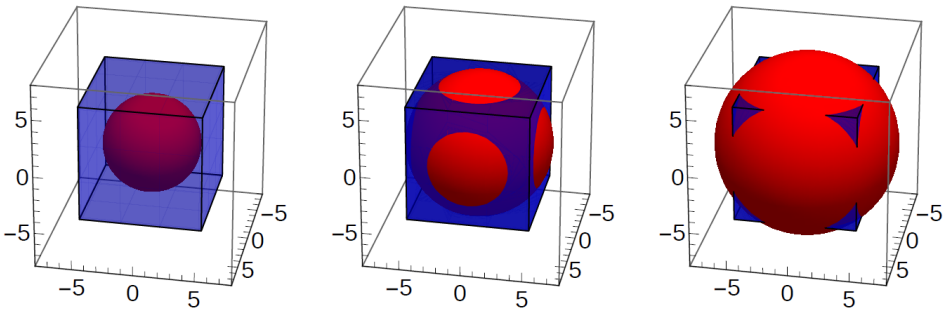

Figure A.6: Calculation of $p_r(r)$ for the three different ranges $r < 5$ (left plot), $5 < r < 5\sqrt{2}$ (medium plot) and $5\sqrt{2} < r < 5\sqrt{3}$ (right plot). Only the part of the red sphere, that is inside the cube, contributes to the distribution function $p_r(r)$.

integrating over the full range of $x_1 = y_1$. The density function for $x_1 - x_2$ can be derived similarly using the transformation $y_1 = x_1$ and $y_2 = x_1 - x_2$:

$$p_{x_1-x_2}(x_1 - x_2) = p_{y_2}(y_2) = \int p_{x_1}(x_1)p_{x_2}(y_2 + x_1)\mathrm{d}x_1. \tag{A.94}$$

The technique of convoluting two density functions are used to proceed from density functions of basic variables to more complex ones.

A.7 Distribution for r with finite size effect

Section 2.5.1 derived the density function $p_r(r)$ without finite size effect as

$$p_r(r) \sim r^2. \tag{A.95}$$

In the following paragraph, the distribution function $p_r(r)$ is calculated including the finite size of the cube. We use the fact, that the probability to measure a specific value of r is proportional to the surface of a sphere with radius r.

The finite size of the system is represented by a cube of length l. Only the part of the surface of the sphere, which is inside of this cube, does contribute to the probability density function $p_r(r)$. Figure A.6 visualizes this setup for three different values of r. We calculate the function $p_r(r)$ differently for these values of r, where we discriminate between three ranges:

1. $r \in [0, l/2]$,
2. $r \in [l/2, \sqrt{2}l/2]$, and
3. $r \in [\sqrt{2}l/2, \sqrt{3}l/2]$.

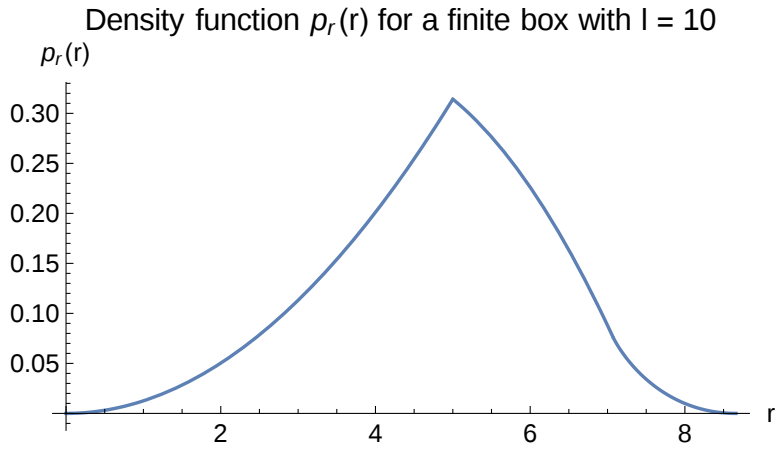

Figure A.7: Plot of $p_r(r)$ for a finite box with length $l = 10$. The critical points are at $r = 5$, $r = 5\sqrt{2} = 7.07$ and $r = 5\sqrt{3} = 8.66$.

For larger values of r, the complete surface of the sphere is on the outside of the cube. Hence, the probability for these values is 0.

In the first interval, the full surface is on the inside of the cube. In this case, the finite size does not influence the probability density function and we obtain $p_r(r)$ from Equation (A.95) as $p_r^{(1)}(r) = 4\pi r^2$.

For $p_r^{(2)}(r)$, the part of the surface, which is not inside the cube, can be described as four spherical caps (see Figure A.6). One spherical cap has the surface $S_{cap} = 2\pi rh$, where h is the height of the cap. Hence, $h = r - l/2$. The full surface inside the cube becomes

$$p_r^{(2)}(r) = S_{sphere}(r, l) = 4\pi r^2 - 6\, S_{cap} = 6\pi lr - 8\pi r^2. \tag{A.96}$$

The third function $p_r^{(3)}(r)$ can be obtained by integrating over this area:

$$p_r^{(3)}(r) = 24r^2 \int_{\sqrt{r^2-(l/2)^2-(l/2)^2}}^{l/2} \int_{\sqrt{r^2-(l/2)^2-y^2}}^{l/2} \frac{l}{2(\sqrt{x^2+y^2+(l/2)^2})^3}\, \mathrm{d}x\, \mathrm{d}y \tag{A.97}$$

The composite function is normalized and then presented in Figure A.7. It agrees with numerical results of the simulation. This derivation shows as an example, how the finite size of the box influences the statistics of the spin system.

A.8 Analytical derivation of the density function $p_{Jsp}(J_{sp})$

We obtain a probability density function for J_{sp} from Equation (4.20) as

$$p_{J_{sp}}(J_{sp}) = 0.001 \frac{\mathrm{d}V(J_{sp})}{\mathrm{d}J_{sp}}\,, \tag{A.98}$$

where V is the volume of a sphere-like body around the strong pair. In order to derive an expression for $p_{J_{sp}}$, we investigate the functional dependence of V on J_s and J_{sp}^{fixed}. The equation

$$\frac{1}{r_{il}^3} - \frac{1}{r_{jl}^3} = J_{sp}^{\text{fixed}} \tag{A.99}$$

defines the surface of V. We define the z-axis as the line connecting spins i and j and choose the origin in the middle. Thereby we find

$$r_{il} = \sqrt{(z - d/2)^2 + x^2 + y^2} \tag{A.100}$$
$$r_{jl} = \sqrt{(z + d/2)^2 + x^2 + y^2}. \tag{A.101}$$

The simplification $x = y = 0$ leads to the cubic equation

$$(z + d)^3 - z^3 = J_{sp} \cdot z^3 \cdot (z + d)^3. \tag{A.102}$$

Its solutions define the two intersections z_l and z_r of V with the z-axis:

$$z_r = -\frac{d}{2} + \frac{d}{2}\sqrt{-0.1\sqrt{x} + \frac{6.9282}{\sqrt{x}} + \frac{5}{3}} \tag{A.103}$$
$$z_l = \frac{d}{0.06x + 0.003278x\sqrt{x} - 0.013\sqrt{x} + 2} \tag{A.104}$$

where $x = d^3 \cdot J_{sp} = \frac{J_{sp}}{J_s}$ denotes the ratio of spin-pair interaction and internal pair interaction. Figure A.8 shows an example of z_r and z_l for $d = 0.5$ and $J_{sp} = 10$.

We estimate V as a sphere with radius $\frac{z_l + z_r}{2}$ and obtain the volume of both bodies as

$$V(z_r, z_l) = 2 \cdot c \cdot \frac{4}{3}\pi \cdot \left(\frac{z_l + z_r}{2}\right)^3 = 17.71 \left(\frac{z_l + z_r}{2}\right)^3 \tag{A.105}$$

where we fit $c = 2.11$ from numerical data (Figure C.20 in Appendix C).

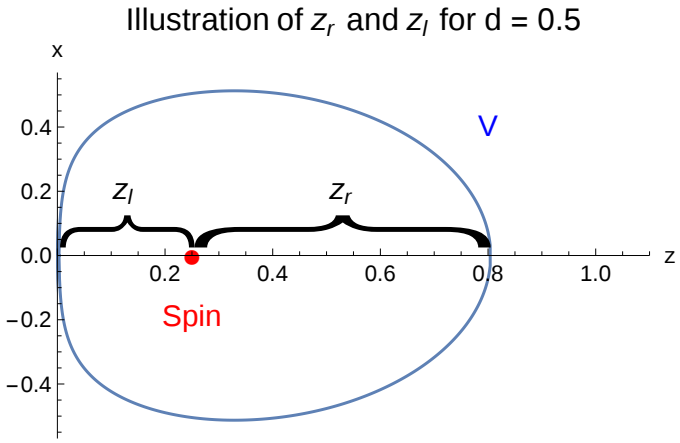

Figure A.8: Definition of the variables z_r and z_l from Equation (A.104). The choice $d = 0.5$ and $J_{sp} = 5$ results in $z_r = 0.554$ and $z_l = 0.246 \approx d/2$. The second spin of the pair is situated at $z = -0.25$.

As a next step, we assume $J_s \gg J_{sp}$. The assumption $J_s \gg J_{sp}$ leads to $x \ll 1$ and results in $z_l \approx d/2$. Likewise, z_r can be approximated as

$$z_r = -\frac{d}{2} + \frac{d}{2}\sqrt{\frac{5}{3} + \frac{6.93}{\sqrt{x}}} \approx -\frac{d}{2} + 1.31\ \frac{d^{1/4}}{J^{1/4}} \tag{A.106}$$

where $x = d^3 \cdot J_{sp}$. Equations (A.105) and (A.106) give

$$V(J_s, J_{sp}) = 2.21\,(z_l + z_r)^3 \approx 2.21\left(1.31\ \frac{d^{1/4}}{J^{1/4}}\right)^3 = 5.04\ J_{sp}^{-3/4}\ J_s^{-1/4} \tag{A.107}$$

where we used $J_s = d^{-3}$.

Now, we return to the calculation of the probability density function $p_{J_{sp}}(J_{sp})$. By using its definition via V, we obtain an approximation for $p_{J_{sp}}(J_{sp})$ holding for $J_s > 1$ as

$$p_{J_{sp}}(J_{sp}) = 0.001\left|\frac{\mathrm{d}V(J_{sp})}{\mathrm{d}J_{sp}}\right| = 0.015\ J_{sp}^{-7/4}\ J_s^{-1/4} \tag{A.108}$$

A.9 Derivation of the probability $p_{\mathbf{link}}$

This section derives the probability p_{link} of a spin pair, to form a link to an arbitrary other pair.

The algorithm determines a link in two steps: First, it examines a strong pair sp_1 with interaction J_s and on-site field h_s. Thereby it finds all spins,

that change the resonance of pair sp_1 (important parameter is the spin-pair interaction J_{sp}). Then, it investigates if spin pairs sp_2 with interaction J_w consisting of one of these spins satisfy the following conditions:

$$\begin{aligned} J_w &< J_s && \text{(A.109)} \\ h_w &< J_w && \text{(A.110)} \\ |h_s - J_s| &< J_{sp} && \text{(A.111)} \\ J_{sp} &> c \cdot J_s && \text{(A.112)} \end{aligned}$$

The probability, that both the first and the second condition are satisfied, is represented by the variable p_{weak}. The third condition refers to the probability p_{strong} and the fourth to p_c. We chose $c = 0.5$.

By multiplying all these probabilities, we obtain the expression

$$p_{\text{Link}} = \int p_{J_{sp}}(x, J_s, \varepsilon)\,(x)\, p_{\text{weak}}(x, J_s, \varepsilon)\, p_{\text{c}}(x, J_s)\, p_{\text{strong}}(x, J_s, \varepsilon)\, \mathrm{d}x \tag{A.113}$$

for the linking probability p_{link}. In the following part we determine each probability separately.

Derivation of p_{weak}

First, we determine the number of weak pairs N, that satisfy the condition

$$J_s > J_w \tag{A.114}$$

for a selected strong pair and a selected spin. We integrate over the distribution of J_w and use $p_J(J) = \frac{J_{\min}}{J^2}$ from Section 2.5.1 to determine the probability for one arbitrary weak pair as

$$p^{\text{single}} = \int_{J_{\min}}^{J_s} \frac{J_{\min}}{J^2} \mathrm{d}J = \left(1 - \frac{J_{\min}}{J_s}\right). \tag{A.115}$$

Now we transform the single probability (one selected weak pair) to the probability for one selected spin. This spin has 248 possible partners on average. This number results from two arguments: First, the possible partner has to have the opposite spin polarization. Second, we need a another correction of a factor of 2 because we double count each pair. Finally, we exclude the spins of the strong pair and the single spin from the number of possible partners.

As a result, we obtain the average number of

$$N = 248 \cdot \left(1 - \frac{J_{\min}}{J_s}\right) \tag{A.116}$$

weak pairs with interaction $J_w < J_s$.

Now, we derive the probability p_{weak}, that one of these pairs satisfies its resonant condition. We estimate this probability by using the classical condition $|h_{ij}| < J_{ij}$ and obtain

$$p_{\text{RC}} = 2\frac{J_w}{\varepsilon} - \frac{J_w^2}{\varepsilon^2} \tag{A.117}$$

for a weak pair with interaction J_w. The resulting probability p_{weak} follows as

$$p_{\text{weak}} = 1 - (1 - p_{\text{RC}})^N \approx 1 - e^{-N \cdot p_{\text{RC}}}, \tag{A.118}$$

where $N = 248 \cdot \left(1 - \frac{J_{\min}}{J_s}\right)$.

Derivation of $p_{\mathbf{c}}$

The variable p_{c} represents the probability, that $J_{pp} > c \cdot J_s$ holds. Both variables are not free and we obtain

$$p_{\text{c}} = \Theta(J_{pp} - c \cdot J_s)\,, \tag{A.119}$$

where $\Theta(x)$ denotes the Heaviside step function. In the simulation, we use $c = 0.5$.

Derivation of $p_{\mathbf{strong}}$

The probability p_{strong} describes the likelihood, that condition

$$|h_s - J_s| < J_{sp} \tag{A.120}$$

is satisfied for a given strong pair and given variable J_{sp}.

First, we calculate p_{strong} for $J_s > J$. In order to satisfy condition (A.120), we require that $J_s - J_{sp} < h_s < J_s - J_{sp}$ holds. Since J_s and J_{sp} are fixed, we obtain p_{strong} by integrating over the remaining variable h_s as

$$p_{\text{strong}} = \int_{J_s - J_{sp}}^{J_s + J_{sp}} p_h(h)\ \mathrm{d}h = \frac{2}{\varepsilon^2} \int_{J_s - J_{sp}}^{J_s + J_{sp}} (\varepsilon - h)\ \mathrm{d}h = \frac{4J_{sp}}{\varepsilon^2}\,(\varepsilon - J_s)\ , \tag{A.121}$$

where we used $p_h(h)$ from Equation 2.42. Similar, we obtain p_{strong} for $J_s > J$ as

$$p_{\text{strong}} = \int_{0}^{J_s + J_{sp}} p_h(h)\ \mathrm{d}h = \frac{1}{\varepsilon^2}\left(\varepsilon(J_s + J_{sp}) - \frac{1}{2}(J_s + J_{sp})^2\right)\ . \tag{A.122}$$

Appendix B

Algorithms

B.1 Classical resonant pair routine

First, the simulation constructs a list of all spin pairs (i, j) where $i < j$ and $i, j = 1 \ldots 1000$. In total, that gives the number of 499500 pairs. For every pair, we calculate its energy splitting h_{ij} and its interaction J_{ij} as

$$\begin{aligned} h_{ij} &= h_i - h_j \\ J_{ij} &= \frac{u_0 \left(1 - 3\cos^2 \theta_{ij}\right)}{r_{ij}^3} \end{aligned}$$

where we obtain the distance r_{ij} of the spins i and j using periodic boundaries:

$$\begin{aligned} r_{ij} &= \sqrt{x_{ij}^2 + y_{ij}^2 + z_{ij}^2} \\ x_{ij} &= \min\left(|x_i - x_j|, |x_i - x_j + x_{\max}|, |x_i - x_j - x_{\max}|\right) \\ y_{ij} &= \min\left(|y_i - y_j|, |y_i - y_j + y_{\max}|, |y_i - y_j - y_{\max}|\right) \\ z_{ij} &= \min\left(|z_i - z_j|, |z_i - z_j + z_{\max}|, |z_i - z_j - z_{\max}|\right) \end{aligned}$$

with the coordinates x_i, y_i, z_i of spin i. We determine the dependence on θ_{ij} as

$$\cos(\theta_{ij}) = z_{ij}/r_{ij} \tag{B.1}$$

As a next step, the routine defines a list *SPs* of pairs, where each spin pair has the parameter (i, j, h_{ij}, J_{ij}). Finally, we sort *SPs* with respect to the absolute value of the pair interactions J_{ij}, where the pair with largest interaction J_{ij} is the first element of *SPs*.

We start identifying resonant pairs by labeling every spin pair as non-resonant. Then, we check the resonance condition

$$|h_{ij}| < J_{ij} \tag{B.2}$$

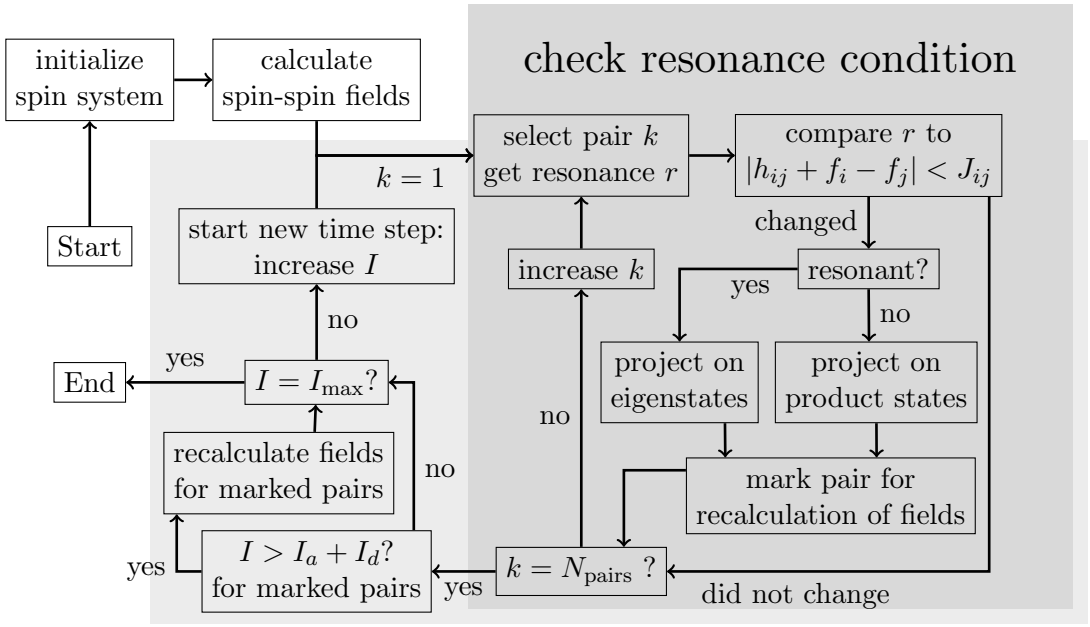

Figure B.1: Flowchart of the evolution algorithm. The light gray rectangle marks the forloop over the time steps I, the dark gray rectangle the subroutine that checks the resonance condition of pair k. The resonance r can be either true or false, dependent whether pair $k = (i, j)$ is labeled a resonant pair or not. Initially, all pairs are labeled as non-resonant.

for every element of *SPs*. We start at the top of the list and proceed downwards. If (B.2) is evaluated true, the simulation determines if one of the two participating spins is already part of another resonant pair. If that is the case, we have a conflict, since one spin is part of at least two resonant pairs. Assume that the second pair has index k_2 in *SPs*, whereas the original pair has index k_1. Since the pair with index k_2 is already labeled resonant, it was checked earlier in the list and we deduce $k_1 > k_2$. By construction of the list it follows that the interaction J_1 of the original pair is smaller than the interaction J_2 of the second pair.

Due to the argumentation from Section 2.2.3, we keep the second pair as resonant and treat the original pair as non-resonant. After the execution of the routine we checked every spin pair whether it is resonant or not. The results of this basic algorithm can be found in Section 2.5.3.

B.2 Time evolution

B.2.1 Initialization

First, the spin system is initialized and fields are calculated and assigned to every spin. We assume that there are no resonant pairs present at initial time $t = 0$.

After the initialization is complete, the algorithm starts the time evolution by executing the first time step. Each time step describes the time evolution from t_n to $t_{n+1} = t_n + \Delta t$ and consists of two main steps:

1. identification of resonant pairs.
2. check of the delay time of pairs and recalculation of fields.

where each step is examines spin pairs individually.

B.2.2 Identification of resonant pairs

Central to this procedure is a list of all spin pairs (i, j), which is ordered with respect to their interaction J_{ij} (starting with the largest value). The routine examines spin pairs individually by going from the top to the bottom of this list. First it checks the resonance condition (2.21). If this condition is evaluated true, the pair is labeled as a resonant pair and all pairs that share a spin with this pair are excluded from the search for resonant pairs in this time step. By this we avoid conflicts (see subsection B.1).

B.2.3 Recalculation of fields

As discussed in the outline of the algorithm, the routine delays the projection on new states and the recalculation of the field by a number of time steps

$$I_d = \lfloor \frac{t_d}{\Delta t} \rfloor = \lfloor \pi \, (2 \; H \; \Delta t)^{-1} \rfloor \,, \tag{B.3}$$

where $\lfloor x \rfloor$ denotes the floor function of x and rounds x down to an integer value.

After the search for resonant pairs, the routine starts again at the top of the list of all spin pairs (i, j) ordered by their interaction J_{ij}. There are two kinds of spin pairs at this point:

- Pairs, for which the basis of their wave functions and their resonance agree. These are non-resonant pairs in product basis or resonant pairs in eigenstate basis.

- Pairs, for which the basis of their wave function and their resonance do not agree. These pairs wait for the projection into their natural basis.

As an example, pairs that changed their resonance in the last search for resonant pairs are of the second kind. For all these pairs, we check if

$$I > I_a + I_d \tag{B.4}$$

holds true. Here, I_a identifies the time step number where the last change of the resonance state of this pair happened. The number I_d represents the delay time t_d and was defined in (B.3).

If Equation (B.4) holds true, the wave function of the pair is projected to the new basis using the probabilities from Equation (A.43) to (A.44). Otherwise nothing happens.

After the projection of ψ, the algorithm adjusts the field the pair imposes on other spins as discussed in Section 2.3.1. If $I_d = 0$, this adjustment happens in the same time step as the identification as a resonant or non-resonant pair. Else, there is a chance, that a spin pair does change its resonance again before its wave function is projected to its natural basis. In this case, we separate between the two possible transitions:
In the first case, an non-resonant pair is identified as resonant at time step I_1 and again as non-resonant at time step I_2. Since $I_d > I_2 - I_1$, the pair has not yet changed to the diagonal basis. Nonetheless, the pair is close to resonance for some time $t = I_1 \cdot \Delta t - I_2 \cdot \Delta t = t_1 - t_2$ and we expect a non-vanishing probability p_{switch} to switch states from $|\uparrow\downarrow\rangle$ to $|\downarrow\uparrow\rangle$ or vice versa.

We calculate this probability by evolving the pair-wave function ψ in time from $t_1 = I_1 \cdot \Delta t$ to $t_2 = I_2 \cdot \Delta t$. Then we determine the projection of ψ at time t_2 on the product states. These projections define the probabilities to remain in the original product state or to flip both spins to produce the second product state. We obtain the probability p_{switch} to switch states in Section A.3.3 as

$$p_{\text{switch}} = \frac{J_{ij}}{h_{ij}^2 + \frac{1}{4}J_{ij}^2} \sin\left(\frac{H}{2}\,(t_1 - t_0)\right) . \tag{B.5}$$

The algorithm switches the product state using the probability p_{switch}. As a result, we obtain an non-resonant pair in its natural basis (product states).

In the second case, a resonant pair is identified as non-resonant at time step I_1 and again as resonant at time step I_2, where we assume that $I_d > I_2 - I_1$

holds. Therefore, the pair has not yet switched to product states. This transition generally happens much faster than in the previous case. Hence, the algorithm keeps the original pair state for the wave function ψ and we obtain a resonant pair in natural basis (eigenstates).

B.2.4 Selection of the time increment Δt

In order to relate the time t to a number of time steps I, we use a time increment Δt: $t = I \cdot \Delta t$. The following passage motivates the choice $\Delta t = 0.5$.

In order to extend the simulation to long times, we have two possibilities:

First, we can increase the number of time steps N. The value of N is bounded by the computational power (at this point we want to thank the BWgrid for support). We can handle a maximum of $N = 10^5$.

Second, we can increase the time increment Δt. On the other hand, the time evolution is depicted properly only, if the time increment Δt is smaller than the typical delay time t_d of fluctuating pairs. This bounds Δt from below. The distribution of different delay times is presented in Figure C.2 (appendix). We are interested in the pairs, that are formed and destroyed and therefore lead to dynamics in the spin system. The distribution of these pairs decreases fast for $t_d < 0.5$. Hence, we choose $\Delta t = 0.5$. Figure C.7 (appendix) shows agreement of the correlation function $C(t)$ for different time increments $\Delta t = 0.02, 0.1, 0.5$.

B.2.5 Calculation of the energy of the system

We determine the energy of the system in two steps: First, we obtain the energy of all resonant pairs as

$$E_{(i,j)} = (H + f_{(i,j)}) \cdot I^z_{(i,j)} + 0.5\kappa, \tag{B.6}$$

where the field $f_{(i,j)}$ was defined in Section 2.2 and κ is obtained from Equation (A.46) in Section 2.2.

Secondly, we calculate the energy contribution of all spins, which do not belong to a resonant pair, as

$$E_k = (h_k + \frac{f_k}{2})\ S^z_k. \tag{B.7}$$

Equations (B.6) and (B.7) yield the total energy as

$$E = \sum_{i=1}^{N_{\text{Spins}}} E_i + \sum_{(n,m)}^{N_{\text{Pairs}}} E_{(n,m)}. \tag{B.8}$$

B.3 Link simulation

The algorithm is divided into three sub functions:

1. The *flagall* function. For each spin pair, this function determines, if the pair is resonant. Then, it calls other functions to link this pair to other pairs. It is similar to the routine described in Section 2.2 about resonant pairs.

2. The *flagPair* function. For a selected pair, which is regarded as strong pair, this function identifies potential weak pairs.

3. The *CheckARC* function. For a selected pair, which is regarded as weak pair, this function checks the advanced resonant condition (4.13). If this condition is evaluated true, it puts links between pairs.

From the initialization process, we obtain the list *SPs* of all pairs, which is ordered with respect to the absolute values of the pair interaction. To accelerate the simulation, we neglect pairs where $h_{ij} \gg J_{ij}$. This is done, by labeling a pair satisfying

$$|h_{ij}| - |J_{ij}| - 10 < 0 \tag{B.9}$$

as *active*. If inequality (B.9) is evaluated false, the spin pair is labeled *inactive* and does not take part in the *flagall* routine. Furthermore, we denote pairs with equal spin state such as $|\uparrow\uparrow\rangle$ as *inactive*. The number of active pairs depends on the value of ε.

As presented in Section 4.2.1, a link always connects two pairs. The pair having the smaller interaction is treated as weak pair, whereas the other pair is denoted as strong pair. A pair can adopt the role of a strong pair for one link, and be the weak pair for other links. We use a two step routine, which is included in the *flagall* function, to find links.

For a selected pair p_k with index k in *SPs*, we first determine its resonance state (see later paragraph on the *checkARC* function). Then, we search for potential weak pairs p_l. Details of this search are given in the following subsections. The resonance condition of these weak pairs was not checked yet, since they have a smaller interaction than p_k and therefore an index larger than k. As a result of this search, we obtain a list of potential weak pairs $l_w(k)$ which belongs to pair p_k and contains all pairs p_l. The function *flagPair* checks every weak pair of $l_w(k)$ on further criteria. If it confirms a potential link, we save this fact on the weak pairs as well. Then, we add k to a list of potential strong pairs $l_s(l)$ of every confirmed potential weak pair $l \in l_w(k)$.

At the start of the *flagall* function, both lists $l_s(l)$ and $l_w(l)$ are empty for all l. By going down the list of spin pairs *SPs*, we fill both lists. If we examine a pair p_k, we already found all potential weak pairs of every pair with an interaction larger than J_{p_k}. Therefore, at this point, the list $l_s(k)$ of potential strong pairs for p_k is complete. If $l_s(k)$ is still empty, p_k has no links to stronger pairs and we use the routine from B.1 to check the resonance condition of p_k. Else, we use the ARC (advanced resonance condition) described in Section 4.1 to determine the resonant state of p_k. This is done by the *CheckARC* routine. If this routine evaluates p_k as resonant, all potential strong pairs of p_k are linked to the pair p_k.

B.3.1 The *flagall* function

The routine is presented as a flowchart in Figure B.2. The search for potential weak pairs of pair p_k with index k and spins (i, j) involves the following steps

1. Check if p_k is *active*.

2. Search for spins s, that can destroy or create the resonance of p_k by a spin flip. The interaction $J_{sp} = J_{is} - J_{js}$ of s and p_k enters the modified resonance condition (2.21) as

$$|h_{ij} \pm \frac{1}{2} J_{sp}| < |J_{ij}|\,, \tag{B.10}$$

   where the fields of all other spins and pairs enter h_{ij}. The sign $\pm$ is determined by the z polarization of spin s. In order to change the resonant state of p_k, J_{sp} must be larger than the previous difference of energy and pair interaction $h_{ij} - J_{ij}$. To test this condition, we use the security range $S_{ij} = h_{ij} - J_{ij}$. If

$$J_{sp} > \pm S_{ij} \tag{B.11}$$

   holds, a spin flip would change the pairs resonance identity. If p_k was originally resonant, S_{ij} is negative. Then the sign in (B.11) is $-$. If p_k was non-resonant, then $S_{ij} > 0$ and the sign in (B.11) is $+$.

3. Check if

$$J_{sp} > 0.5 \cdot |J_{ij}| \tag{B.12}$$

   holds. The previous condition (B.11) can be true if both J_{sp} and S_{ij} are small compared to J_{ij}. But then the eigenstates and therefore the dynamics of p_k would not change much by flipping spin s. By requiring (B.12) we ensure that the eigenstates of p_k change noticeable. For further explanation, see Section 2.2 and especially Figure 2.1.

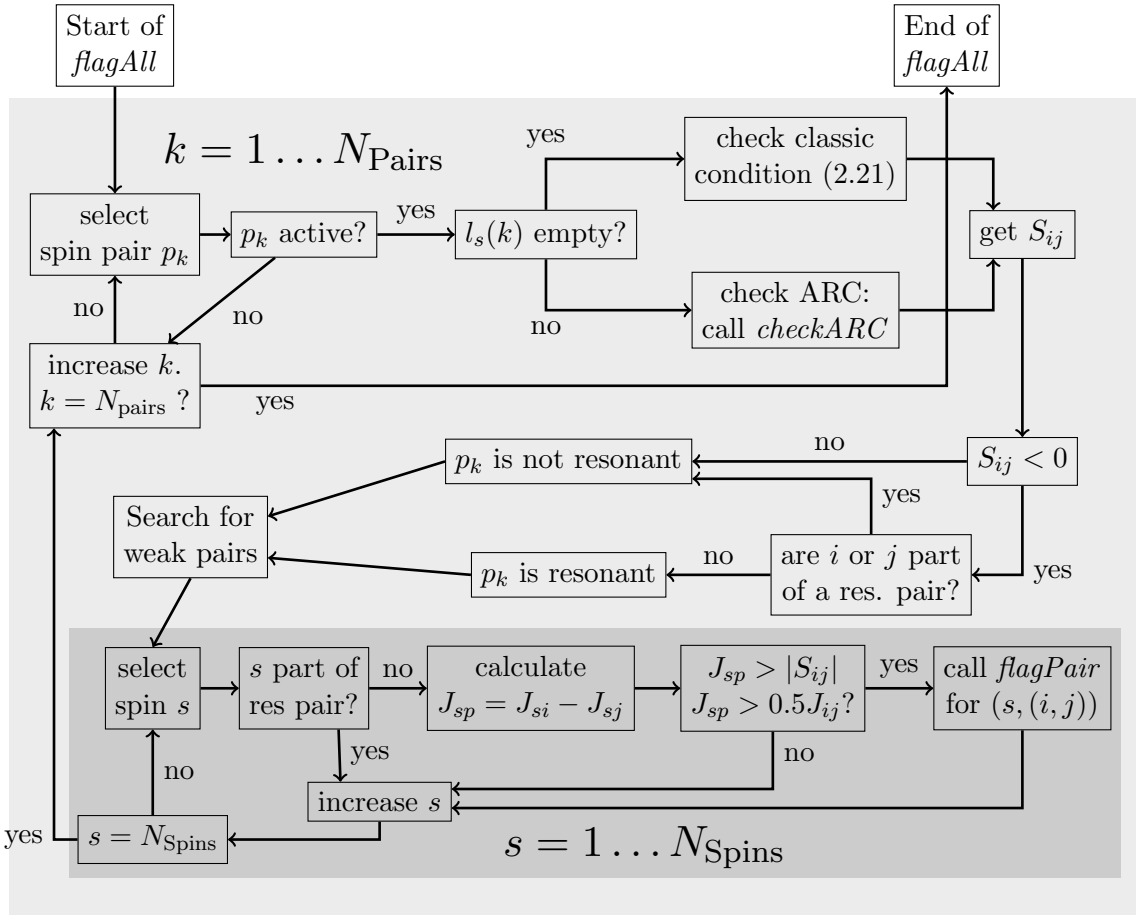

Figure B.2: Flowchart of the *flagAll* routine. The shaded rectangles indicate the two different for-loops of the routine. The search for weak pairs is described in Section B.3.

4. Check if s is part of a resonant pair and ensure that $s \neq i, j$.

To accelerate the simulation, we do not calculate J_{sp} anew but create tables including all possible J_{sp} during the initialization.

As a result of the search for potential weak pairs we obtain a list S_k of spins s, which satisfy all conditions from above. For every element s of S_k, the routine calls *flagPair*.

B.3.2 The *flagPair* function

The input parameter of this function are a spin s and a pair p_k consisting of spins (i, j). It selects pairs $p_l = (s, t)$, which include spin s, and determines if p_k is a strong pair of p_l. If this is true, the routine adds the pair p_k

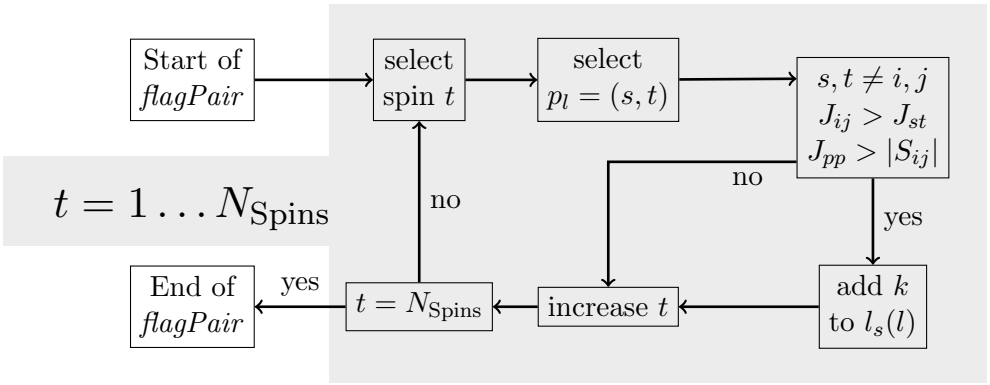

Figure B.3: Flowchart of the *flagPair* routine. The shaded rectangle indicates the for-loop over all spins t as a possible partner for spins s. Both spins create the pair $p_l = (s,t)$. If the conditions described in B.3 are satisfied, the routine adds the pair p_k to the list $l_s(l)$ of strong pairs of p_l.

to the list $l_s(l)$ of p_l. This list $l_s(l)$ is needed to formulate the advanced resonance condition of spin pair p_l. If this condition is evaluated positive, a link between p_k and p_l is established. Before the routine adds k to $l_s(l)$, it checks whether p_l satisfies the following conditions:

1. $s,t \neq i,j$ and p_l is active.
2. $J_{ij} > J_{st}$. This condition ensures that the selected pair p_l is a weak pair of p_k.
3. $J_{pp} > |S_{ij}|$ where $S_{ij} = h_{ij} - J_{ij}$ is the security range of p_k and

$$J_{pp} = |(J_{is} - J_{it}) - (J_{js} - J_{jt})| \tag{B.13}$$

   is the pair-pair interaction of p_k and p_l. From the second condition of the *flagAll* routine we already now, that a spin flip of s would change the resonance of p_k. However, due to symmetry of the spins s and t, the pair-pair interaction $J_{\text{pair-pair}}$ can be much smaller than the spin-pair interaction $J_{\text{spin-pair}}$. We test (B.13) to ensure that a transition $|\uparrow\downarrow\rangle \rightarrow |\downarrow\uparrow\rangle$ of the weak pair p_l would change the resonance of pair p_k.

If all conditions are satisfied, the pair p_k is a potential strong pair of p_l. Hence, the index k is added to the list $l_s(l)$. In order to establish the link between p_k and p_l, the advanced resonance condition of pair p_l has to be satisfied. This check occurs, when the *flagAll* routine arrives at the pair index l and checks the resonance condition of p_l (see Figure B.2).

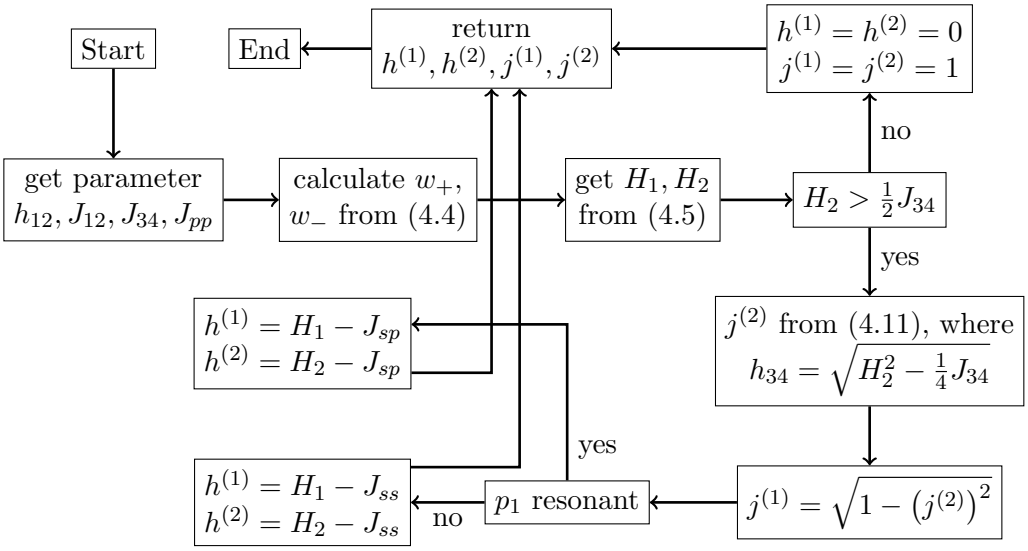

Figure B.4: Flowchart of a subroutine of *CheckARC*. This routine determines the shifts $h^{(1)}, h^{(2)}$ and the transition amplitudes $j^{(1)}, j^{(2)}$ for a strong pair $(1, 2)$ and a weak pair $(3, 4)$.

B.3.3 The *checkARC* function

The *checkARC* routine determines, whether one of the advanced resonance conditions (4.13) of a pair $p_k = (i, j)$ is true or false. It returns the security range S_{ij} of this pair. Thereby, it analyzes the list of potential strong pairs $l_s(k)$, which was created using the functions *flagAll* and *flagPair*. More details on the derivation of the advanced resonance condition can be found in Section 4.1. A sketch of the algorithm is presented in Figure B.5.

First, the algorithm deletes all pairs p_d from the list $l_s(k)$, that are not resonant but include a spin part of another resonant pair. Next, the algorithm calculates for each remaining pair p_l of $l_s(k)$ the values h_{ij}, for which the 4-spin-system has a resonant transition. These values are denoted as shifts $h^{(i)}$. Additionally to two shift values, the routine determines respective transition amplitudes $j^{(i)}$. The calculation of $h^{(1)}, h^{(2)}, j^{(1)}, j^{(2)}$ is done using a distinct subroutine, which is presented in Figure B.4. The derivation of these calculations can be found in Section 4.1.

For clarity we repeat Equation (4.13):

$$\left| h_{34} - \sum_{\pm,s,i} \pm h_s^{(i)} \right| < J_{34} \cdot \prod_{s,i} j_s^{(i)} \tag{B.14}$$

where the parameter s sums over all potential strong pairs in the list $l_s(k)$

and i has values ± 1. We can rewrite (B.14) as

$$\left| h_{34} - \sum_{i_s=\pm 1} \left(\sum_{s=1}^{N_s} \pm h_s^{(i_s)} \right) \right| < J_{34} \cdot \prod_{i_s=\pm 1} \left(\prod_{s=1}^{N_s} j_s^{(i_s)} \right) \tag{B.15}$$

and introduce a vector $p = (i_s)_{(s=1 \ldots N_s)}$, which consists of all values $i_s \in \{-2, -1, 2, 2\}$. Each component p_s has four possible values to represent the four different values of $\pm h^{(i)}$. Therefore, we obtain 4^{N_s} distinct vectors p. We substitute the inner product and sum in (B.15) by the variables

$$E(p) = \sum_{s=1}^{N_s} h_s^{(p_s)} \tag{B.16}$$

and

$$c(p) = \prod_{s=1}^{N_s} j_s^{(p_s)} \,. \tag{B.17}$$

We obtain

$$\left| h_{34} - \sum_{p} E(p) \right| < |J_{34}| \cdot \prod_{p} c(p) \,. \tag{B.18}$$

In order to obtain the rewritten advanced resonance condition (B.18), the algorithm *checkARC* calculates $E(p)$ and $c(p)$ for every possible value of p. Since the size of p and the number of conditions (B.18) grows exponentially as 2^{N_s}, the duration of the simulation strongly depends on the values for N_s. If a weak pair has 10 or more potential strong pairs, we take only the nine strong pairs with largest coupling strength into account.

After the routine set up all conditions (B.18), it checks whether they are true or false. If all conditions are evaluated false, the weak pair p_k is not resonant and is not linked to any of the potential strong pairs. If at least one condition is evaluated true, all potential strong pairs of the list $l_s(k)$ are linked to the weak pair p_k and p_k is labeled as a resonant pair. The resonance of the potential strong pairs does not change during the progress.

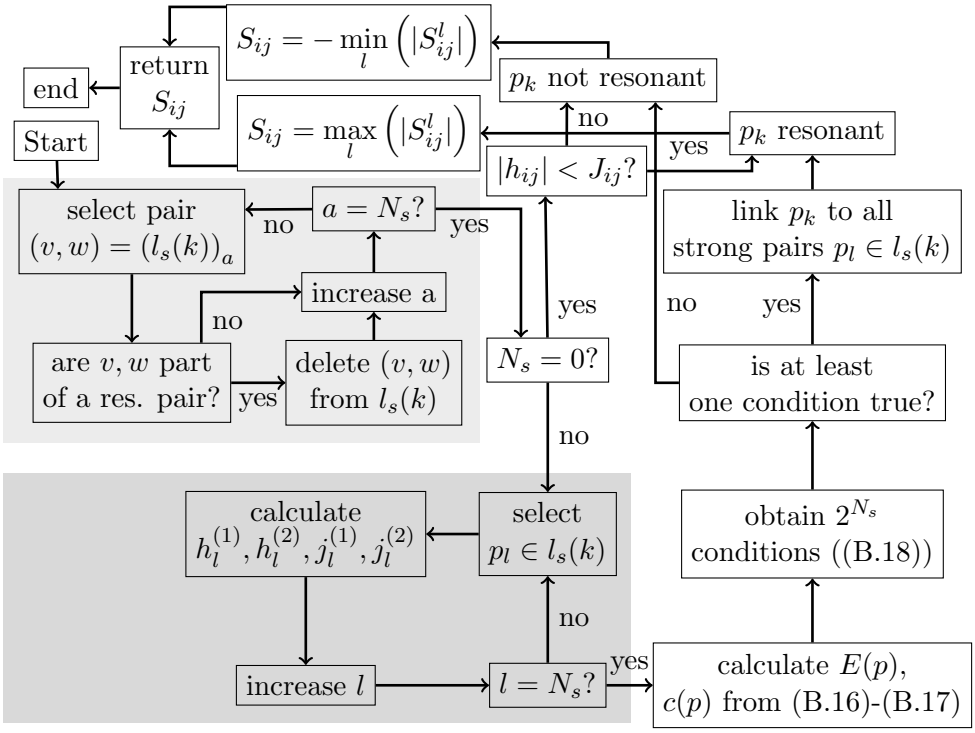

Figure B.5: Flowchart of *CheckARC*. This routine determines the advanced resonance conditions (B.18) for a weak pair p_k and links p_k to every potential strong pair of $l_s(k)$ if (B.18) is evaluated true.

Appendix C

Additional figures

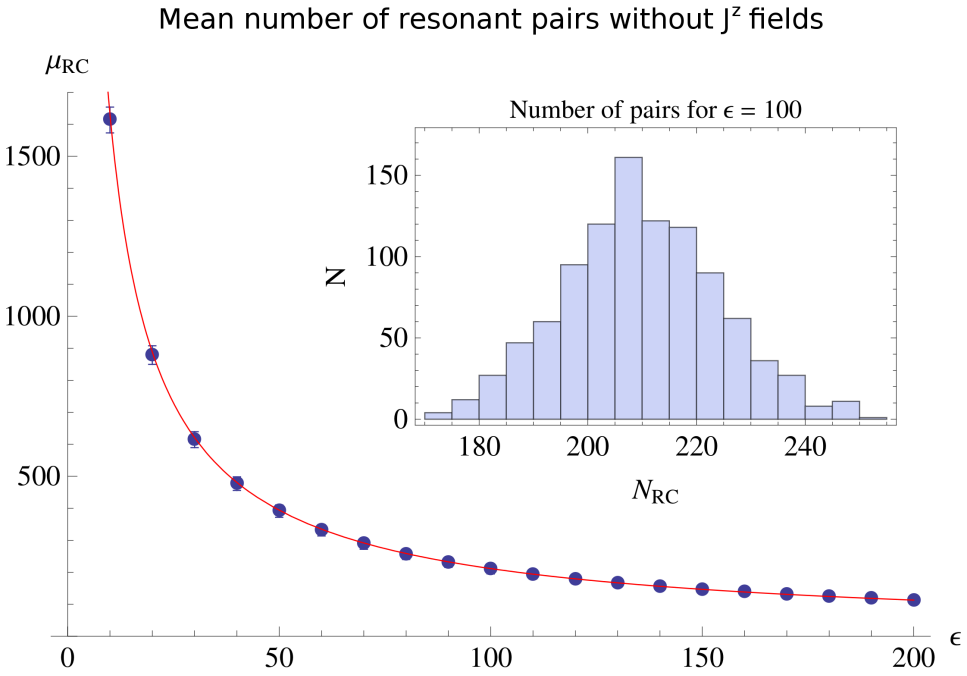

Figure C.1: The main plot shows the dependence of the averaged number of resonant conditions μ_{RC} on the disorder ε using isotropic r^{-3} interaction without J^z fields. For each disorder value, 1000 different initial configurations of the spin system were examined. The mean values μ_{RC} of the resulting distributions of N_{RC} are indicated by blue dots, the standard derivation by an error bar. The distribution of N_{RC} for $\varepsilon = 100$ is presented as inset. The red curve represents the fit from Equation (2.46).

C.1 Time Evolution

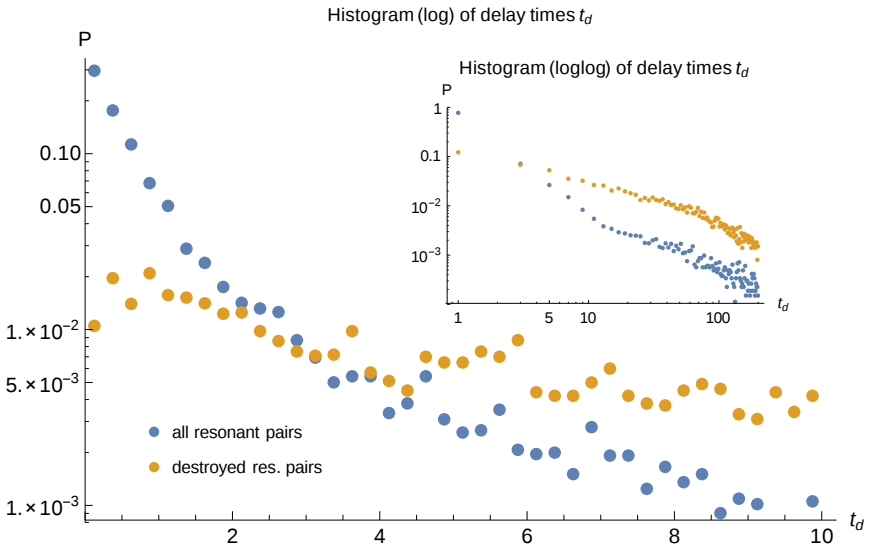

Figure C.2: Histogram of the delay times for disorder $\varepsilon = 0$. The main plot shows a logarithmic plot of short times $t_d < 10$, the inset shows a log-log plot of long times $t_d \in [0, 200]$. Blue dots show the distribution of t_d for all resonant pairs present in the system and yellow dots mark the distribution of deleted pairs. Only the second kind of pairs leads to a fluctuation of fields and therefore contributes to the dynamics in the system.

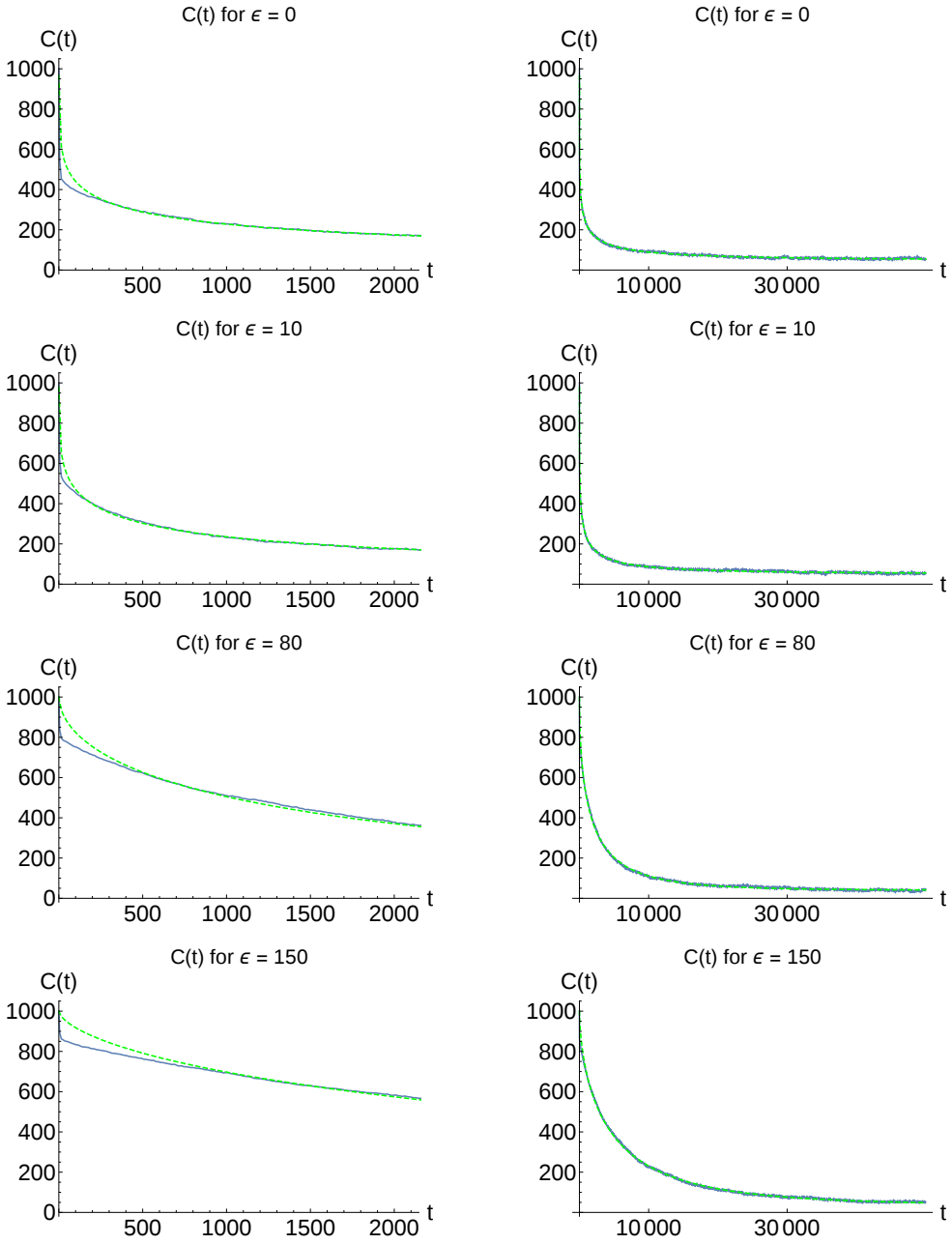

Figure C.3: Linear plots of the correlation function $C(t)$ for disorder $\varepsilon = 0, 10, 80, 150$. We present one plot for times $t \in [0, 2000]$ and one plot for $t \in [0, 50000]$, thereby we averaged over about 35 different initial configurations of spins. The blue dots indicate the data obtained from the simulation whereas the green line is a stretched exponential function as defined in (3.4).

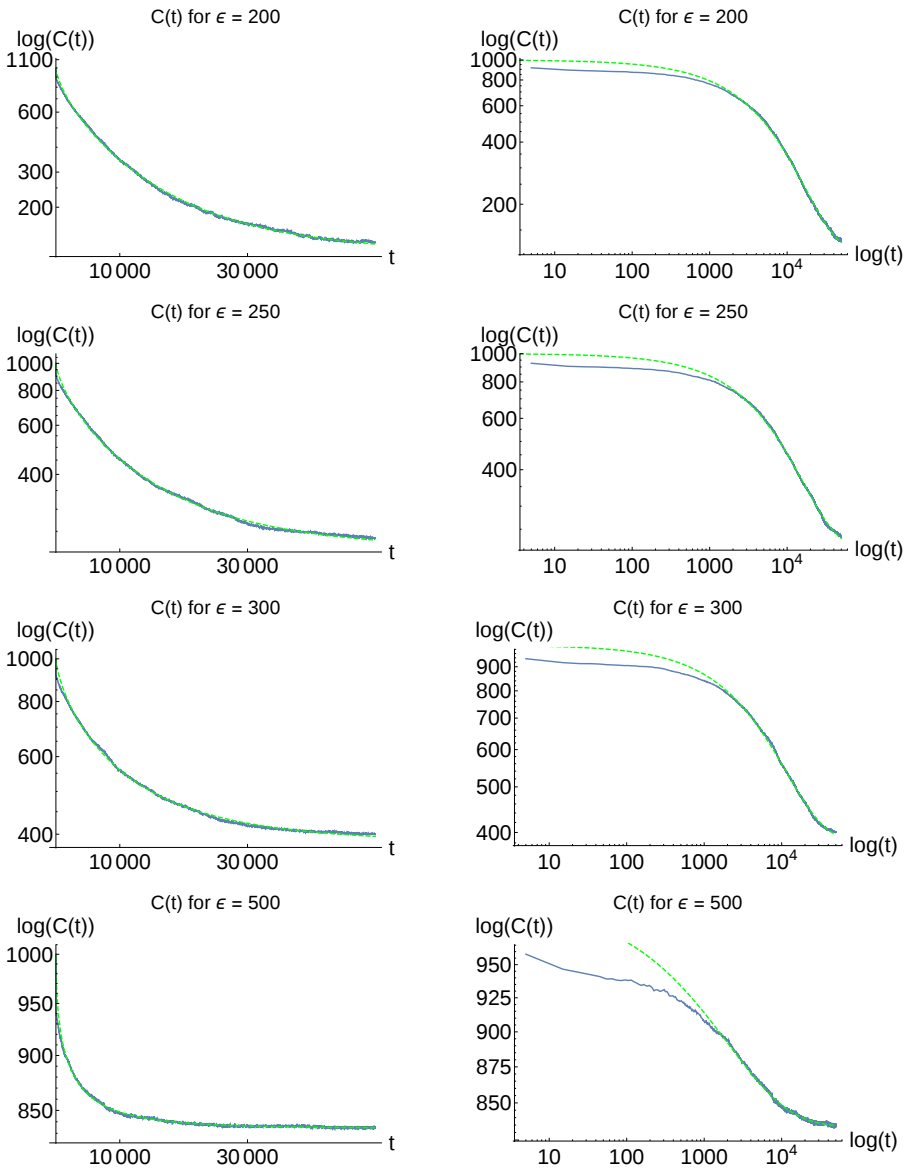

Figure C.4: Collection of logarithmic plots of the correlation function $C(t)$ for disorder values $\varepsilon = 200, 250, 300, 500$ and a time increment $\Delta t = 0.5$ for long times. We averaged over about 35 different initial configurations of spins. The blue dots indicate the data obtained from the simulation whereas the green line is a stretched exponential function as defined in (3.4).

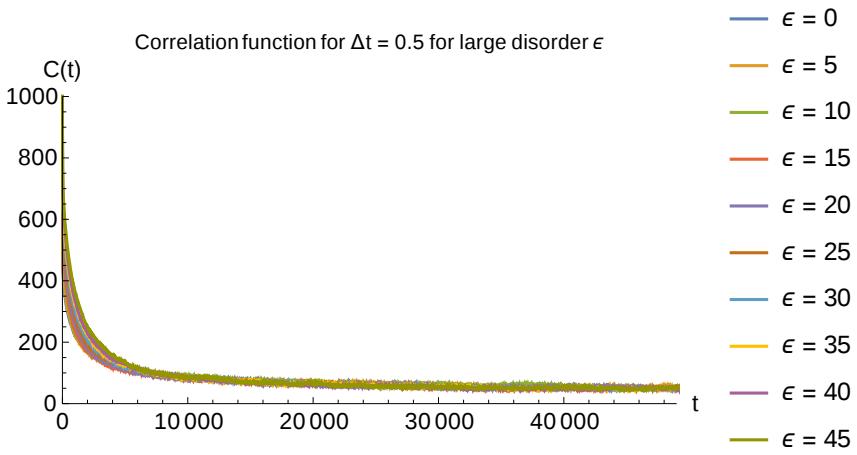

Figure C.5: Plot of the correlation function $C(t)$ for about 70 different initial configurations and time increments $\Delta t = 0.5$.

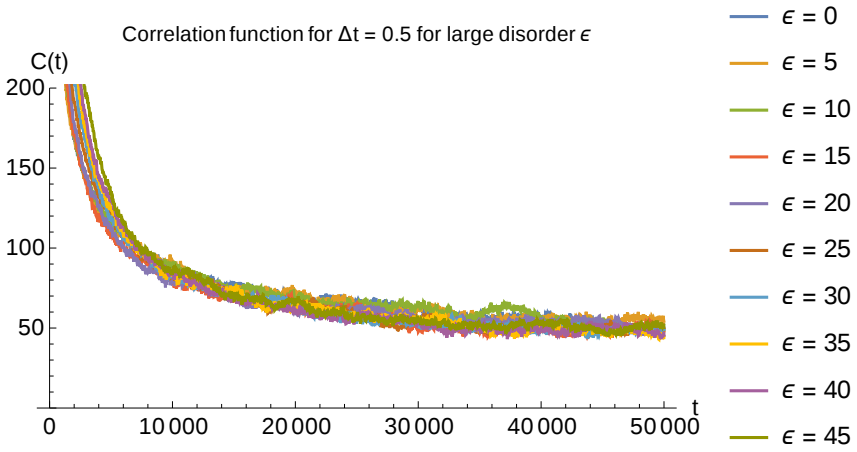

Figure C.6: Plot of the correlation function $C(t)$ for about 70 different initial configurations and time increments $\Delta t = 0.5$.

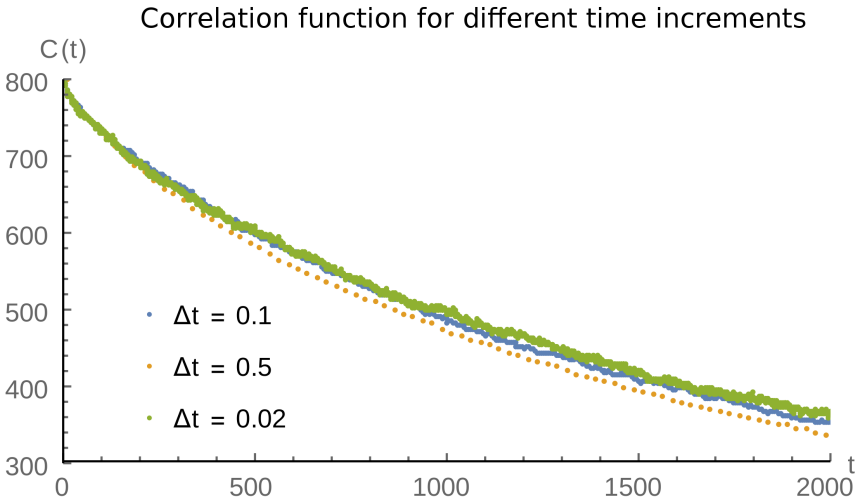

Figure C.7: Plot of the correlation function $C(t)$ for $\varepsilon = 70$ and different time increments Δt.

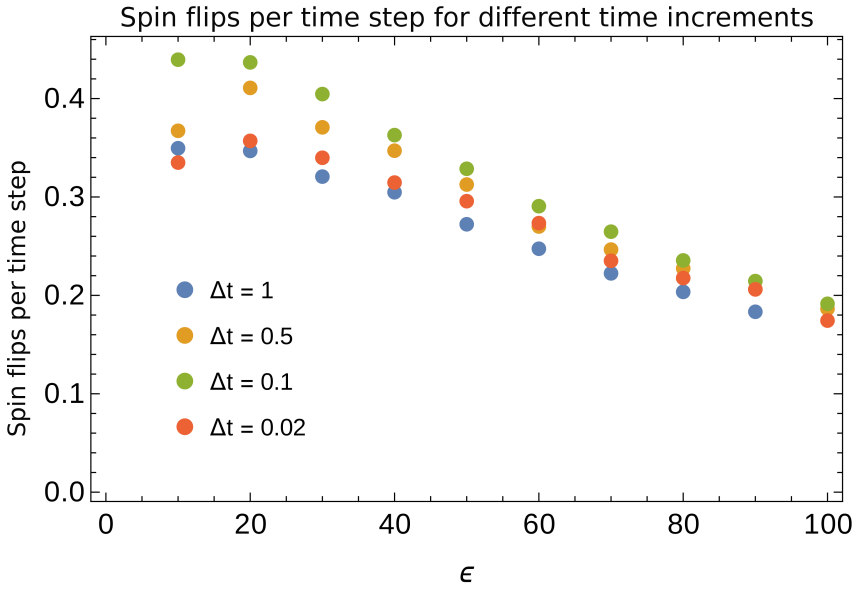

Figure C.8: Mean number of spin flips per time step for a system with disorder $\varepsilon = 70$ and for different time increments Δt.

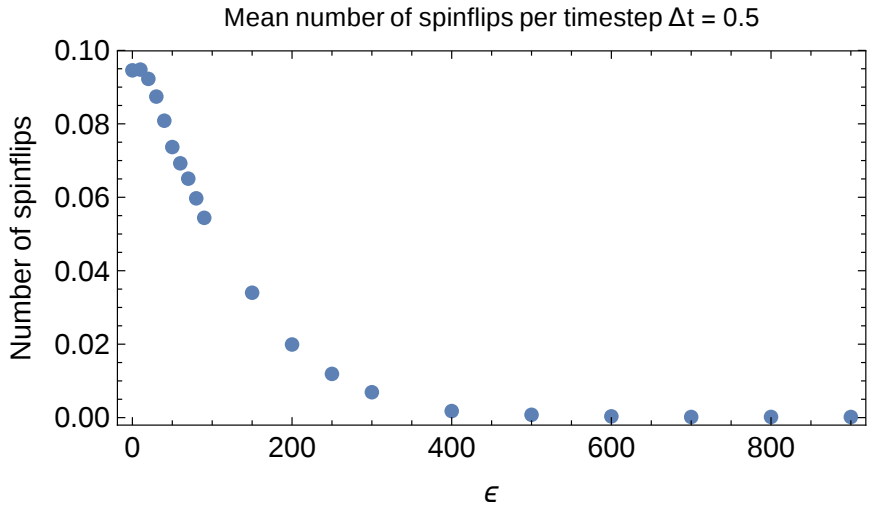

Figure C.9: Number of spin flips per time step.

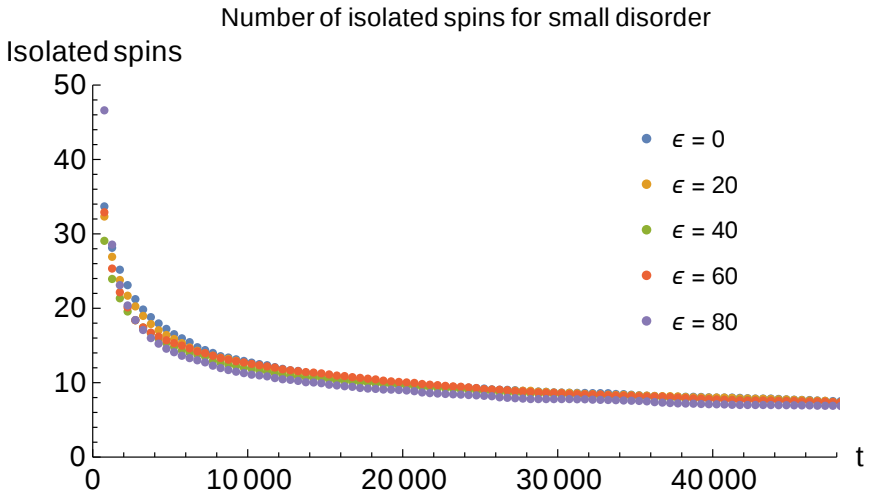

Figure C.10: Number of isolated spins over time t for small disorder $\varepsilon < 100$.

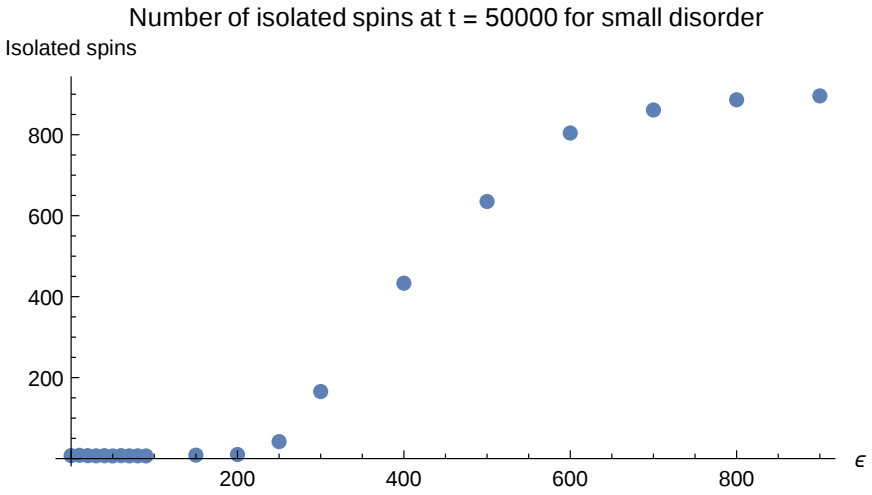

Figure C.11: Number of isolated spins at time $t = 50000$ over time t for varying disorder ε.

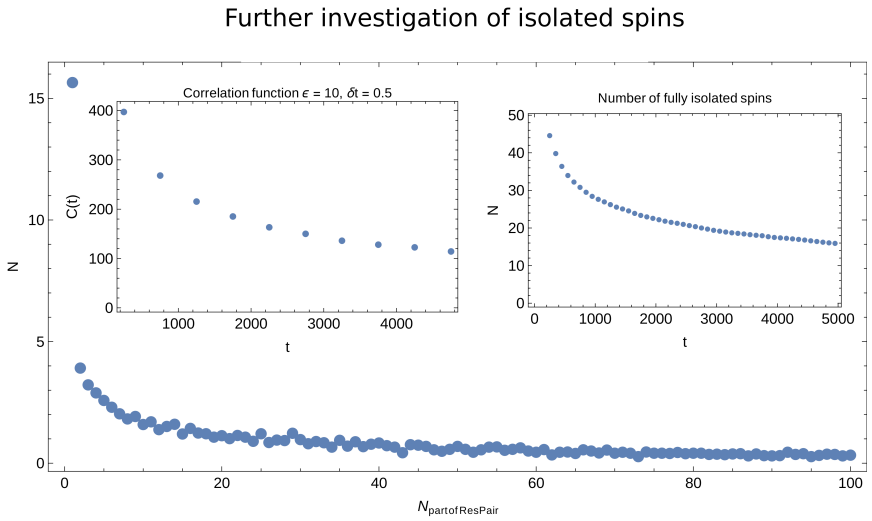

Figure C.12: This histogram examines spins, that did not flip up to a time $t = 5000$ for $\varepsilon = 10$ and $\Delta t = 0.5$. On the x-axis, the Figure presents the number of times, these spins have been part of a resonant pair. For $x = 0$, we obtain fully isolated spins (spins, that never have been part of a resonant pair). Even though these spins form a clear maximum, they are only responsible for ca. 20% of all non-flipped spins (≈ 100). The left inset shows the correlation function $C(t)$ for this data set, whereas the right inset shows the number of fully isolated spins over time t.

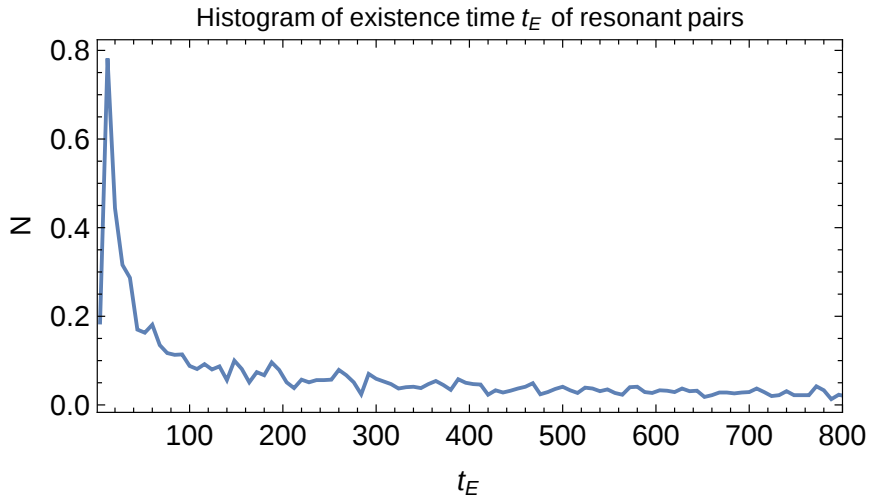

Figure C.13: Histogram of the absolute existence time t_E for $\varepsilon = 10$, $\Delta t = 0.5$. We averaged over 100 different initial configurations.

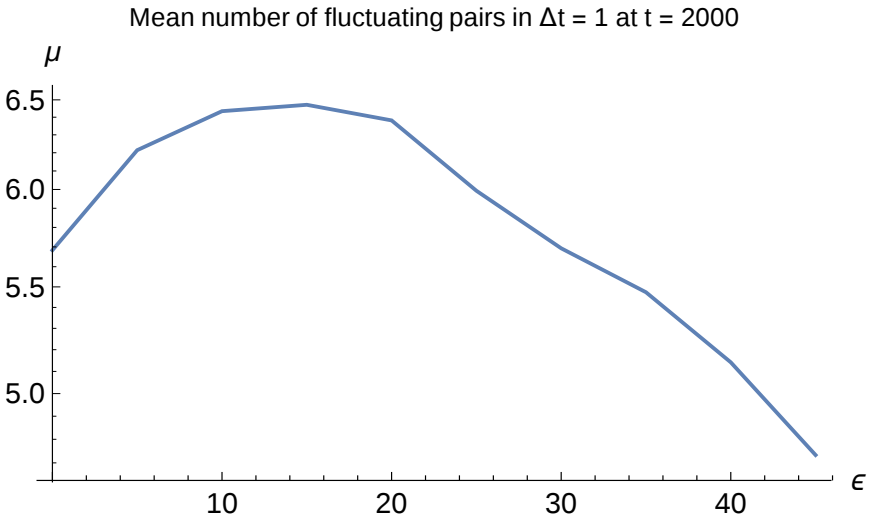

Figure C.14: Mean number of fluctuating pairs at $t = 50000$ for small disorder value ε.

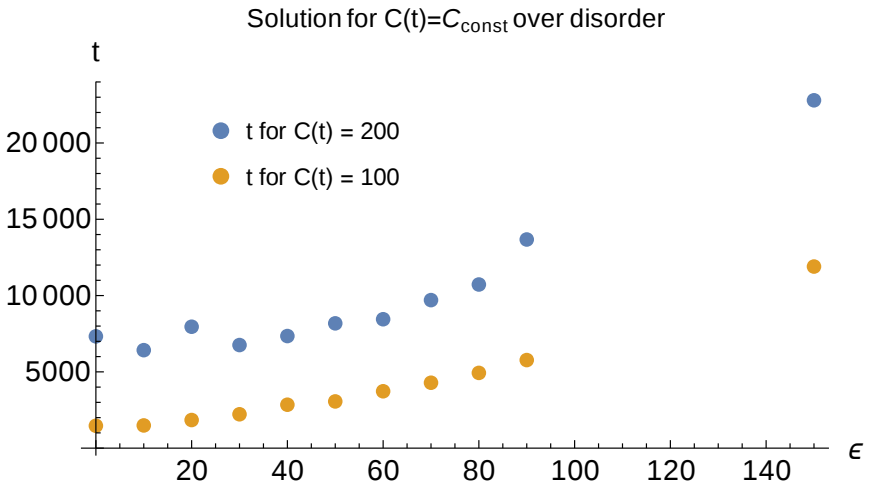

Figure C.15: Solution of the Equation $C(t) = C_{\text{const}}$ for $C_{\text{const}} = 100$ and $C_{\text{const}} = 200$. The difference is shown in Figure C.16.

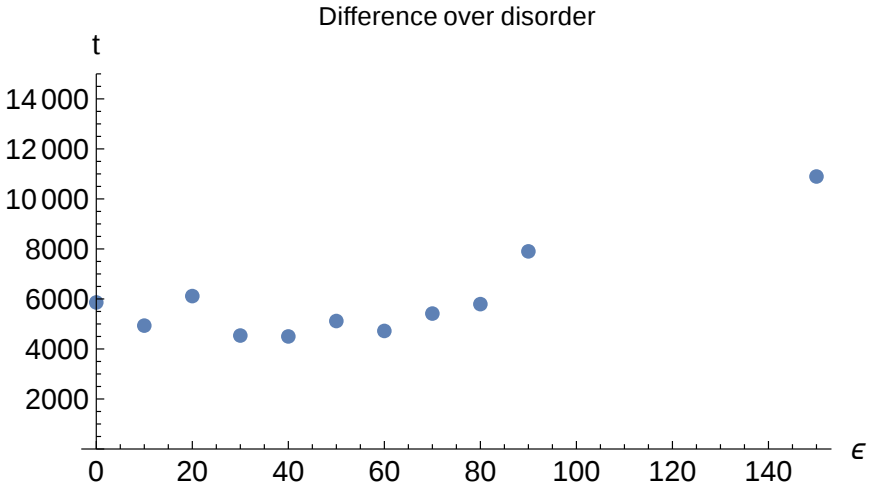

Figure C.16: Difference of the two curves from Figure C.15.

C.2 Cluster formation

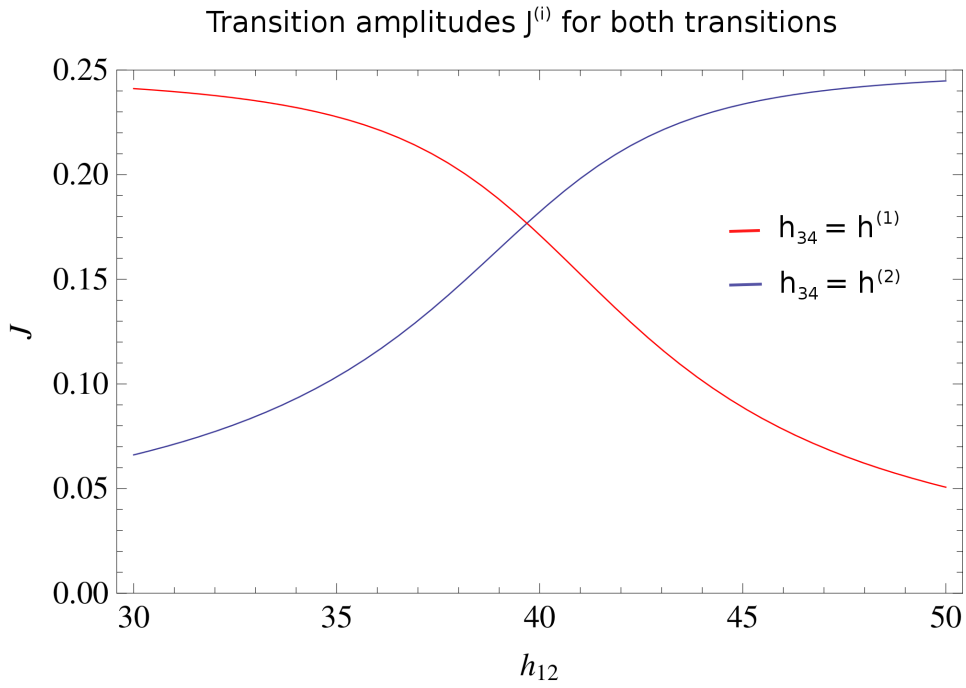

Figure C.17: Transition amplitudes for a system with variable h_{12} and $J_{12} = 10$, $J_{pp} = 80$ and $J_{34} = 1$. The transition between the two eigenstates at $h_{34} = h^{(1)}$ is represented by the red, the transition at $h_{34} = h^{(2)}$ by the blue curve. The two curves cross at $h_{12} = 40 = \frac{J_{pp}}{2}$ where $J = \frac{1}{\sqrt{2}}\frac{1}{4}J_{34} \approx 0.175$.

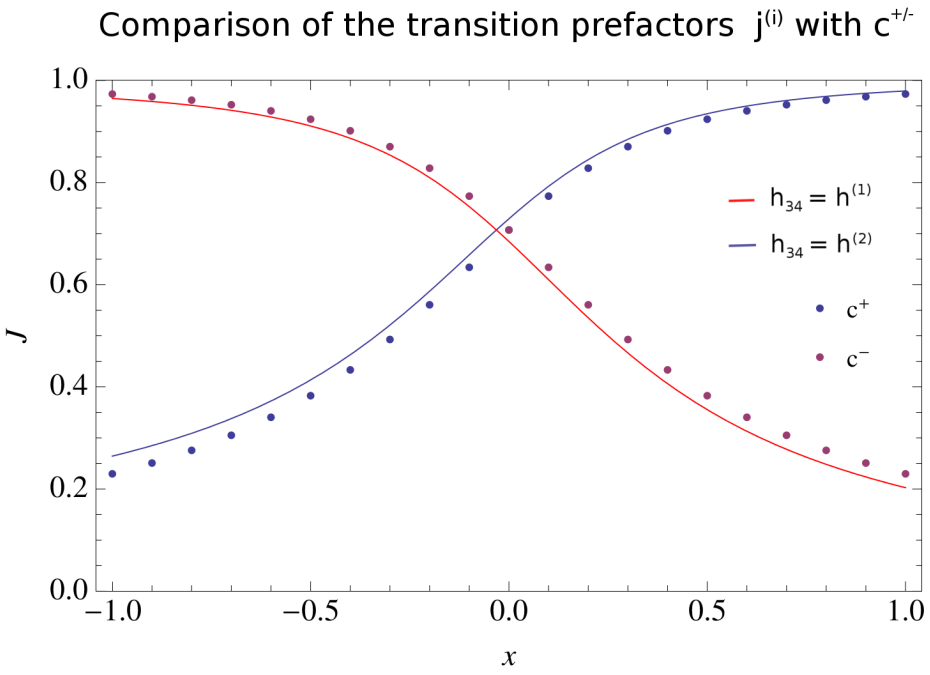

Figure C.18: Comparison of the transition prefactors $j^{(i)}$ for $h_{34} = h^{(1)}$ (red line) and $h_{34} = h^{(2)}$ (blue line) from Figure C.17 with the functions $c^{\pm}(x)$ (dots) from Equation (2.13), where $x = \frac{h_{12}}{J_{12}}$.

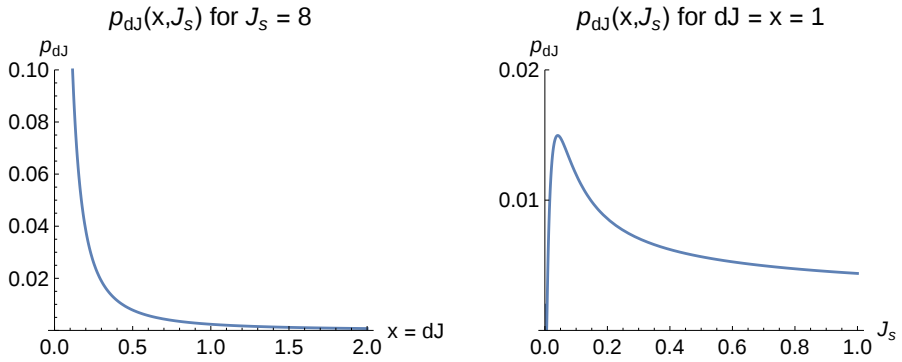

Figure C.19: The left plot shows the density function $p_{J_{sp}}(x)$ for fixed strong pair interaction J_s. In the right plot we fix x at 1 and vary the interaction J_s of the strong pair.

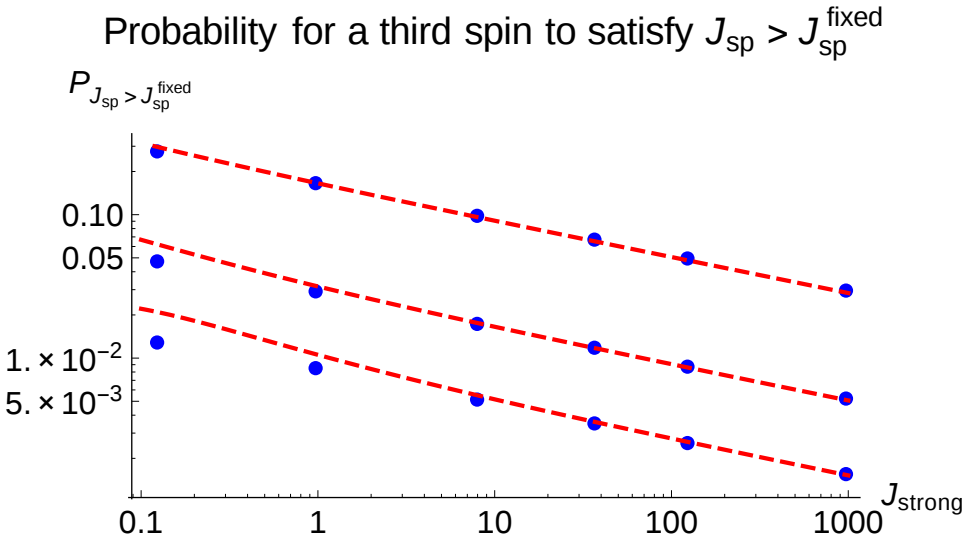

Figure C.20: Comparison of the analytical expression $V = 0.7 \cdot (z_l + z_r)^3$ (red dashed line) with numerical data (blue dots) for $J_{sp}^{\text{fixed}} = 0.01, 0.5, 0.1$.

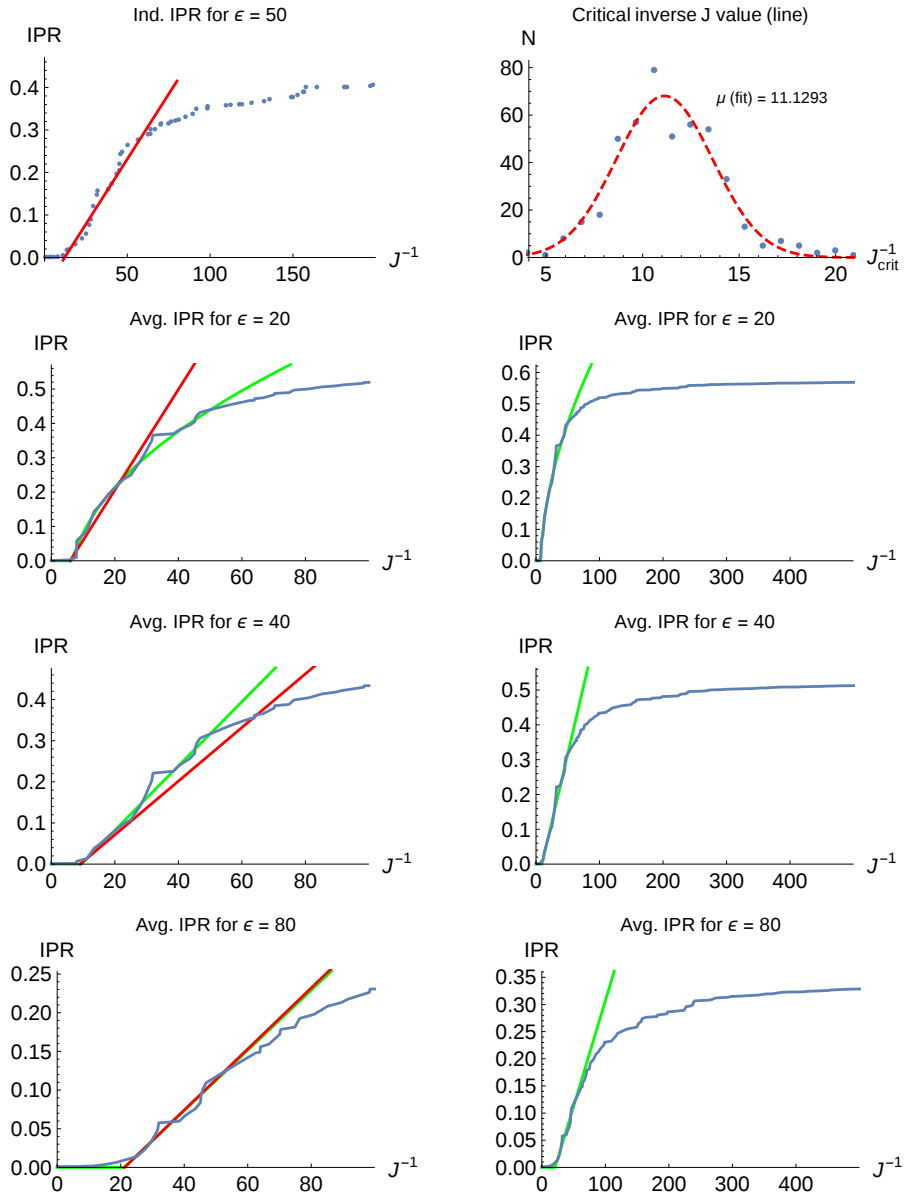

Figure C.21: The bottom six plots (second to fourth row) represent the averaged IPR function defined in (4.17) for the three disorder values $\varepsilon = 20, 40, 80$. For each disorder value we show a small scale ($J^{-1} \in [0, 100]$, left column) and a larger scale ($J^{-1} \in [0, 500]$, right column). The two fits represent a straight line fitted at J_{ip}^{-1} (red line) and a square root function (green line). Each plot was obtained by averaging over about 500 initial configurations.In the top left plot we present the IPR function for a lattice for $\varepsilon = 40$. The top right pot shows a histogram of the values of J_{crit}^{-1} obtained from $\varepsilon = 40$ and 462 different initial configurations. The Gaussian fit (red dashed line) has a standard deviation of $s = 2.5$.

Acknowledgments

First of all, I want to thank my advisor Boris Fine. He has an incredible intuition for physics and never lacked ideas, how to continue the research. Moreover, I would like to thank Studienwerk Villigst e.V., the Heidelberg Center for Quantum Dynamics, the Heidelberg Graduate School for Fundamental Physics and the Institute for Theoretical Physics Heidelberg for financing the research of this thesis.

Additionally, I want to thank the members of the Institute of Theoretical Physics in Heidelberg. In summary, I spend more time here than in any other building in Heidelberg, and I enjoyed it very much. From all my nice colleagues, I want to express special thanks to Kambiz Veshgini, Walter Hahn, and David Breyel. Not only did they help me by proofreading large parts of this manuscript, but often joined in helpful discussions on scientific and non-scientific topics.

Moreover, I would like to thank my parents for the support during the time of my phd, and during my whole life. This phd thesis is the final result of a long way of education, which you shaped essentially.

Last but not least, I am grateful for having met Lisa Feustel, who is the most important person of my life.

Bibliography

[1] Anatole Abragam. *The principles of nuclear magnetism*. Oxford Univ. Pr., 2011.

[2] E. Abrahams, P.W. Anderson, D.C. Licciardello, and T.V. Ramakrishnan. Scaling theory of localization: Absence of quantum diffusion in two dimensions. *Phys. Rev. Lett.*, 42:673, 1979.

[3] E. Akkermans and G. Montambaux. *Mesoscopic Physics of Electrons and Photons*. Cambridge Univ. Press, 2007.

[4] P.W. Anderson. Absence of diffusion in certain random lattices. *Physical Review*, 109:1492, 1958.

[5] P.W. Anderson, B.I. Halperin, and C. Varma. Anomalous low-temperature thermal properties of glasses and spin glasses. *Phil.Mag.*, 25:1–9, 1972.

[6] Alain Aspect. Direct observation of anderson localization of matter waves in a controlled disorder. *Nature*, 453:891–894, 2008.

[7] D.M. Basko, I.L. Aleiner, and B.L. Altshuler. Metalinsulator transition in a weakly interacting many-electron system with localized single-particle states. *Annals of Physics*, 321:1126, 2006.

[8] Doru Bodea and Alois Wuerger. Interaction-driven relaxation of two-level systems in glasses. *PRL*, 97:165505–1, 2006.

[9] A.L. Burin and Yu. Kagan. Low-energy collective excitation in glasses. new relaxation mechanism for ultralow temperatures. *JETP*, 80:761, 1995.

[10] A.L. Burin, Yu. Kagan, L.A. Maksimov, and I.Ya. Polishchuk. Dephasing rate in dielectric glasses at ultralow temperatures. *PRL*, 80:2945(4), 1997.

[11] N.Y. Ching and D.L. Huber. Numerical studies of energy levels and eigenfunctions localization in dilute three-dimensional systems. *Phys. Rev. B*, 25:1096, 1982.

[12] R. Dalichaouch, J. P. Armstrong, S. Schultz, P. M. Platzman, and McCall. Microwave localization by two-dimensional random scattering. *Nature*, 354:53–55, 1991.

[13] B.I. Halperin. Properties of a particle in a one-dimensional random potential. *Adv. Chem. Phys.*, 13:123, 1967.

[14] J.A. Kjäll, J.H. Bardarson, and F. Pollmann. Many-body localization in a disordered quantum ising chain. *Phys. Rev. Lett.*, 113:107204, 2014.

[15] P. A. Lee and T. V. Ramakrishnan. Disordered electronic systems. *Rev. Mod. Phys.*, 53:287–337, 1985.

[16] N.F. Mott and W.D. Twose. The theory of impurity conduction. *Adv. Phys.*, 10:107, 1961.

[17] A. Pal and D.A. Huse. Many-body localization phase transition. *Phys. Rev. B*, 82:174411, 2010.

[18] A. Papoulis and S.U. Pillai. *Probability, random variables, and stochastic processes*. McGraw-Hill Europe, 2002.

[19] J.C. Phillips. Stretched exponential relaxation in molecular and electronic glasses. *Rep. Prog. Phys.*, 59:1133–1207, 1996.

[20] W.A. Phillips. Tunneling states in amorphous solids. *J. Low. Temp. Phys.*, 7:351, 1972.

[21] I. Y. Polishchuk and A. L. Burin. Thermal conductivity of glasses induced by nuclear quadrupole interaction at ultra low temperatures. *J. Low. Temp. Phys. 7*, 162:509, 2010.

[22] Alberto Rodriguez, Louella J. Vasquez, Keith Slevin, and Rudolf A. Romer. Multifractal finite-size scaling and universality at the anderson transition. *Phys. Rev. B*, 84:134209–1, 2011.

[23] S. Rogge, D. Natelson, and D. D. Osheroff. Evidence for the importance of interactions between active defects in glasses. *Phys. Rev. Le*, 76:3136, 1996.

[24] F. Scheffold, R. Lenke, R. Tweer, and G. Maret. Localization or classical diffusion of light? *Nature*, 398:206–270, 1999.

[25] C.P. Slichter. *Principles of Magnetic Resonance*. Springer, 1996.

[26] R. Vosk and E. Altman. Many-body localization in one dimension as a dynamical renormalization group fixed point. *Phys. Rev. Lett.*, 110:67204, 2013.

[27] R. L. Weaver. Anderson localization of ultrasound. *Wave Motion*, 12:129–142, 1990.

[28] C.C. Yu and A.J. Leggett. Low temperature properties of amorphous materials: Through a glass darkly. *Comments Condens. Matter Phys.*, 14:231, 1988.

[29] R.C. Zeller and R.O. Pohl. Thermal conductivity and specific heat of noncrystalline solids. *Phys. Rev. B*, 4:2029, 1971.